May 25, 2004

Dr. Jeff Amthor
Environmental Science Division
Department of Energy
19901 Germantown Rd.
Germantown, MD 20874

RE: Final Technical Progress Report
Award No. DE-FG03-01DF63065, *Direct Experiments on the Ocean Disposal of Fossil Fuel CO_2*

Dear Jeff,
We have completed the final report for Award No. DE-FG03-01DF63065 concerning, *Direct Experiments on the Ocean Disposal of Fossil Fuel CO_2*. I have appended below our final progress report on that project. I have also appended the recent progress report from our NETL award, since these studies are closely intertwined. We appreciate support from the program greatly, and we are now progressing quite well on our continuing support from the Office of Science.

Sincerely,

James P. Barry
Associate Scientist

Final Technical Progress Report
Award No. DE-FG03-01DF63065, *Direct Experiments on the Ocean Disposal of Fossil Fuel CO_2*

Introduction

From 2001 to early 2004, we performed field and laboratory experiments, and developed technology to investigate the feasibility and biological consequences of direct ocean CO2 injection as a sequestration strategy to mitigate rising levels of CO2 in the atmosphere. These activities were performed using support from the Monterey Bay Aquarium Research Institute (MBARI) and DoE, through the combined efforts of MBARI ships, ROVs, and science, engineering and operations personnel. DoE support included funding from NETL (Award DE-FC26-00NT40929 :*Feasibility of large-scale ocean CO2 sequestration* –Drs. Brewer and Barry) and DoE Office of Science Award DE-FG03-01DF63065 (*Direct Experiments on the Ocean Disposal of Fossil Fuel CO_2* - Drs. Barry and Brewer). Activities supported by the Office of Science award were intertwined closely with those funded by NETL and MBARI, but were associated most closely studies by postdoctoral fellows. The major results of activities supported by the NETL award are listed in the attached technical progress report which includes several scholarly publications related to this research.

Field Experiments

Several deep-sea field experiments were performed off the California coast during 2001 to 2003. Each of these experiments involved a logistically complicated process of pressurizing and transporting small quantities (~20 to 150 l) of liquid CO2 to the seafloor using the ROV *Tiburon*, launched from the R/V *Western Flyer*, operated by MBARI. Five of these small-scale CO2 release experiments were used to evaluate the response of deep-sea organisms to changes in seawater chemistry caused by the addition of CO2 to the ocean. During each experiment, small pools of liquid CO2 were created on the seafloor, after which the CO2 would dissolve slowly into seawater, carrying a CO2-rich dissolution plume downstream over sediments inhabited by infaunal organisms and past small cages holding experimental animals. Changes in seawater chemistry were detected mainly by pH meters; the addition of CO2 to seawater elevates its CO2 levels, and reduces its pH (i.e. increases the acidity of seawater). We assessed the survival of various organisms (microbes, meiofauna [nematodes, amoebae, flagellates], macrofauna [sediment-dwelling worms and crustaceans], and megafauna [snails, sea urchins, sea cucumbers, octopus, fish] during month-long exposure to elevated CO2 levels in the dissolution plumes.

The major results of these field experiments indicates that direct ocean injection of CO2 in the deep-sea will have variable, but generally negative effects on deep-sea ecosystems. Elevated CO2 levels cause physiological stress in many marine organisms, including respiratory stress, acidosis of intra- and inter-cellular spaces, and narcosis. The severity of effects on individual physiology vary among taxa, with echinoderms as the most sensitive taxon studies. The potential consequences for population and species level effects remain unknown. Effects will be most pronounced near sites of CO2 release, and the severity and scope of effects will depend on the volume of CO2 released. These

results also have implications for the future rise in ocean CO2 levels due to air-sea gas exchange and ocean mixing.

Our field experiments during the past year or so have included collaborators from other institutions who are funded by the Office of Science for carbon sequestration studies. Kevin Carman (LSU) and Dave Thistle (FSU) are funded to investigate various aspects of the effects of CO2 on deep-sea meiofauna. Jim Kennett (UCSB) and Joan Bernhard (WHOI) are funded to investigate the effects of elevated CO2 on deep-sea foraminifera. Carman and Thistle have accompanied us on research cruises during 2002 and 2003, and we collected samples for Kennett and his students during these years. We will continue these collaborations during 2004/2005.

Technology Development and Laboratory Studies

Several technology develop efforts are associated with this project. These include; 1) the design, fabrication, and deployment of a deep-sea fish-trap respirometer, to study the physiology of deep-sea fishes, including their sensitivity to elevated CO2 levels, 2) development of a chilled seawater aquarium system with fine control of gas concentrations to allow long-term studies of CO2 effects on marine animals, and 3) upgrading our benthic respiration system to allow measurements of pH, CO2, and oxygen, as well as adding sample injection / withdrawal syringes to allow manipulation of CO2 levels inside the chamber.

Deep-sea Fish Trap / Respirometer

In order to examine the physiological response of apex predators to deep-sea carbon sequestration we have developed a hyperbaric trap respirometer. This project was funded by the Office of Science as a supplement to award DE-FG03-01DF63065. The goal is to capture deep-water fishes at depths of up to 4000m and return the specimens to the surface alive at *in situ* pressure for controlled laboratory experiments. The system consists of a stainless steel pressure cylinder (1.2 m long, 30 cm ID, 4000m rated) that is deployed as a free vehicle. The organism is captured at depth with a batied hook which draws the fish inside. A pressure-retaining door is sealed and a messenger float is released, which floats to the surface. The trap is recovered by sending an acoustic signal to the system which will release its anchor weight and float to the surface . Upon recovery and transfer of the system to the laboratory, high-pressure pumps maintain a flow of seawater and a pressure accumulator and regulator system controls pressure within the trap. Internal instrumentation includes a circulating pump, oxygen optode, and low light camera. The goal is to maintain fishes for up to 30 days to monitor their respiration rates and behavioral response to varying levels of CO2 exposure.

The trap has been developed, tested and deployed at sea four times. This system has proven to self-seal at depth and return to the surface with 95+% of the in situ pressure. We have successfully captured a deep-sea fish, *Coryphaenoides acrolepis*, returned it alive to the shore-based laboratory, and measured its oxygen consumption rate. A scholarly publication describing this system is in preparation.

Benthic Respiration System

The upgraded benthic respiration system will allow injection of acid to mimic the effects of carbon dioxide sequestration, and will be completed in Fall 2004. We will then

begin deployments of the system, altering seawater chemistry in the chambers and measuring changes in oxygen uptake and carbon remineralization, if any.

Chilled, gas-controlled aquarium system

We have nearly completed the design and assembly of a highly sopohisticated aquarium system that will allow us to control closely the gas concentrations and temperature of 3 aquarium systems. Using this system, we intend to hold deep-sea animals (from depths to ~1500m) for extended periods (months) to evaluate changes in growth and potentially reproductive effort that are associated with various levels of dissolved CO2. These systems will also regulate water for respiration measurements on animals using the respiration system we've developed for this project. The focus of our investigations of the CO2 sensitivities of marine animals is shifting from field experiments to laboratory studies. This aquarium system, funded by MBARI and DoE, will play a large role in those studies.

National and International Conferences

Both Barry and Brewer have continued to be involved in carbon management issues at national and international levels. Brewer is a lead author on the IPCC chapter under development concerning climate change and ocean carbon sequestration. Barry is a contributing author on this report. Each has presented numerous papers and seminars at international meetings concerning ocean carbon sequestration.

Scholarly Publications (* indicates paper appended at end of final report)

*Barry, J.P., Kurt R. Buck, Chris F. Lovera, Linda Kuhnz, Patrick J. Whaling, Edward T. Peltzer, Peter Walz, and Peter G. Brewer (2004). Effects of Direct Ocean CO2 Injection on Deep-Sea Meiofauna (in press, Journal of Oceanology).

*Carman, K.R., Thistle, D., Fleeger, J., Barry, J.P. (2004). The influence of introduced CO2 on Deep-Sea metazoan meiofauna (in press, Journal of Oceanography).

*Barry, J.P., Seibel, B.A., Drazen, J.C., Tamburri, M.N., Buck, K.R., Lovera, C., Kuhnz, L., Peltzer, E.T., Osborn, K., Whaling, P.J, Walz, P., Brewer, P.G. (2003). Deep-sea field experiments on the biological impacts of direct deep-sea CO2 injection. Proceedings of the Second Annual Conference on Carbon Sequestration, May 5-8, 2003, Alexandria, VA.

Thistle, D., Carman, K.R., Sedlacek, L., Brewer, P.G., Fleeger, J.W., Barry, J.P. Deep-ocean experimental tests of the sensitivity of sediment-dwelling animals to imposed CO_2 gradients. (revised ms submitted to Marine Ecology Progress Series).

Barry, J.P., Drazen, J., Seibel, B., Tamburri, M., Buck, K., Lovera, C., Kuhnz, L., Whaling, P.J., (in prep.). Biological Responses of Deep-sea organisms to direct CO2 injection. (manuscript in preparation for submission to J. Geophysical Research for special issue of proceedings from the SCOR/IOC Symposium on "The Ocean in a High CO2 World", Paris, France 2004)

Barry, J.P., Seibel, B.A., Drazen, J.C., Tamburri, M.N., Buck, K.R., Lovera, C., Kuhnz, L., Osborn, K., Whaling, P.J. Biological consequences of deep-sea CO_2 sequestration (ms in revision for resubmission).

Drazen, J.C., Bird, L., Barry, J.P. A deep-sea, pressurized, fish trap respirometer for studies of the physiology of abyssal fishes. (manuscript in preparation for submission to Limnology & Oceanography).

Abstracts

Barry, J.P., Seibel, B., Lovera, C. Deep-sea field studies on the biological consequences of direct ocean CO2 sequestration. Eos Trans. AGU, 82(47), Fall Meet. Suppl., Abstract U32B-09, (2001)

Barry, J., Seibel, B., Drazen, J., Tamburri, M., Lovera, C., Brewer, P. (2002). Field experiments on direct ocean CO2 sequestration: the response of deep-sea faunal assemblages to CO2 injection at 3200 m off Central California. Eos Trans. AGU, 83, Spring Meet. Suppl., Abstract OS51F-02

Barry, J.P., J.C. Drazen, K.R. Buck, B.A. Seibel, M.N. Tamburri, C. Lovera and L. Kuhnz. Field experiments on the biological impacts of deep-sea Co2 injection. Tenth International Deep-sea Biology Symposium

Thistle, D., K.R. Carman, L. Sedlacek, J.P. Barry, P.G. Brewer and J.W. Fleeger. Consequences for the deep-sea fauna of injection of liquid carbon dioxide: preliminary results. Tenth International Deep-sea Biology Symposium

Drazen, J.C., Bird, L. and Barry, J.P. Development of a fish trap respirometer for studies of the physiology of deep-sea fishes. Tenth International Deep-sea Biology Symposium

TITLE: The Effects of Direct Ocean CO_2 Injection on Deep-Sea Meiofauna

AUTHORS:

James P. Barry (barry@mbari.org), Kurt. R. Buck, Chris Lovera, Linda Kuhnz, Patrick J.

Whaling, Edward. T. Peltzer, Peter Walz, Peter.G. Brewer

Monterey Bay Aquarium Research Institute, 7700 Sandholdt Road, Moss Landing, CA 95039

RUNNING TITLE
Effects of ocean CO_2 injection

ABSTRACT

Purposeful deep-sea carbon dioxide sequestration by direct injection of liquid CO_2 into the deep water of the ocean has the potential to mitigate the rapid rise in atmospheric levels of greenhouse gases. One issue of concern for this carbon sequestration option is the impact of changes in seawater chemistry caused by CO_2 injection on deep-sea ecosystems. The effects of deep-sea carbon dioxide injection on infaunal deep-sea sea organisms were evaluated during a field experiment in 3600 m depth off California, in which liquid CO_2 were released on the seafloor. Exposure to the dissolution plume emanating from the liquid CO_2 resulted in high rates of mortality for flagellates, amoebae, and nematodes inhabiting sediments in close proximity to sites of CO_2 release. Results from this study indicate that the large changes in seawater chemistry (i.e. pH reductions of ~0.5-1.0 pH units) near CO_2 release sites will cause high mortality rates for nearby infaunal deep-sea communities.

INTRODUCTION

Warming of 0.75 ^{o}C over the Earth during the last century (Mann *et al.*, 1999) has been accompanied by broad changes in marine and terrestrial ecosystems (Parmesan and Yohe, 2003; Root *et al.*, 2003), and is thought to be associated with the simultaneous rapid increase in atmospheric greenhouse gas concentrations, driven by emissions from the burning of fossil fuels. Earth's climate is expected to warm even more rapidly during this century, as global CO_2 emissions increase from present rates near 7 to 15 $GtCy^{-1}$ or more by 2050 (Marland *et al.*, 2001). Estimates of warming expected through the 21st century vary among models, but all are responsive to levels of carbon dioxide in the atmosphere.

Direct injection of CO_2 into the ocean was suggested over 25 years ago (Marchetti, 1977) as one of several carbon sequestration alternatives to offset the accelerating rise in anthropogenic greenhouse gases (Reichle et al, 1999; Brewer *et al.*, 1999). Sequestration would be accomplished by injecting carbon dioxide stripped from the flue gases of fuel-burning power plants into the bottom waters (~3000 m) of the deep-sea, where the circulation time of the world ocean would prevent CO_2 out-gassing to the

atmosphere for centuries, thereby mitigating the peak atmospheric CO_2 levels expected during the next 200-300 years.

To be effective, an ocean CO_2 injection program would require that large quantities of CO_2 (i.e. billions of tons of carbon) be injected into the deep waters of the ocean. Dissolution of the liquid CO_2 into seawater will elevate CO_2 levels (hypercapnia) and, through a response of the carbonate buffering system of seawater, reduce its pH. Depending on the period and volume of injection, an ocean carbon sequestration program could eventually result in pH reduction of possibly up to tenths of pH units for the bottom waters of the entire world ocean. Acidification near sites of CO_2 injection would be far more severe, with pH values close to 4.0 at the seawater / CO_2 interface, and shifts of 1 unit or greater over meters to potentially 10s to 100s of kilometers.

Immersion in CO_2-laden, acidic seawater from CO_2 injection poses physiological challenges to marine animals that respond by tolerance, compensation, or death. Responses are based on physiological adaptation of species that have evolved to tolerate the range of natural environmental variability encountered. Animals that evolved in highly stable conditions typical of deep-ocean waters are, in general, more sensitive to a variety of environmental perturbations than shallow-water animals, including those associated with CO_2 injection (Seibel and Walsh, 2003). The main CO_2-related stresses can include acidosis of intra- and extra-cellular fluids, requiring pH compensation and inducing respiratory stress, and metabolic suppression, associated with hypercapnia (Pörtner and Reipschläger, 1996). Changes in ocean pH caused by direct sequestration or air/sea exchange that fall within the range of normal environmental variation are expected to be less stressful than more extreme perturbations. Over the world ocean, seawater pH varies today from ~7.3 to ~8.5, (www.nodc.noaa.gov), and differs among ocean basins. pH varies most in the upper ocean; the mean (SD) pH in depths <1000 m for the Atlantic and North Pacific Oceans are 8.2 (0.15) and 7.9 (0.22), respectively, representing variation of 0.6 and 0.9 pH units). Deep-sea environments are less variable; pH between 3000-4000 m for these areas is 8.0 (0.02) and 7.8 (0.05), variation of 0.1 and 0.2 pH units. Individuals and populations are likely to experience even less natural pH variability.

Ecological impacts resulting from physiological stress during exposure to hypercapnic, low pH waters produced through CO_2 injection are an important concern regarding the role, if any, that ocean sequestration should play in a national or global carbon management strategy. Changes in pH caused by CO_2 injection are expected to exceed, in some cases by a large margin, the natural range of pH variability encountered by deep-sea organisms. In addition, the physiological literature on deep-sea animals suggests that they are much more sensitive to CO_2 related stresses than their shallow-water counterparts (Seibel and Walsh, 2003).

Nor are the ecological impacts of elevated oceanic CO_2 levels limited to those associated with a deep-sea CO_2 sequestration program. Air-sea gas exchange quickly equalizes CO_2 levels in the atmosphere and surface waters of the ocean, and has led to a rise in ocean CO_2 levels since the Industrial Revolution (Keeling and Whorf, 2002; Barnola *et al.*, 2003), which will continue in the future (Marland *et al.*, 2001). Roughly $1/3^{rd}$ of current fossil fuel CO_2 emissions (~7 $GtCO_2y^{-1}$) enter the sea surface through air-sea exchange (Houghton *et al.*, 1990; McNeil et al, 2003), and have already acidified the upper ocean by–0.1 pH units (Sabine *et al.*, 2002). Continued acidification of the surface

ocean (-0.3 pH units by 2100; Haugan and Drange, 1992; Drange *et al.*, 2001; Harvey, 2003) may place coral reefs and other shallow marine ecosystems in peril (Kleypas et al, 1999; Knowlton, 2001).

Together, the physiological challenges posed by hypercapnia and acidification of the surface ocean or in the deep-sea by direct CO_2 injection, elevate the importance of understanding the ecosystem consequences of these global perturbations of ocean chemistry. Ocean sequestration would reduce atmospheric emissions, but would add to the accumulating burden of fossil fuel CO_2 in the ocean. And while "dangerous anthropogenic interference" with the climate system has been debated widely, there has been little or no consideration of acceptable levels of anthropogenic change in ocean CO_2 levels. Thus, although direct deep-sea CO_2 injection is technically feasible (IPCC, 2001), the environmental consequences of large-scale CO_2 sequestration remain unknown and may be substantial (Seibel and Walsh, 2003). In view of the potential for significant changes in ocean pH, due either to continued invasion of anthropogenic CO_2 in the ocean surface (Caldeira *et al.*, 2003), or to direct sequestration of CO_2 in the deep ocean, research concerning the biological and ecological impacts of elevated CO_2 on marine biota is a high priority. In addition, comparison of the sensitivities of deep and shallow-living marine biota to elevated CO_2 levels should receive considerable attention prior to initiating a direct ocean CO_2 injection as a carbon management strategy. Here we present the initial results of *in situ* deep-sea CO_2 release experiments designed to evaluate the sensitivity of sediment-dwelling deep-sea meiofauna to CO_2-rich, low pH seawater plumes emanating from deep-sea CO_2 pools.

METHODS

We measured the survival of deep-sea infaunal meiofauna to direct deep-sea CO_2 injection during an *in situ* experiment during June – July, 2001, in which organisms were exposed to the CO_2-rich dissolution plume from pools of liquid CO_2 released into PVC "corrals" on the seafloor. Our experiments were designed to investigate the potential effects of direct ocean CO_2 sequestration and develop deep-sea experimental techniques for controlled ecosystem CO_2 enrichment (e.g. DeLucia *et al.*, 1999).

The study was performed at the base of the continental rise at 3600 m depth, 85 km west of Moss Landing, California (36^o 42' 33.4" N, 123^o 31' 22.0"W). This site is a flat, soft sediment environment with little relief at the base of the continental slope (Fig. 1). The local megafaunal assemblage is typical of abyssal deep-sea communities in the eastern Pacific, with moderate densities of macrourid (*Coryphaenoides armatus*) and zoarcid fishes (*Pachychara* sp.), octopus (*Benthoctopus* sp.), echinoderms (holothurians – *Peniogone* sp., *Abyssocucumis abyssorum, Scotoplanes globosa*), echinoids (*Cystechinus loveni, Aporocidaris milleri*), gastropod molluscs (*Mohina vernalis*), ophiuroids (unknown sp.), and a variety of less abundance species. The infaunal macrofaunal assemblage at this site is dominated by tube-dwelling ampeliscid amphipods (*Haploops lodo*), but also includes numerous other crustacean, polychaeta, mollusca, and cnidarians. Sediment-dwelling meiofauna are abundant, and dominated by nematodes, flagellates, and amoebae, with lesser densities of ciliates, foraminifera, and other groups.

Experimental CO_2 Treatments

Three small (48 cm diameter x 15 cm high) PVC rings ("corrals") placed on the seafloor were filled with ~20 liters of liquid CO_2 using an ROV-mounted CO_2-release system (Brewer *et al.*, 1999) developed by the Monterey Bay Aquarium Research Institute (Fig. 2). Liquid CO_2 is slightly heavier than seawater at this depth, and dissolves slowly into the overlying seawater, producing a CO_2-rich, low-pH dissolution plume that is carried downstream in the prevailing current. Because it is rich in CO_2, the dissolution plume is also slightly heavier than seawater, and flows downstream across the seafloor as a dense plume, thereby exposing sediment-dwelling infauna (especially those inhabiting the surface) to seawater chemistry expected with a large scale CO_2 sequestration program. Release of liquid CO_2 into pools on the seafloor, selected here because it is experimentally tractable, is only one of many variants of proposed ocean CO_2 injection strategies (Haugan and Drange, 1992; Drange et al, 2001; Caldeira and Rau, 2000).

The PVC corrals were filled with liquid CO_2 in late June, 2001, refilled 2 weeks later, and the experiment was terminated in late July, 2001. The liquid CO_2 persisted in liquid form, with a hydrate skin, throughout the study, and we did not observe large volume changes from massive hydrate formation (Brewer *et al.*, 1999).

Three additional PVC corrals were placed on the seafloor nearby (~30 to 50 m away) to serve as control corrals. Although these corrals were not filled with liquid CO_2, samples were collected near these corrals in the same manner used for experimental corrals.

Meiofaunal Assemblage Samples

Meiofaunal organisms were sampled using sediment cores, which were collected prior (June,, 2001) to dispensing the CO_2 and after (July, 2001) 35d exposure, from the area immediately adjacent to both the CO_2 and control corrals. Three cores (7.5 cm diameter x 20 cm deep) were collected near (<1 m from the corral) each CO_2 corral and each control corral, from which subsamples were collected by extracting the top 1 cm of the sediment from a portion of the core using a 60 cc syringe with the Luer end removed. Subsamples were preserved immediately in a 2% glutaraldehyde solution in 0.1 M cacodylate buffered, filtered seawater. A Percoll density-gradient centrifugation technique was used to extract meiofauna from aliquots of the subsampled sediment. Details of this technique are discussed in Buck *et al.* (2000). Counts and biovolume measurements of meiofauna stained with the fluorochrome DAPI were made using epifluorescence microscopy. Estimates of abundance in each core represented the total biovolume estimated from the sample. Tissue condition (live / dead) was assessed for a subsample of nematode individuals collected. Individual nematodes stained with DAPI were inspected under epifluorescence microscopy for the presence (live) or absence (dead) of intact cell nuclei.

Physical Measurements

Changes in seawater chemistry caused by the dissolution plume were measured using SeaBird pH sensors attached to a SeaBird model 16 CTD. The pH probes were

positioned 3-5 cm above the seafloor and located 1 m from CO_2 corrals. Seawater pH, as well as temperature, conductivity, and depth, was recorded at 10 minute intervals throughout the experiment to determine the intensity and duration of plume exposure near CO_2 corrals.

The direction and speed of near-bottom currents at the site were measured using an acoustic doppler current meter (ADCP) deployed 2 m above the bottom.. This ADCP measured current speed at 10-minute intervals for bins 4 to 50 m above the seafloor. The current speed 10 m above the bottom was used to characterize the direction and speed of local currents.

Variation in pH and current speed were compared using spectral analyses to determine the dominant period of variation for the flow and pH changes near the corrals. Progressive vector diagrams were also plotted to determine the short (i.e. days) to medium (weeks) pattern of current flow.

Statistical Analyses

The abundance of each meiofaunal taxon was compared between treatment (CO_2) and control groups by ANOVA at the beginning (prior to CO_2 release) and end of the experiment (after 1 month of exposure to CO_2). Because replicate cores used to estimate meiofaunal abundance were taken near each corral, these data were analyzed using a nested ANOVA design (corrals nested within treatments; Zar, 1999). Prior to analysis by ANOVA, variances of biovolume data for each meiofaunal taxon were compared between groups (treatment & control) using an F test (Zar, 1999). Square-root transformations were applied to biovolume data for taxa (Amoebae, Nematodes) with significantly ($p<0.05$) different variances between treatments, after which, F-tests were non-significant.

The percentage of individuals that were dead for nematodes was compared between CO_2 and control treatments at the end of the experiment using a nested ANOVA, after applying an arcsine transformation to the percentage data. An F-test was used to evaluate heteroscedasticity among groups.

RESULTS

Upon returning to the 3600 m CO_2 release experiment site with the ROV, our initial observations determined that much of the CO_2 released had dissolved, although a small amount of liquid CO_2 or CO_2 hydrate, or both, remained n some corrals. The sediment was disturbed in some corrals, apparently due to "frost heave" by the CO_2 hydrate, but the sediment surrounding the corrals, where samples were collected for meiofaunal analyses, was undisturbed.

The pH of seawater near corrals containing liquid CO_2 was highly variable during the experiment (Fig. 3), due to continued dissolution of the liquid CO_2 and shifting direction of bottom currents. This resulted in large peak pH perturbations ($\Delta pH \sim -1.5$ units were observed within 1 m of the CO_2 corrals) during periods when currents were flowing over pH sensors, and little or no pH change when currents carried the CO_2 dissolution plume away from pH sensors. Excursions in pH greater than 1 unit were rare (<5% of the time) even near CO_2 pools, and reductions of ≥ -0.2 units occurred only 25% of the time. Due to failure of a pH sensor placed near a control corral located 40 to 80 m

from the CO_2 corrals, perturbations to seawater chemistry were not measured near these control corrals. However, it is expected that little to no variation in pH occurred near control corrals, based on subsequent measurements of pH versus distance that showed little to no pH perturbation at distances of ~50 m from CO_2 corrals.

Near-bottom currents were generally sluggish, but highly variable in direction (Fig. 4), as expected from the observed pH variability. Currents averaged 4.4 $cm \cdot s^{-1}$, with net transport to the SE at 1.7 $cm \cdot s^{-1}$, and rotated clockwise throughout the day over inertial periods, reversing direction about every 12 hours. Fourier analysis of currents and variation in pH values each indicated strong periodicity near 12.4 h, associated with the major semidiurnal lunar tidal constituent (M2). In effect, the inertial and tidal periodicity of bottom currents caused the seafloor in each direction around a CO_2 corral to be bathed in CO_2-rich waters (ΔpH –1.0 or greater) for ~30 minute periods, twice per day. The rotary character of currents then shifted the dissolution plume progressively to the right, eventually bathing the entire seafloor around the corral with CO_2-rich seawater. When the plume was not flowing over one section of the seafloor surrounding the corral, it was bathed in normal seawater.

The population density or tissue condition of sediment-dwelling meiofauna declined after exposure to intense CO_2 stress, indicating that survival rates were low. Prior to CO_2 injection, no differences in the biovolume of any meiofauna taxon sampled (flagellates, amoebae, allogromiid foraminiferans, ciliates, and nematodes) were detected in samples collected near control corrals and CO_2 corrals ($p>0.05$ for nested ANOVA tests). After ~one month intermittent exposure to the dissolution plume with pH perturbations up to –1.7 pH units, we detected significant differences in the biovolumes of the two dominant groups (Fig. 5). Flagellates increased slightly in biovolume near control corrals, but declined near CO_2 corrals, leading to a large difference in biovolume ($F=12.0$, $p<0.003$) by the end of the experiment. Amoebae exhibited a similar pattern of divergence in biovolume between control and CO_2 corrals. By the end of the experiment, control corral locations had a higher ($F=6.7$, $p<0.02$) biovolume of amoebae than CO_2 corral sites. Reduced densities of both groups probably reflect the death and nearly complete decay of individuals impacted by CO_2 exposure. Although decay rates are unknown, observations of degradation rates for much larger macrofaunal amphipods from this site indicated that significant tissue loss occurs over the month-long experiment. In view of their much smaller size, it is likely that small meiofaunal taxa may degrade completely during a similar period.

Unlike flagellates and amoebae, ciliates and allogromiid foraminifera did not decrease in biovolume during exposure to the CO_2 dissolution plume. Because these taxa are relatively low in abundance, however, our sampling design may be inadequate to detect small changes in abundance or biovolume.

Nematodes, the most prevalent meiofaunal taxon inhabiting the sediment, also declined significantly in biovolume near CO_2 pools during the experiment ($F=7.9$, $p<0.02$), and even higher rates of mortality were indicated from analyses of tissue condition. Detailed inspection of individuals stained with DAPI under epifluorescence microscopy (indicating the presence / absence of intact cell nuclei; Fig. 6), indicated that the most (63.0%, SE=12.1) individuals collected near CO_2 corrals had died prior to preservation. The percentage of decaying nematodes near control corrals (16.4%,

SE=5.8) was significantly (F=5.9, $p<0.02$) lower than near CO_2 corrals. These metazoans likely require longer decay times due to their chitinous cuticle.

DISCUSSION

These results provide a glimpse of the types of ecological impacts to deep-sea benthos that are likely to occur near sites of CO_2 injection during a direct ocean CO_2 injection program. In areas where CO_2 injection results in relatively large perturbations to seawater chemistry (i.e. $\Delta pH > -1.0$ units), even for short periods as observed in these experiments, it is likely that meiofaunal taxa will exhibit high rates of mortality. All abundant meiofauna experienced high mortality near CO_2 pools, shown by reductions in abundance or biovolume, or higher percentages of dead individuals at the end of the experiment.

Although we were unable to perform any physiological measurements on these organisms, it is very likely that acidosis from immersion in hypercapnic waters exerted lethal physiological stresses. Meiofauna, including the amoebae, euglenoid flagellates, and ciliates studied here, as well as relatively primitive metazoans (nematodes), lack complex respiratory or circulatory systems that could be impaired by acidosis, but their ability to maintain normal physiological function is, nevertheless, linked to acid-base balance. CO_2-related acidosis, an imbalance in the optimal acid-base status of inter- and intracellular fluids, impairs physiological function in several ways, including changes in the activity of key enzymes and enzyme-protein interactions that affect even the most basic metabolic functions (Hochachka and Somero, 2002). Some pH compensation, via the buffering capacity of intracellular fluids, coupled with active proton-equivalent ion transport may restore normal internal pH for some degree of environmental pH perturbation (Seibel and Walsh, 2003). Failure to maintain optimal pH levels, however, will be lethal, or require a reduction in energy allocated to activity, growth, or reproduction. Physiological stresses caused by hypercapnia and acidosis often act together due to the bicarbonate buffering, and the separate effects of these remain somewhat obscure.

Our results support the expectation (Seibel and Walsh, 2003) that deep-sea species may be sensitive to pH stress that will accompany a direct CO_2 injection sequestration program. The perturbations to pH near our CO_2 corrals was large compared to that expected over large regions of the oceans during a CO_2 sequestration program, but also have relevance for smaller pH perturbations that will occur distant from CO_2 release sites. CO_2-related physiological stress, if not lethal as observed in this study, will convey higher "costs of living" through the energetic costs of acid / base balance, restricted aerobic capacity, and inhibition of protein synthesis. These costs are expected to be highest for deep-sea organisms, which typically have limited metabolic capacity, as well as narrow ranges of tolerance to environmental variation. Physiological responses of individuals to increased CO_2 levels may translate into changes in the survival, growth, and reproduction rates of populations, and shifts in the ecosystem dynamics of deep-sea communities.

The integrated impacts of a direct CO_2 sequestration program on deep-sea ecosystems will depend on the depths, locations, method of injection, and certainly the volume of CO_2 injected. If liquid CO_2 is released undiluted, it will produce a CO_2

dissolution plume near ~pH4 in the boundary layer at the release site. The plume will disperse and mix downcurrent, finally approaching background levels a distance determined by several factors, including current speed, injection method, total CO_2 injected, rate of injection, and other factors. Animals in close proximity to disposal sites are at risk of high mortality rates, as observed for benthic meiofauna in this study. Plume effects over larger scales may be estimated coarsely from expected pH fields. For example, if 0.25 to 4 $GtCy^{-1}$ as CO_2 is injected for 100 y beneath 3000 m and disperses worldwide (see methods), the pH of the deep-waters of the entire world ocean will shift by –0.02 to –0.3 units. Even larger pH perturbations will occur in mixing zones that may extend 10s to 100s of km around disposal sites (Haugan and Drange, 1992; Caldeira and Wickett, 2002).

Direct deep-sea CO_2 sequestration could mitigate the anthropogenic rise in atmospheric pCO_2 that wi program should include careful consideration of the balance between the lesser of two evils – the unabated effects of climate warming or acidification, or both, on terrestrial and shallow marine ecosystems, or damage to deep-sea ecosystems by CO_2 sequestration. Ongoing research should provide guidance concerning the risks of direct CO_2 injection, and may mandate other methods or more environmentally benign CO_2 sequestration approaches (e.g. accelerated carbonate dissolution; Caldeira and Rau, 2000). Clearly, an ocean carbon sequestration program will be successful only if its intended benefits – a stabilization of atmospheric CO_2 and mitigation of climate warming consequences for terrestrial and shallow water ocean systems, outweigh its liabilities – energy expended on sequestration and damage to deep-sea ecosystems. Lacking presently is sufficient information on both sides of this balance.

KEYWORDS:
CO_2 sequestration, , meiofauna, ecological impacts, deep-sea biology, hypercapnia

REFERENCES

Barnola, J.-M., D. Raynaud, C. Lorius, & N.I. Barkov (2003). Historical CO_2 record from the Vostok ice core. In *Trends: A Compendium of Data on Global Change*. Carbon Dioxide Information Analysis Center, Oak Ridge National Laboratory, U.S. Department of Energy, Oak Ridge, Tenn., U.S.A

Brewer, P.G., G. Friederich, E.T. Peltzer, & F.M. Orr Jr. (1999) Direct experiments on the ocean disposal of fossil fuel CO_2. *Science* 284, 943-945

Buck, K.R., J.P. Barry, and, A.G.B. Simpson (2000); Monterey Bay cold seep biota: euglenozoa with chemoautotrophic bacterial epibionts. Europe. J. Protistology, 35, 117-126.

Caldeira, K. & M.E. Wickett, (2002). Comparing pH impacts of oceanic CO_2 injection and atmospheric CO_2 release. *Eos Trans. AGU,* 83(1), Spring Meet. Suppl., Abstract OS51F-01

Caldeira, K., & G.H. Rau (2000). Accelerating carbonate dissolution to sequester carbon dioxide in the ocean: Geochemical implications. *Geophys. Res. Let*. 27, 225-228.

Caldeira, K., A.K. Jain, & M.I. Hoffert (2003) Climate sensitivity uncertainty and the need for energy without CO_2 emission. *Science*, 299, 2052-2054.

DeLucia, E. H., J.G. Hamilton, S.L. Naidu, R.B. Thomas, J.A. Andrews, A. Finzi, M. Lavine, R. Matalama, J.E. Mohan, G.R. Hendrey, and W.H. Schlesinger. (1999) Net primary production of a forest ecosystem with experimental CO_2 enrichment. *Science*, 284, 1177- 1179.

Drange, H., G. Alendal, & O.M. Johannessen, (2001) Ocean release of fossil fuel CO_2: A case study. *Geophys. Res. Lett*. 28, 2637-2640.

Harvey, L.D.D. (2003) Impact of deep-ocean carbon sequestration on atmospheric CO_2 and on surface-water chemistry. *Geophys. Res. Lett.* 30, 1237-1240.

Haugan, P.M., & H. Drange, (1992) Sequestration of CO_2 in the deep ocean by shallow injection. *Nature* 357, 318-320.

Hochachka, P.W. and G.N. Somero (2002). *Biochemical Adaptation: mechanism and process in physiological evolution.* Oxford University Press, Oxford, 466 pp.

Houghton, J.T. *et al.*, (1990) *Climate Change: The IPCC Scientific assessment. Intergovernmental Panel on Climate Change*, Cambridge University Press

IPCC. (2001) In *Climate Change 2001: The Scientific Basis* (eds Houghton, J.T., *et al.*, Cambridge University Press, Cambridge, 896 pp.

Keeling, C.D. & T.P. Whorf, (2002) Atmospheric CO_2 records from sites in the SIO air sampling network. In *Trends: A Compendium of Data on Global Change*. Carbon Dioxide Information Analysis Center, Oak Ridge National Laboratory, U.S. Department of Energy, Oak Ridge, Tenn., U.S.A.

Kleypas, J.A.., R.W. Buddemeier, D. Archer, J.-P. Gattuso, C. Langdon, & B.N. Opdyke (1999). Geochemical consequences of increased atmospheric carbon dioxide on coral reefs. *Science* 284, 118-120.

Knowlton, N. (2001). The future of coral reefs. *Proc. Nat. Acad. Sci.* 98, 5419-5425

Mann, M.E., R.S. Bradley, & M.K. Hughes (1999). Northern hemisphere temperatures during the past millennium: interferences, uncertainties, and limitations. *Geophys. Res. Lett*. 26, 759-762

Marchetti, C. (1977) On geoengineering and the CO_2 problem. *Climate Change* 1, 59-69.

Marland, G., T.A. Boden, & R.J. Andres, (2001) Global, Regional, and National CO_2 Emissions. In *Trends: A Compendium of Data on Global Change*. Carbon Dioxide Information Analysis Center, Oak Ridge National Laboratory, U.S. Department of Energy, http://cdiac.esd.ornl.gov/trends/trends.htm).

McNeil, B., R.J. Matear, R.M. Key, J.L. Bullister, & J.L. Sarmiento, (2003) Anthropogenic CO_2 uptake by the ocean based on the global chlorofluorocarbon data set. *Science* 299, 235-239.

Parmesan, C. & G. Yohe, (2003) A globally coherent fingerprint of climate change impacts across natural systems. *Nature* 421, 37-42

Pörtner, H.-O. & A. Reipschläger, (1996) In, *Ocean Storage of CO_2. Environmental, Workshop 2: Environmental Impact* (eds Ormerod, B., Angel, M.) 57-81 (IEA Green house and Gas R & D Programme, Southampton Oceanography Centre, UK)

Reichle, D., J. Houghton, S. Benson, J. Clarke, F.R.. Dahlman, G. Hendrey, H. Herzog, J. Hunter-Cevera, G. Jacobs, R. Judkins, B. Kane, J. Ekmann, J. Ogden, A. Palmisano, R. Socolow, J. Stringer, T. Surles, A. Wolsky, N. Woodward, & M. York (1999) *Carbon Sequestration: Research and Development* (Office of Science, Office of Fossil Energy, U.S. Dept. of Energy

Root, T.L., J.T. Price, K.R. Hall, S.H. Schneider, C. Rosenzweig, & J.A. Pounds (2003) Fingerprints of global warming on wild animals and plants. *Nature* 421, 57-60

Sabine, C.L.,R.A. Freely, R.M. Key, J.L. Bullister, F.J. Millero, K Lee, T.-H. Peng, B. Til brook, T. Ono & C.S. Wong (2002) Distribution of anthropogenic CO_2 in the Pacific Ocean. *Global Biogeochemical Cycles* 16, 1083-1099.

Seibel, B.A. & P.J. Walsh, (2003) Biological impacts of deep-sea carbon dioxide injection inferred from indices of physiological performance. *J. Exp. Biol.* 206, 641-650

Zar, J.H., (1999) *Biostatistical analysis*, 4th edition. Prentice-Hall, Englewood Cliffs, NJ

ACKNOWLEDGEMENTS

This research was supported by MBARI (projects 200001, 200002), the U.S. Dept. of Energy, Fossil Energy Group (Grant DE-FC26-00NT40929), and the U.S. Department of Energy, Ocean Carbon Sequestration Program, Biological and Environmental Research (BER), (grant #DE-FG03-01ER63065). Deep-sea experiments would not have been possible without the excellent support of the crews of the R/V *Western Flyer* and ROV *Tiburon*.

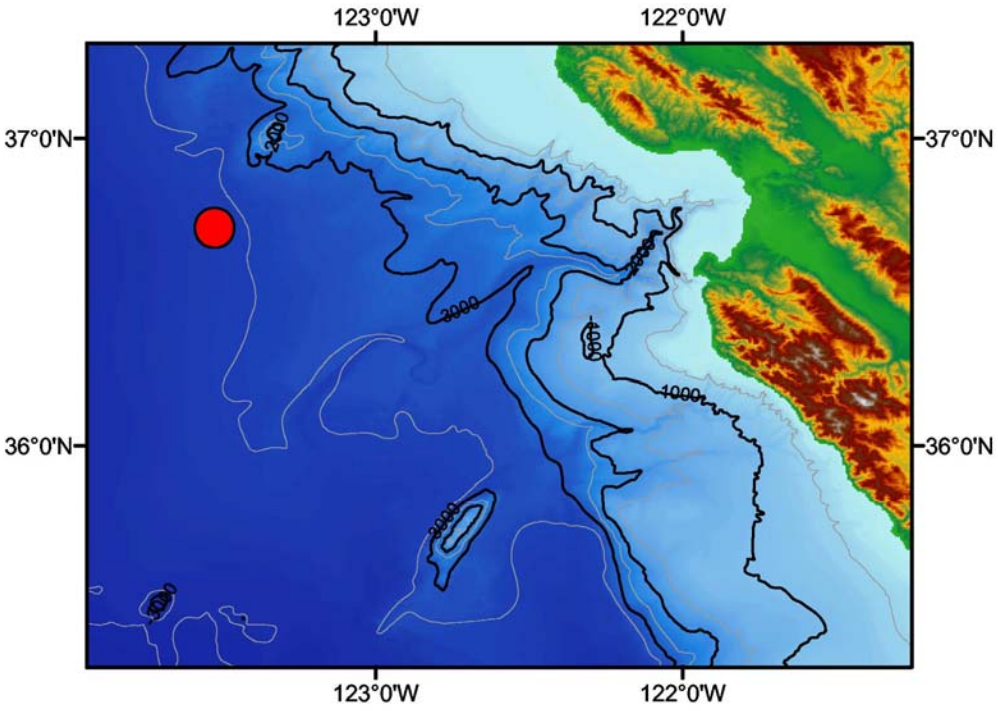

Fig. 1. Map of CO_2 Sequestration Study site, 85 nm west of Moss Landing, California. Water depth at site (red dot) is 3600 m.

Fig. 2. Photograph of CO_2 corrals during filling operations. Liquid CO_2 is visible as a clear liquid partially (1) or fully (2) filling the corrals. Some sediment has been entrained in the CO_2 inside corral 2. Some CO_2 hydrate is also visible in corral 2. By the end of the experiment, much of the CO_2 had dissolved.

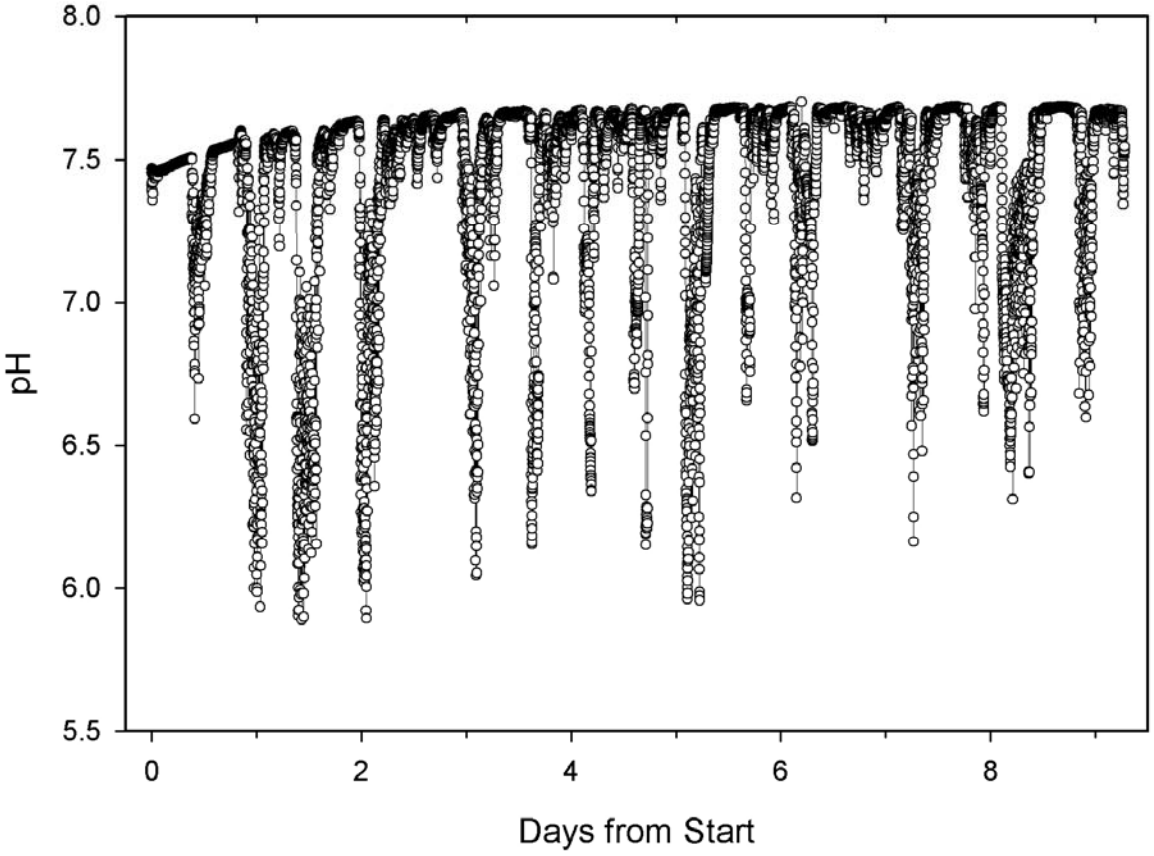

Fig. 3. pH perturbations near CO_2 corrals during CO_2 dissolution. Normal (background) pH is near 7.65 at this depth, and is reflected by the upper boundary of values recorded during the experiment. Note the large pH reductions approximately every 12 hours, which represent the advection of the dissolution plume over the pH sensor. Maximum pH shifts were near –1.7 pH units. The initially low background values (near 7.5) were due to the early equilibration of the instrument with the background deep-sea water pH, and are not due to the CO_2 dissolution plume.

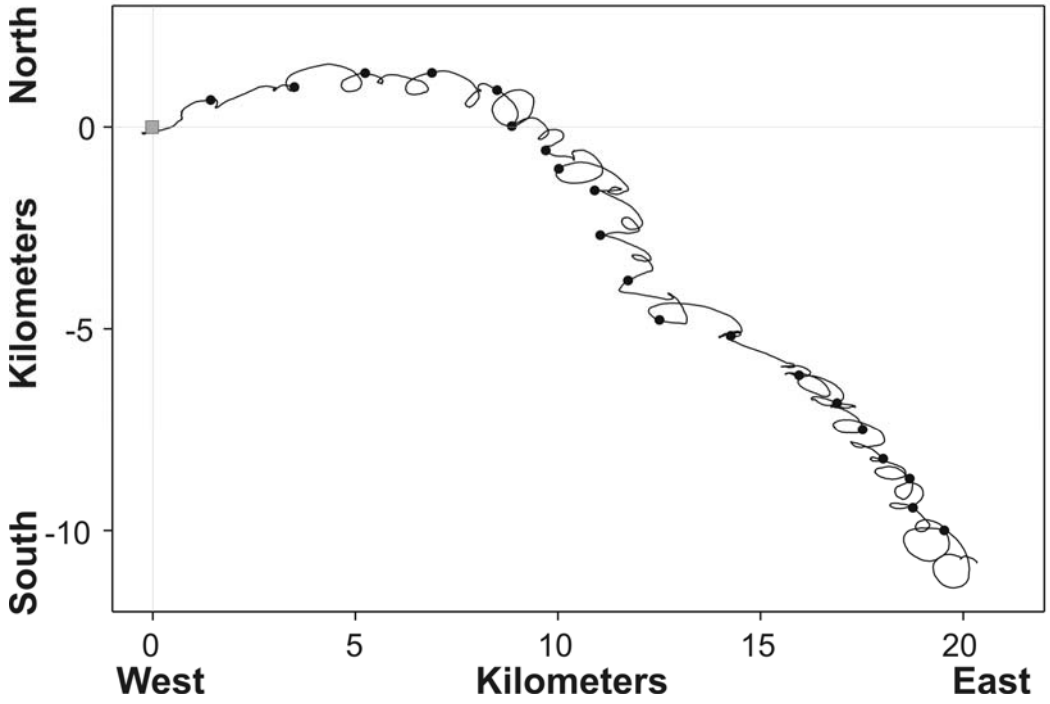

Fig. 4. Progressive vector diagram illustrating flow at 15 meters above bottom at 3600 m depth during the CO_2 experiment. The flow path of a parcel of water in the region is described by the advective transport from the starting point (gray box) to the end point (lower right corner). A black circle notes the start of each day. Note the rotary flow, which will disperse the CO_2 plume in several directions, even though the mean flow is to the SE. The major periodicity in both flow direction and speed is 12.5 hours, corresponding the semidiurnal lunar tidal constituent.

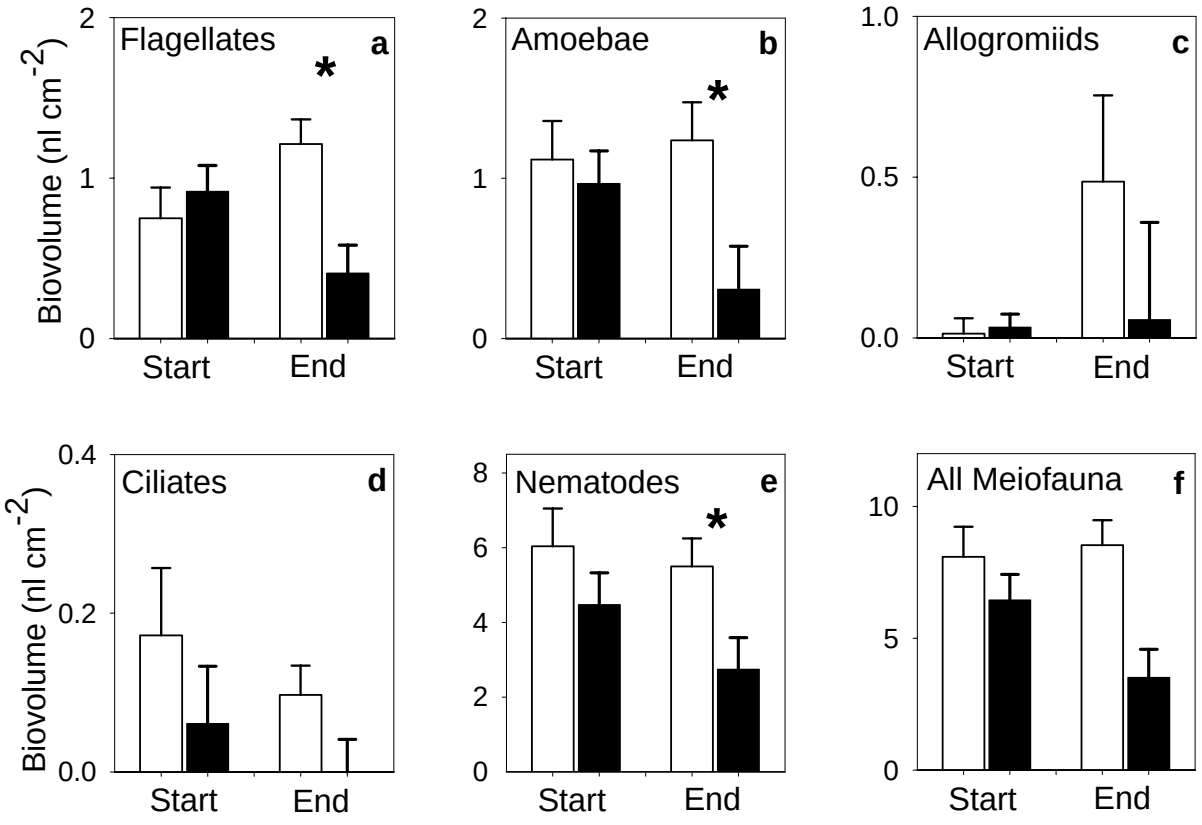

Fig. 5. Changes in abundances of meiofaunal taxa after exposure to CO_2 dissolution plume.
Open bars indicate core samples collected near control corrals. Dark bars are core samples collected near CO_2 corrals. Bars indicate mean (+ SE) of treatments from nested ANOVA analyses. Start was at the beginning of the experiment prior to CO_2 injection into CO_2 corrals. End was after 4.5 weeks of exposure. Asterisk indicates significant (nested ANOVA, $p<0.05$) different in abundance between control and CO_2 abundances.

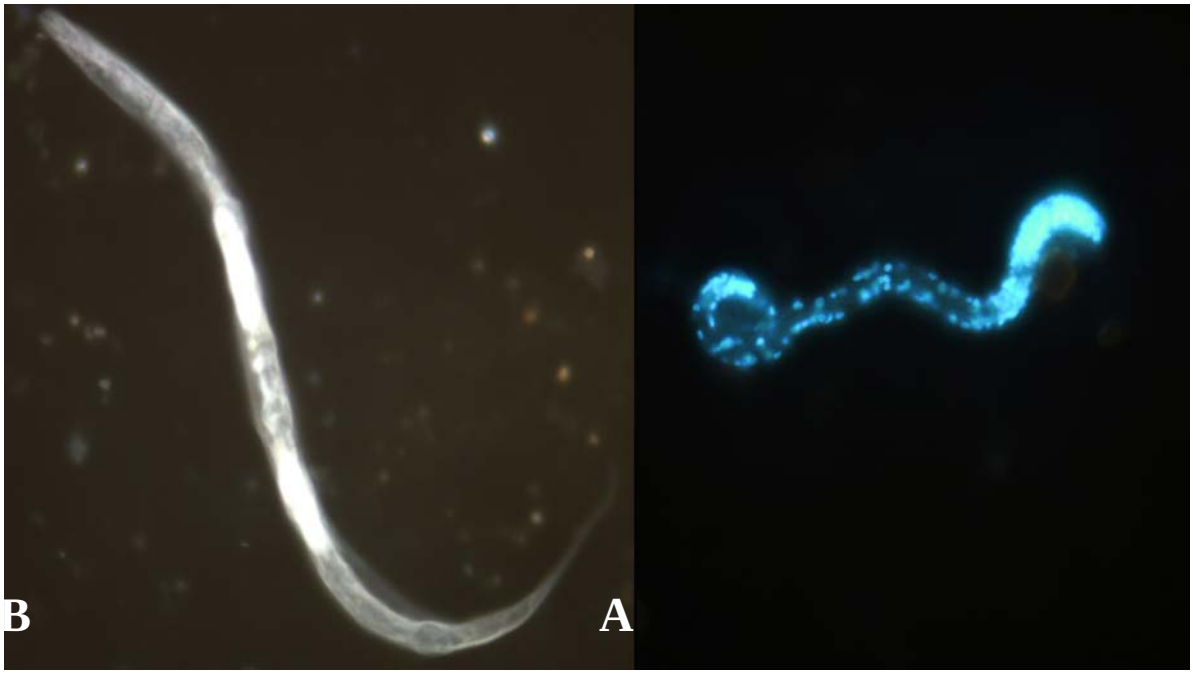

Fig. 6. Condition of nematodes exposed to CO_2 dissolution plume. A. Microscopic image of DAPI stained nematode with intact cell nuclei (light blue dots) indicating the individual was live immediately prior to preservation. B. Gray image of degrading nematode. This individual is also stained with DAPI, but exhibited no epifluorescence, and thus, no intact nuclei, indicating death prior to preservation. Individuals of this type were commonly observed near CO_2 corrals.

Deep-sea field experiments on the biological impacts of direct deep-sea CO_2 injection

J.P. Barry, B.A. Seibel, J.C. Drazen, M.N. Tamburri, K.R. Buck, C. Lovera, L. Kuhnz, E.T. Peltzer, K. Osborn, P.J. Whaling, P. Walz, P.G. Brewer

Monterey Bay Aquarium Research Institute, 7700 Sandholdt Road, Moss Landing, CA 95039

ABSTRACT

Direct injection of CO_2 into the ocean, a radical idea suggested 25 years ago (Marchetti 1977), is among several carbon sequestration alternatives under consideration to offset the accelerating rise in anthropogenic greenhouse gases (Reichle et al 1999, Brewer et al. 1999). This issue raises important questions concerning the impacts of pH changes and elevated CO_2 levels for marine ecosystems and the role, if any, ocean sequestration should play in a national or global carbon management strategy. While there is uncertainty concerning physical responses to greenhouse gas forcing (Caldeira et al 2003), there is no doubt that oceanic CO_2 levels have risen significantly (Keeling and Whorf 2002, Barnola et al. 2003) and will continue to do so (Marland et al. 2001). Roughly $1/3^{rd}$ of current fossil fuel CO_2 emissions (~7 $GtCO_2y^{-1}$) enter the sea surface through air-sea exchange (Houghton et al. 1990, McNeil et al 2003), thereby acidifying the upper ocean (Sabine et al. 2002). Continued acidification by air/sea CO_2 exchange (Haugan and Drange 1992) or direct ocean CO_2 sequestration (Drange et al. 2001, Harvey 2003) will challenge the physiological tolerances of species inhabiting both shallow (Kleypas et al. 1999, Knowlton 2001) and deep (Tamburri et al. 2000, Seibel and Walsh 2003) marine ecosystems. Here we present the initial results of *in situ* deep-sea CO_2 release experiments off Central California, showing that various deep-sea taxa are sensitive to short-term (~ 1 mo.) exposure to CO_2-rich, low pH plumes emanating from deep-sea CO_2 pools.

INTRODUCTION

Warming of 0.75 ^oC over the Earth during the last century (Mann et al. 1999) has been accompanied by broad changes in marine and terrestrial ecosystems (Parmesan and Yohe 2003, Root et al. 2003). In this century, however, Earth's climate is expected to warm more rapidly; global CO_2 emissions are expected to increase from present rates near 7 GTCy-1 to 15 GtCy-1 by 2050 (Marland et al. 2001). Simultaneously, acidification of the surface ocean (-0.3 pH units by 2100; Haugan and Drange 1992) may place coral reefs and other shallow marine ecosystems in peril (Kleypas et al 1999, Knowlton 2001). Ocean sequestration would reduce atmospheric emissions, but would add to the accumulating burden of fossil fuel CO_2 in the ocean. And while "dangerous anthropogenic interference" with climate has been debated widely, no such debate has taken place over acceptable oceanic CO_2 levels. Thus, although direct deep-sea CO_2 injection is technically feasible (IPCC 2001), the environmental consequences of large-scale CO_2 sequestration remain unknown and may be substantial (Seibel and Walsh 2003).

Immersion in CO_2-laden, acidic seawater from CO_2 injection poses physiological challenges to marine animals that respond by tolerance, compensation, or death. Responses are based on physiological repertoires that have evolved over thousands of generations to tolerate the range of natural environmental variability encountered. Animals that have evolved in highly stable conditions typical of deep-ocean waters are, in general, more sensitive to a variety of environmental perturbations than shallow-water animals, including those associated with CO_2 injection (Seibel and Walsh 2003). The main CO_2-related stresses can include acidosis of intra-

and extra-cellular fluids, requiring pH compensation and inducing respiratory stress, and metabolic suppression, associated with hypercapnia (Pörtner and Reipschläger 1996). Changes in ocean pH caused by direct sequestration or air/sea exchange that fall within the range of normal environmental variation are expected to be less stressful than more extreme perturbations. Over the world ocean, seawater pH varies today from ~7.3 to ~8.5, (www.nodc.noaa.gov), and differs among ocean basins. pH varies most in the upper ocean; the mean (SD) pH in depths <1000 m for the Atlantic and North Pacific Oceans are 8.2 (0.15) and 7.9 (0.22), respectively, representing variation of 0.6 and 0.9 pH units). Deep-sea environments are less variable; pH between 3000-4000 m for these areas is 8.0 (0.02) and 7.8 (0.05), variation of 0.1 and 0.2 pH units. Individuals and populations are likely to experience even less natural pH variability.

We evaluated the biological impacts of direct CO_2 injection on deep-sea animals *in situ* during two experiments (E1, E2) exposing deep-sea animals to the dissolution plume from pools of liquid CO_2 released into PVC "corrals" on the seafloor at 3600 m depth off California (Fig. 1). Our experiments were designed to investigate the potential effects of direct ocean CO_2 sequestration and develop deep-sea experimental techniques for controlled ecosystem CO_2 enrichment (e.g. DeLucia et al. 1999). Liquid CO_2 is heavier than seawater at this depth, but dissolves slowly, producing a CO_2-rich, low-pH dissolution plume. We measured the survival of various groups of deep-sea organisms exposed to these plumes. Creation of a dissolving pool of CO_2 on the seafloor[0], selected here because it is experimentally tractable, is only one of many variants of proposed ocean CO_2 injection strategies (Haugan and Drange 1992, Drange et al 2001, Caldeira and Rau 2000).

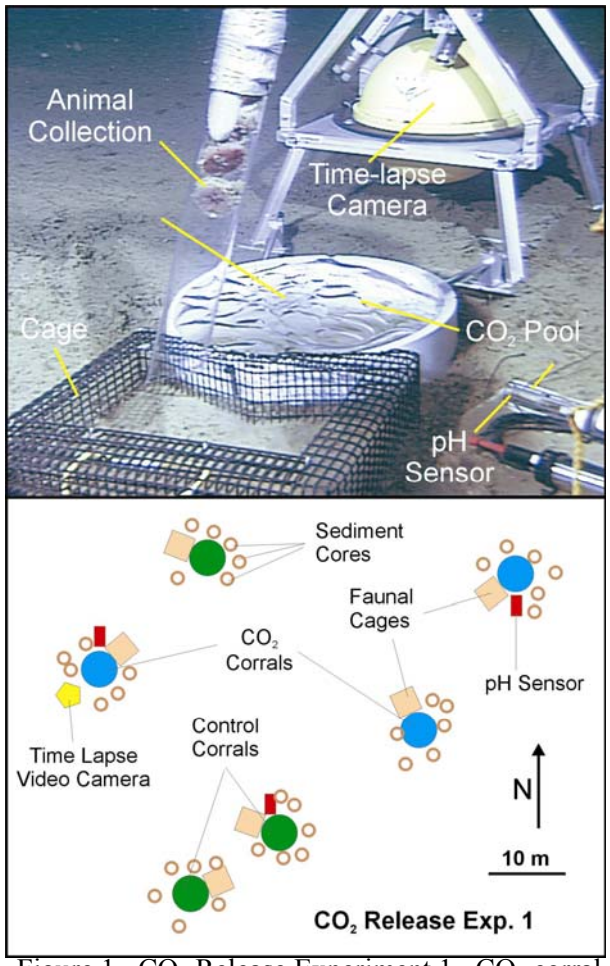

Figure 1. CO_2 Release Experiment 1. CO_2 corral filled with liquid CO_2, animal cage used to hold megafauna, pH sensor, and time-lapse video camera used in E1 (top). Sea urchins and holothurians are visible in acrylic tube, used as suction sampler to collect and deploy megafauna. Experimental layout of CO_2 release E1 at 3600 m depth shown in bottom image.

METHODS

An ROV-mounted CO_2-release system (Brewer et al. 1999) developed by the Monterey Bay Aquarium Research Institute was used to inject liquid CO_2 into PVC corrals placed on the seafloor on the continental rise in 3600 m depth, 85 nm off Moss Landing, CA (36° 42' 33.4" N, 123° 31' 22.0"W). The CO_2 persisted in liquid form, with a hydrate skin, throughout the study. We did not observe large volume changes from massive hydrate formation (Brewer et al. 1999).

In the first experiment (E1), 3 small (48 cm diameter x 15 cm high) PVC corrals were filled with ~twenty liters of liquid CO_2 (Fig. 1), and study animals were held in mesh cages (46 x

46 x 20 cm) placed nearby (<1m). The survival rates of megafauna held in cages and organisms inhabiting sediments adjacent to CO_2 corrals were compared with control groups near three empty corrals. Several individuals each of urchins (*Cystechinus* sp.) and holothurians (*Abyssocucumis* sp.) were collected from the seafloor nearby using a suction sampler and placed carefully in each mesh cage adjacent to CO_2 corrals (n=3) and control corrals (n=3). Sediment cores (7.5 cm diameter x 20 cm deep) were collected to obtain mud samples for microbial, meiofaunal, and macrofaunal counts and analyses (n=6 per corral). Sets of sediment cores were collected prior to dispensing the CO_2 and after 35d exposure. Macrofaunal samples were sieved (300 μm). Meiofaunal analyses were based on percol-gradient centrifugation technique. Microbial counts performed under epifluorescence microscopic inspection of DAPI-stained samples. Abundance, biovolume, or indices of mortality (e.g. tissue degradation) were compared among treatments at the beginning and end of the experiment.

A second experiment (E2) was similar, but used a single, larger (93 cm diameter x 30 cm high) corral containing ~75 l of liquid CO_2. Study organisms included urchins and infaunal organisms used in E1, and common fishes (eelpout, *Pachycara sp.*; rattail, *Coryphaenoides armatus*). Fishes were collected in baited traps prior to CO_2 release. Fish traps and urchin cages were positioned 1, 5, 10, and 50 m from the central CO_2 pool. Infaunal organisms were sampled from sediment cores at these distances. CO_2 in experimental corrals was replenished after ~2 weeks in each experiment to ensure continued CO_2 dissolution. Both experiments were terminated after ~1 month.

The intensity of plume exposure was estimated from pH sensors positioned 3-5 cm above the seafloor and located 1 m (E1), 5 m, and 50 m (E2) from CO_2 corrals. Time-series records of pH were obtained from 1 m away from a CO_2 pool during E1, and from 5 m, and 50 m from the central CO_2 corral during E2.

The direction and speed of near-bottom currents at the site were measured using an acoustic doppler current meter deployed 2 m above the bottom during E1. Currents 15 m above the bottom were used for analyses. Current records were not obtained during E2.

CO_2 corrals used in E1 were 15 cm high, and filled completely with liquid CO_2, leading to fairly rapid dissolution, likely due to the direct exposure of the CO_2 surface to near bottom currents. During E2, a single larger PVC corral (33 cm high x 94 cm diameter) was filled only 2/3 full, partially insulating the CO_2 surface from bottom currents. This appears to have resulted in a slower dissolution rate and perhaps smaller pH excursions around the corral.

Because all animals collected from 3600 m depths died upon ascent to the surface, mortality caused by CO_2 exposure was distinguished from death during ascent by assessing amphipod tissue condition. A rating system from 1 (intact, "recent death") to 5 (nearly entirely degraded, tissues translucent to transparent, exoskeleton fragile) was used for tissue condition. Ratings of $\geq$4 had been dead for $\geq$2 weeks, based on comparisons with tissue degradation rates of amphipods measured at the site in separate assays. Mortality (% individuals dead) was calculated as the percentage of all individuals with tissue ratings of $\geq$4.

Natural variation in ocean pH was determined from inspection of pH measurements throughout the world ocean available from the National Ocean Data Center (http://www.nodc.noaa.gov/). Estimates of pH changes in the deep-sea caused by 100 y of CO_2 sequestration using injection rates of 0.25 and 4 gtCy-1 were calculated assuming no outgassing of injected CO_2 from the volume of the bottom 1 km of the ocean (~3.6 x 108 km^{-3}), alkalinity = 2400 $\mu m \cdot kg^{-1}$, depth = 3500 m, T = 1.5 ^{o}C, initial ΣCO_2 = 2350 $\mu m \cdot kg^{-1}$, and ending ΣCO_2 = 2356 and 2443 $\mu m \cdot kg^{-1}$, respectively.

RESULTS

In the first experiment (E1) changes in seawater pH around corrals were highly variable owing to changes in current direction with the tides, leading to large peak pH perturbations (ΔpH ~ –1.5 units were observed within 1 m of the CO_2 corrals) during periods when currents were flowing over pH sensors, and little or no pH change when currents carried the CO_2 dissolution plume away from pH sensors. Excursions in pH greater than 1 unit were rare (<5% of the time) even near CO_2 pools, and reductions of $\geq$ –0.2 units occurred only 25% of the time.

In the second experiment (E2) maximum pH shifts recorded 5 and 50 m from the CO_2 pool showed moderate (-0.2 pH units) to minor (-0.05 units) peak pH changes, and small average pH changes (-0.008, -0.003 units), respectively. Shifts of $\geq$ -0.2 units were recorded less than 2% of the time 5 m from the CO_2 pool. Unfortunately, the pH sensor adjacent (1 m) to the central CO_2 corral failed during E2.

Due to the rotary character of inertial and tidal currents at the site, pH perturbations were cyclical, exposing organisms to elevated CO_2 levels during short periods when they were in the path of the dissolution plume. Adoption of more complex experimental techniques analogous to terrestrial ecosystem studies (DeLucia et al. 1999) may be necessary to create steady pH fields. Near-bottom currents during E1 averaged 4.4 $cm \cdot s^{-1}$, with net transport to the SE at 1.7 $cm \cdot s^{-1}$. Fourier analysis of currents and variation in pH 1m (E1) and 5 m (E2) from CO_2 corrals all indicated strong periodicity near 12.4 h, associated with the major semidiurnal lunar tidal constituent (M2). In effect, organisms 1m from CO_2 pools (E1) were bathed in CO_2-rich waters

TABLE 1. Summary of CO_2 Impacts

	1 m (E1)	1 m (E2)	5 m (E2)	10 m (E2)	50 m (E2)
Change in pH units: Max (mean)	-1.0 (-0.2)		-0.1 (-0.008)		-0.01 (-0.003)
Bacteria	-2 ns	0	0	0	0
Meiofauna					
Flagellates	64 **	65	33	23	0
Amoebae	67 *	68	34	24	0
Nematodes	63 **	0	0	0	0
Macrofauna					
Amphipod (*Haploops lodo*)	95 ***	15 *	2 ns	3 ns	3 ns
Epibenthic Megafauna					
Urchin – *Cystechinus* sp.	100 **	100	80	0	0
Holothurian – *Abyssocucumis* sp.	100 **				
Near-Bottom Deep-sea Fishes					
Zoarcid – *Pachychara* sp.		0	0		0
Macrourid - *Coryphaenoides armatus*		100	100		100

Table 1. Summary of faunal impacts during CO_2 release experiments. Changes in pH represent the maximum and (mean) perturbations to ambient pH levels during each experiment. Values for each taxon are percentage mortality estimates based on comparisons of CO_2 vs. Control treatments (E1) or initial vs. end samples (E2). CO_2 impacts were high for samples within areas of large pH shifts, and undetectable or non-significant for small pH shifts. Negative mortality listed for bacteria indicates an increase in cell counts. Failure of pH sensors prevented measurements of pH shifts near (1m) the CO_2 pool during E2. All faunal groups except bacteria exhibited high rates of mortality near CO_2 pools in E1. E1, E2 indicate Experiment 1, and 2, respectively. Blanks indicate no data. ns, *, **, *** indicate non-significant, $p<0.05$, $p<0.01$, $p<0.001$ for t-tests.

(ΔpH –1.0 or greater) for ~30 minutes, twice per day. The CO_2 plume was an order of magnitude weaker at 5 m during E2, where pH shifts of ≥0.1 unit persisted for ~15 minutes, twice per day.

Most organisms were sensitive to large pH changes in CO_2 dissolution plumes very near CO_2 pools. Urchins and holothurians mortality near (<1m) CO_2 corrals was high during exposure and dissolution of skeletal elements was observed in several urchins. Urchins in control cages appeared unharmed, and all holothurians in control cages were absent, and presumably escaped. Survival of the amphipod, *Haploops lodo*, was low after intense CO_2 exposure during E1. Its abundance and tissue condition were initially similar among treatments, but differed greatly after one month, indicating high mortality rates near CO_2 pools, and very low mortality near control corrals. Sediment-dwelling meiofauna showed similar declines in population density or condition after exposure to intense CO_2 stress. The abundance of flagellates and amoebae were similar near CO_2 and control corrals before CO_2 injection, but declined near CO_2 pools by the end of the experiment. Reduced densities of both groups probably reflect the death and decay of individuals impacted by CO_2. Nematodes, the most prevalent meiofaunal taxon declined only slightly in biovolume near CO_2 pools, apparently due the slow degradation of their chitinous cuticle. Detailed inspection of individuals stained with DAPI using epifluorescence microscopy (indicating the presence / absence of intact cell nuclei), however, indicated that most nematodes near CO_2 had died compared to low mortality near control stations. Unexpectedly, cell counts of sediment bacteria were similar between CO_2 and control corrals, despite the large pH shift and mortality of other groups, and even increased during the study near CO_2 pools.

Faunal responses to the apparently milder CO_2 plume produced during the second experiment were less severe than observed during E1, and decreased at distances of 5 m or greater where pH shifts were very small (Table 1). Urchins held in cages within 1m of the central CO_2 pool died during E2, but no obvious skeletal degradation was observed. Most urchins 5 m from CO_2 also died after exposure to pH reductions of only 0.1 to 0.3 units for less than 2% of the time during E2 and an average pH shift of only –0.008. No CO_2 effects were detectable for urchins held in distant cages (10, 50 m) where pH changes were small (ΔpH =< –0.05 units less than 1% of E2). The mortality rate for amphipods (*Haploops lodo*) near (1m) the CO_2 pool was much lower during E2 than measured in E1, but was greater than before CO_2 release (Table 1). Densities of the smallest meiofaunal groups (flagellates and amoebae) declined near the CO_2 pool, with detectable changes up to 10 m from the pool. Nematode mortality was low, however, suggesting that they were somewhat more tolerant to the milder pH changes during E2 than smaller taxa.

DISCUSSION

Our results support the expectation (Seibel and Walsh 2003) that deep-sea species may be sensitive to pH stress that will accompany a direct CO_2 injection sequestration program. CO_2-related physiological stress, if not lethal, will convey higher "costs of living" through the energetic costs of acid / base balance, restricted aerobic capacity, and inhibition of protein synthesis. These costs may be highest for deep-sea organisms, which typically have limited metabolic capacity. Physiological responses of individuals to increased CO_2 levels may translate into changes in the survival, growth, and reproduction rates of populations, and shifts in the ecosystem dynamics of deep-sea communities.

The scale of ecosystem impacts from a direct CO_2 sequestration program depends on the depths, locations, and certainly the volume of CO_2 injected. Since any CO_2 released will result in CO_2 dissolution plumes from pH ~4 in the boundary layer to background values, animals in close proximity to disposal sites are at risk. Plume effects over larger scale may be estimated coarsely from expected pH fields. For example, if 0.25 to 4 $GtCy^{-1}$ as CO_2 is injected for 100 y beneath 3000 m and disperses worldwide (see methods), the pH of the deep-waters of the entire world ocean will shift by –0.02 to –0.3 units. These levels are comparable to the pH changes observed ~5 m from our CO_2 pools, and overlap or exceed the present range of natural deep-ocean pH

variability. Even larger pH perturbations will occur in mixing zones that may extend 10s to 100s of km around disposal sites (Haugan and Drange 1992, Caldeira and Wickett 2002).

Direct deep-sea CO_2 sequestration could partially mitigate the anthropogenic rise in atmospheric pCO_2 that will almost certainly accelerate through this century. Although fossil fuel conservation and alternative energy sources should be primary carbon management strategies, the decision to implement a direct ocean CO_2 sequestration program hinges on the balance between the lesser of two evils – the unabated effects of climate warming or acidification, or both, on terrestrial and shallow marine ecosystems, or damage to deep-sea ecosystems by CO_2 sequestration. Moreover, because most climate stabilization scenarios assume that CO_2 emissions will be balanced by removal, where the ocean is the largest CO_2 sink, it is likely that ocean pH will continue to decrease, with consequences that are currently not understood. Ongoing research should provide guidance concerning the risks of direct CO_2 injection, and may mandate other methods or more environmentally benign CO_2 sequestration approaches (e.g. accelerated carbonate dissolution; Caldeira and Rau 2000). Clearly, an ocean carbon sequestration program will be successful only if its intended benefits – a stabilization of atmospheric CO_2 and mitigation of climate warming consequences for terrestrial and shallow water ocean systems, outweigh its liabilities – energy expended on sequestration and damage to deep-sea ecosystems. Lacking presently is sufficient information on both sides of this balance.

REFERENCES

Barnola, J.-M., Raynaud, D., Lorius, C., & Barkov, N.I. Historical CO_2 record from the Vostok ice core. In *Trends: A Compendium of Data on Global Change*. Carbon Dioxide Information Analysis Center, Oak Ridge National Laboratory, U.S. Department of Energy, Oak Ridge, Tenn., U.S.A (2003).

Brewer, P.G., Friederich, G., Peltzer, E.T., & Orr, F.M. Jr. Direct experiments on the ocean disposal of fossil fuel CO_2. *Science* 284, 943-945 (1999).

Caldeira, K. & Wickett, M.E. Comparing pH impacts of oceanic CO_2 injection and atmospheric CO_2 release. *Eos Trans. AGU,* 83(1), Spring Meet. Suppl., Abstract OS51F-01 (2002).

Caldeira, K., & Rau, G.H. Accelerating carbonate dissolution to sequester carbon dioxide in the ocean: Geochemical implications. *Geophys. Res. Let*. 27, 225-228 (2000).

Caldeira, K., Jain, A.K., & Hoffert, M.I. Climate sensitivity uncertainty and the need for energy without CO_2 emission. *Science*, 299, 2052-2054 (2003).

DeLucia, E. H., J.G. Hamilton, S.L. Naidu, R.B. Thomas, J.A. Andrews, A. Finzi, M. Lavine, R. Matalama, J.E. Mohan, G.R. Hendrey, and W.H. Schlesinger. (1999) Net primary production of a forest ecosystem with experimental CO_2 enrichment. *Science*, 284, 1177-1179.

Drange, H., Alendal, G., & Johannessen, O.M. Ocean release of fossil fuel CO_2: A case study. *Geophys. Res. Lett*. 28, 2637-2640 (2001).

Harvey, L.D.D. Impact of deep-ocean carbon sequestration on atmosphereic CO_2 and on surface-water chemistry. *Geophys. Res. Lett.* 30, 1237-1240 (2003).

Haugan, P.M., & Drange, H. Sequestration of CO_2 in the deep ocean by shallow injection. *Nature* 357, 318-320 (1992).

Houghton, J.T. et al., *Climate Change: The IPCC Scientific assessment. Intergovernmental Panel on Climate Change*, Cambridge University Press (1990).

IPCC. In *Climate Change 2001: The Scientific Basis* (eds Houghton, J.T., et al., Cambridge University Press, Cambridge, 896 p, 2001).

Keeling, C.D. & Whorf, T.P. Atmospheric CO_2 records from sites in the SIO air sampling network. In *Trends: A Compendium of Data on Global Change*. Carbon Dioxide Information Analysis Center, Oak Ridge National Laboratory, U.S. Department of Energy, Oak Ridge, Tenn., U.S.A. (2002)

Kleypas, J.A. *et al*., Geochemical consequences of increased atmospheric carbon dioxide on coral reefs. *Science* 284, 118-120 (1999).

Knowlton, N. The future of coral reefs. *Proc. Nat. Acad. Sci.* 98, 5419-5425 (2001).

Mann, M.E., Bradley, R.S. & Hughes, M.K. Northern hemisphere temperatures during the past millennium: interferences, uncertainties, and limitations. *Geophys. Res. Lett*. 26, 759-762 (1999).

Marchetti, C. On geoengineering and the CO_2 problem. *Climate Change* 1, 59-69 (1977).

Marland, G., Boden, T.A., & Andres, R.J. Global, Regional, and National CO_2 Emissions. In *Trends: A Compendium of Data on Global Change*. Carbon Dioxide Information Analysis Center, Oak Ridge National Laboratory, U.S. Department of Energy (2001; http://cdiac.esd.ornl.gov/trends/trends.htm).

McNeil, B., Matear, R.J., Key, R.M., Bullister, J.L., & Sarmiento, J.L. Anthropogenic CO_2 uptake by the ocean based on the global chlorofluorocarbon data set. *Science* 299, 235-239.

Parmesan, C. & Yohe, G. A globally coherent fingerprint of climate change impacts across natural systems. *Nature* 421, 37-42 (2003).

Pörtner, H.-O., Reipschläger, A. In, *Ocean Storage of CO_2. Environmental, Workshop 2: Environmental Impact* (eds Ormerod, B., Angel, M.) 57-81 (IEA Green house and Gas R & D Programme, Southampton Oceanography Centre, UK, 1996).

Reichle, D. et al. *Carbon Sequestration: Research and Development* (Office of Science, Office of Fossil Energy, U.S. Dept. of Energy, 1999).

Root, T.L., et al. Fingerprints of global warming on wild animals and plants. *Nature* 421, 57-60 (2003).

Sabine, C.L., et al. Distribution of anthropogenic CO_2 in the Pacific Ocean. *Global Biogeochemical Cycles* 16, 1083-1099 (2002).

Seibel, B.A. & Walsh, P.J. Biological impacts of deep-sea carbon dioxide injection inferred from indices of physiological performance. *J. Exp. Biol.* 206, 641-650 (2003).

Tamburri, M.N., Peltzer, E.T., Friederich, G.E., Aya, I., Yamane, K., & Brewer, P.G. A field study of the effects of CO_2 ocean disposal on mobile deep-sea animals. *Mar. Chem.* 72, 95-101 (2000).

ACKNOWLEDGEMENTS

This research was supported by MBARI (projects 200001, 200002), the U.S. Dept. of Energy, Fossil Energy Group (Grant DE-FC26-00NT40929), and the U.S. Department of Energy, Ocean Carbon Sequestration Program, Biological and Environmental Research (BER), (grant #DE-FG03-01ER63065). Deep-sea experiments would not have been possible without the excellent support of the crews of the R/V Western Flyer and ROV Tiburon.

TITLE: The Influence of Introduced CO_2 on Deep-Sea Metazoan Meiofauna

AUTHORS:

Kevin R. Carman[1*] (zocarm@lsu.edu), David Thistle[2] (dthistle@garnet.acns.fsu.edu), John W. Fleeger[1] (zoflee@lsu.edu), James P. Barry[3] (barry@mbari.org)

*** - Corresponding author**

1 – Dept. of Biological Sciences, Louisiana State University, Baton Rouge, LA USA 70803

2 – Dept. of Oceanography, Florida State University, Tallahassee, FL USA 32306

3 – Monterey Bay Aquarium Research Institute, 7700 Sandholdt Rd., Moss Landing, CA USA 95039

RUNNING TITLE:

Effects of CO_2 on meiofaunal

Key words: CO_2 sequestration, meiofauna, deep sea

ABSTRACT

An experiment was performed to determine the effect of injected CO_2 on the deep-sea (3200 m) meiofaunal community in the Monterey Canyon. Approximately 20 L of liquid CO_2 was added to each of three cylindrical corrals (PVC rings pushed into the seabed) that were arranged in a triangular array 10 m on a side. After a 30-day, sediment cores were collected within an area exposed to CO_2 and at a reference site approximately 40 m away; cores were also collected from within two of the CO_2 corrals. Sediment cores were sectioned into 0-5, 5-10, and 10-20 mm layers. Abundances of major taxa (harpacticoid copepods, nematodes, nauplii, kinorhynchs, polychaetes, and total meiofauna) were determined for each layer. CO_2 exposure did not significantly influence the abundances or vertical distributions of any of the major taxa. However, other evidence suggests that abundance alone did not accurately reflect the effect of CO_2 on meiofauna. We argue that slow decomposition rates of meiofaunal carcasses can mask adverse effects of CO_2 and that longer experiments and/or careful examination of meiofaunal condition are needed to accurately evaluate CO_2 effects on deep-sea meiofaunal communities.

INTRODUCTION

Since the industrial revolution, the atmospheric concentration of CO_2 has increased by approximately 30% as a consequence of the increased use of fossil fuels and deforestation (Keeling and Whorf 1998). This rate of increase is unprecedented in the past 400,000 years and has raised concerns that it may lead to accelerated global warming (Reichle et al. 1999). During the 1980's, the combustion of fossil fuels created approximately 5.5 ± 0.5 Gt C y^{-1} (Gt = gigaton = billion metric tons) of CO_2, of which approximately 2.2 Gt C y^{-1} was removed from the atmosphere. The consensus is that most (approximately 2 Gt y^{-1}) of this carbon was absorbed by the ocean (Reichele et al. 1999) and that the rest was removed by the terrestrial biosphere. In spite of these large CO_2 sinks, atmospheric CO_2 increased at a rate of approximately 3.3 Gt C y^{-1} (Schimel et al. 1995), and thus atmospheric CO_2 concentrations continued to rise (Reichele et al. 1999). Reichele et al. (1999) estimate that atmospheric CO_2 carbon will need to be decreased by about 1 Gt y^{-1} by the year 2025 and by up to 4 Gt y^{-1} by 2050 in order to stabilize the atmospheric CO_2 concentration. Attempts to reduce atmospheric CO_2 concentrations by curtailing global CO_2 emissions have been relatively unsuccessful and fall well short of the goals identified above. The world ocean represents a tremendous potential sink for excess atmospheric CO_2 (Reichele et al. 1999) and thus the ocean is being considered as a reservoir in which excess CO_2 can be sequestered. Although various strategies for direct injection of CO_2 into the ocean have been proposed (Haugan and Drange 1992, Caldeira and Rau 2000, Drange et al. 2001, Yamasaki 2003), we lack an understanding of how increased CO_2 concentrations will influence marine ecosystems

(Tyler 2003,). Here we examine the ecological effects of directly injecting CO_2 onto the seabed of the deep ocean (Ormerod 1996).

As CO_2 is moved from the sea surface to depth, the increased pressure dramatically changes its physical properties. Below 3000 m, liquid CO_2 is denser than seawater (Brewer et al. 2000). Therefore CO_2 can most effectively be isolated from surface water and the atmosphere if it is directly injected at depths of $\geq$ 3000 m. Very little is known about the potential effects of CO_2 sequestration on deep-sea organisms (Shirayama 1995; Omori et al. 1996). Toxicity models assume that reductions in pH associated with elevated CO_2 concentrations are the primary mechanism by which organisms are adversely affected (e.g., Auerbach et al. 1997). Tamburri et al. (2000), however, showed that mobile, deep-sea scavengers suffer from respiratory distress when exposed to hypercapnic conditions (and that this effect was not associated with decreased pH). Thus, it appears possible that injection of CO_2 into the deep sea may adversely affect organisms both directly (via elevated CO_2 concentrations) and indirectly (via reduced pH).

Our research focuses on the injection of CO_2 into the deep sea and examines the influence of elevated CO_2 concentrations and associated acidification of seawater on meiofaunal benthic invertebrates (animals that pass through a 50 μm sieve and are retained on a 32 μm sieve) in the deep sea. Meiofauna are well-suited for studies of environmental disturbances (anthropogenic or natural). They are small and have higher metabolic rates and faster turnover times than do macrobenthos. Meiofauna therefore respond to disturbances over relatively short time scales (Coull and Chandler 1992, Carman et al. 1997). Meiofauna typically lack larval dispersing stages and spend almost

all of their life cycle in the sediment. Thus emigration/immigration events do not ordinarily contribute substantially to their community structure, so causality of changes in abundance and community structure over time can be more reliably linked to a disturbance event. In addition to these practical advantages, the meiofauna are worth studying in their own right. They are the most abundant deep-sea metazoans, and their representation in the deep-sea fauna increases with depth (Thiel 1979). Further, their diversity in the deep sea far exceeds that of the megafauna and macrofauna (Lambshead 1993).

MATERIALS AND METHODS

Our study site was located in the Monterey Canyon off Monterey, CA, USA (36˚ 22.8', N 122˚ 40.7' W) at a depth of 3250 m (Fig. 1). All sampling and experimental manipulations were conducted with the ROV *Tiburon*, which is operated from the R/V *Western Flyer*. In October 2002, approximately 20 L of liquid CO_2 was pumped into each of three 48-cm diameter plastic pipes that had been set into the seabed such that each extended ~15 cm into the water (Fig. 2). These "corrals" were positioned at the apexes of an equilateral triangle 10 m on a side (Fig. 2). The injected CO_2 was dispersed passively, primarily by tidal currents. When we returned after 30 days, no CO_2 was visible (CO_2 can be seen because its refractive index differs from water, Fig. 2) in the corrals or on the seabed adjacent to the corrals. The CO_2 had mixed with the near-bottom water and flowed out of the corrals and onto the seabed. We collected 7-cm inner diameter cores from an area ~2 m away from a corral (treatment) and an area ~40 m away from the nearest corral (control); cores were also collected from within two of the corrals.

Immediately upon retrieval, cores were transferred to a controlled temperature room and held at 4^{o} C.

Prior to administration of CO_2 in October, one emergence trap was placed in both the control and CO_2-treatment areas (Fig. 2). Emergence traps consisted of cylindrical PVC (20 cm diameter, 14.6 cm height) with a removable lid on the top and an inverted funnel (1.8-cm opening) on the bottom. Traps were supported by 4 legs that rested on the sediment and elevated the bottom edge of the trap ~5 cm above the seabed. The traps were deployed to test the efficacy of the design, with the ultimate goal of using these traps to determine if exposure to elevated CO_2 influences emigration of meiofauna from sediments into overlying water. As part of the test, we added 100 frozen (dead) individuals of *Amphiascoides atopus* (Lotufo and Fleeger, 1995; collected from a laboratory culture) to each trap prior to deployment. The *A. atopus* individuals (which are easily distinguishable from extant deep-sea harpacticoid species) were added to the traps to determine the loss rate of copepods through decomposition during a 30-day deployment. Emergence traps were recovered after 30 days; the contents of the each trap were collected on a 32-µm sieve and fixed in buffered formaldehyde.

pH of sediment was determined prior to extrusion and collection of sediments (Thistle et al. in preparation). Overlying water from each core was then collected by aspiration and concentrated on a 32-µm sieve. A subcore (1.9-cm diameter) was inserted into the center of each core. Sediment was extruded from cores and subcores and sectioned vertically at 0-5, 5-10, 10-20, and 20-30 mm intervals. Subcore samples were frozen and subsequently used for analysis of lipid storage material in harpacticoid copepods (Thistle et al. in preparation). The sediment collected from outside of the

subcore was fixed in 4% formaldehyde solution buffered to neutrality with borax, and stained with Rose Bengal. Particulate material from overlying water captured on the 32-μm sieve was added to the 0-5 mm sediment layer collected from outside the subcore. For each vertical layer, meiofauna were sorted to major taxon and enumerated. Data were expressed as abundance 10 cm^{-2}.

Meiofaunal abundance data from control and CO_2 –treatment areas were analyzed with SAS Version 9 for Windows. Data were standardized to a count of individuals per vertical centimeter of sediment for each of the three sediment core-depth categories then weighted in the analysis by the number of centimeters represented by each sediment core-layer category. We applied a generalized linear mixed-model ANOVA with a Poisson error distribution. In order to account for the non-independence of the observations of each sediment-layer category within a sediment core, variance and covariance for the repeated measures on each core were modeled with an exponential semivariogram. The Type-3 tests of fixed effects and least-square means were calculated with the SAS glimmix macro. Analyses were performed for total meiofauna and the most abundant taxa (harpacticoid copepods, nematodes, kinorhynchs, polychaetes and nauplii). Data from the two replicate cores collected from corrals were not included in the statistical analysis but were included in figures for qualitative comparisons.

RESULTS AND DISCUSSION

Vertical distributions and abundances of total meiofauna, nematodes, copepods, kinorhynchs, polychaetes, and nauplii are illustrated in Fig. 3. For total meiofauna and all individual taxa, abundances were significantly influenced by sediment layer but not by CO_2 exposure (Table 1). Further, the layer x CO_2-exposure interaction was not

significant in any of the analyses. Taken at face value, these results suggest that meiofauna were not adversely affected by exposure to CO_2 (i.e., abundance did not decrease) and that they did not respond by altering their vertical position within the sediment. However, other evidence suggests that this conclusion is premature and may be an artifact of the relatively short (1-month) duration of this experiment.

Using samples from the experiment presented here, Thistle et al. (in preparation) demonstrated that pH within sediments of the CO_2-treatment area was lower by 0.45-1.0 pH units. Thus, the lack of significant effects on meiofaunal abundance was not because the experiment failed to expose meiofauna to elevated CO_2 concentrations and associated acidic conditions.

Relatively little is known about the effects of reduced pH and/or elevated CO_2 concentrations on marine benthic invertebrates. A few correlative field studies have considered pH or CO_2 as physicochemical variables that might influence the abundance of (primarily shallow-water) benthic organisms. Results are either equivocal (e.g., pH covaries with a variety of other environmental variables such as O_2 or H_2S), or apparent effects are minimal (Meadows et al. 1994; Vopel et al. 1996; Paula et al. 2001; Siemens et al. 2001). Thiermann et al. (1997) observed reduced abundances of benthic fauna in the immediate vicinity of a shallow-water hydrothermal vent, where pH was as low as 6. Further, around deep-sea hydrothermal vents, low pH (5.2) has adverse effects on calcareous foraminifera (carbonate dissolution is enhanced, Jonasson et al. 1995). Nevertheless, deep-sea organisms are highly adapted to stable pH and CO_2 conditions and have greatly reduced buffering capacities relative to shallow-water species. Therefore,

even slight changes in pH should have important influences on their metabolic activities (Seibel and Walsh, 2001, 2003).

Sediment within CO_2 corrals was unambiguously blanketed with several centimeters of liquid CO_2, and thus animals were maximally exposed to hypercapnia and acidosis. However, faunal abundances in CO_2 corrals were comparable to or greater than abundances found in CO_2 treatments and controls (Fig. 3). We consider it likely that most meiofauna in corral samples were killed by exposure to CO_2 and that the animals recovered in sediment cores were dead at the time of collection, but the carcasses had not yet decomposed. We note that the abundance of harpacticoid copepods in the 0-5 mm layer of corral sediments was approximately twice that in the same layer of CO_2 and control treatments, while nematode abundance in corrals was similar to that of other samples. We speculate that corrals might have acted as a trap for taxa with the ability to disperse (such as harpacticoids, see below). Meiofaunal individuals would presumably be killed by CO_2 exposure when entering the corral and thus accumulate in surface sediment. We further speculate that if dead meiofauna did not decompose in CO_2 corrals, it is possible that meiofauna killed within the CO_2-treatment area had also not decomposed.

Data from emergence traps provide further evidence that dead meiofauna may require longer than 30 days to decompose. Of the 100 frozen *Amphiascoides atopus* added to emergence traps, 98 in one trap and 100 in the other were recovered after 30 days of exposure to ambient deep-sea water. The *A. atopus* individuals in emergence traps were not in sediment, and their decomposition rates may have been faster if they had been in contact with sediments. Nevertheless, their virtually complete recovery

supports the hypothesis that meiofauna killed as the result of exposure to CO_2 might not have decomposed during the experimental period.

Further, Thistle et al. (in preparation) examined the condition of harpacticoid copepods (based on anatomical features) from this experiment and found that 70-100% of harpacticoids from the CO_2-treatment were partially decomposed, but only 0-40% of harpacticoids from control sediments were partially decomposed. The relatively poor condition of harpacticoids in the CO_2-treatment area suggests that elevated CO_2 and corresponding acidic conditions adversely affected this taxon. Based on DNA staining methods, Barry et al. (this symposium) similarly concluded that nematodes and foraminifera suffered high mortality in a similar experiment conducted at 3600 m.

Almost all meiofaunal animals are motile and adjust their vertical positions in response to changing environmental conditions. Even in the deep sea, differences in factors such as sediment type (Carman et al. 1987) and hydrodynamic conditions (Thistle and Levin 1998) can alter vertical distributions. Meiofaunal movement rates are millimeters per minute, so a several-week experiment should detect vertical movement induced by exposure to CO_2 if it occurred. We anticipated that exposure of meiofauna to CO_2-enriched water (and associated acidic conditions) would induce them to move deeper into the sediment or, for animals with the ability to swim, to move into the overlying water. However, the sediment layer x CO_2 interaction term was not significant for any taxon (Table 1), indicating that CO_2 did not induce major changes in the vertical distribution of meiofauna within sediment. Furthermore, if CO_2 exposure induced meiofauna to migrate out of sediment into the overlying water, we would have expected decreased abundances in the 0-5 mm sediment layer of cores from the CO_2-treatment

area. In shallow marine environments, many harpacticoid copepod species swim into overlying water in response to various environmental cues (Walters 1991). However, abundances of harpacticoids (and other taxa), were not significantly reduced in the 0-5 mm layer (or deeper layers) of CO_2-exposed sediments (Fig. 3, Table 1), suggesting that exposure to CO_2 did not induce a major exodus from sediments. Some resident harpacticoid copepod species (and no other meiofaunal taxa) were captured in emergence traps (data not shown), illustrating that at least some species have the ability to exit the seabed. It is possible that harpacticoid copepods near corrals were overwhelmed by CO_2 before they were able to escape. It is possible that copepods further away from corrals, and thus exposed to lower CO_2 concentrations, were able to escape. Future experiments involving gradients of exposure will be required to examine this possibility.

Collectively, our observations suggest that exposure to CO_2 adversely affected the meiofaunal community, but, because of slow decomposition rates (> 30 days), the effects were not reflected by conventional abundance data. Adverse environmental conditions from elevated CO_2 concentrations did not trigger a detectable escape response by meiofauna, which may exacerbate the susceptibility of meiofauna to hypercapnia or acidosis.

To our knowledge, decomposition rates of meiofauna have not been previously examined in the deep sea. It is well established, however, that bacterial metabolic rates in abyssal sediments are very low in comparison to shallow-water sediments (Jannasch et al. 1971). Assuming that bacterial activity is primarily responsible for meiofaunal decomposition, slow decomposition rates of meiofauna might be expected. Our results have important implications for the design and interpretation of experimental tests of CO_2

effects on deep-sea benthos. Tests of CO_2 effects should include assays that determine the viability of animals and not be based on abundance alone. The condition indexes employed by Thistle et al. (in preparation) and Barry et al. (this symposium) are examples of how the viability of animals can be assessed. Nevertheless, longer-term experiments may be needed to fully evaluate CO_2 effects.

ACKNOWLEDGEMENTS

This research was supported by DOE grant # DE-FG02-02ER63456, Office of Science, Biological and Environmental Research. We are grateful for the shipboard and technical assistance of K. Buck, L. Kunz, T. Marshall, L. Sedlacek, H. Sofranko, J. Zukowski, and the Captain and crew of the R/V *Western Flyer* and ROV *Tiburon*.

BIBLIOGRAPHY

Auerbach, D. I., J. A. Caulfield, E. E. Adams and H.J. Herzog (1997): Impacts of ocean disposal on marine life: I. A toxicological assessment integrating constant-concentration laboratory assay data with variable-concentration field exposure. *Environ. Model. Asses*. **2**, 333-343.

Barry, J. P., B. A. Seibel, K. R. Buck, C. Lovera, E. T. Peltzer, K. Osborn, P. J. Whaling, P. Walz, and P. G. Brewer (2004): The effects of direct ocean CO_2 on deep-sea meiofauna. [this issue] *J. Oceanography*.

Brewer, P. G, G. Friederich, E. T. Peltzer, and F. M. Orr, Jr. (1999): Direct experiments on the ocean disposal of fossil fuel CO_2. *Science* **284**, 943-945.

Caldeira, K. and G. H. Rau (2000): Accelerating carbonate dissolution to sequester carbon dioxide in the ocean: Geochemical implications. *Geophys. Res. Let.* **27**, 225-228.

Carman, K. R., J. W. Fleeger and S. M. Pomarico (1997): Response of a benthic food web to hydrocarbon contamination. *Limnol. Oceanogr.* **42**, 561-571.

Carman, K. R., K. M. Sherman and D. Thistle (1987): Evidence that sediment type influences the horizontal and vertical distribution of nematodes at a deep-sea site. *Deep-Sea Res.* **34**, 45-53.

Coull, B. C. and G. T. Chandler (1992): Pollution and meiofauna: field, laboratory, and mesocosm studies. *Oceangr. Mar. Biol. Ann. Rev.* **30**, 191-271.

Drange, H, G. Alendal and O. M. Johannessen (2001): Ocean release of fossil fuel CO_2: A case study. *Geophys Res. Let.* **28**, 2637-2640.

Jannasch, H. W., K. Eimhjellen, C. O. Wirsen and A. Farmanfarmaian (1971): Microbial degradation of organic matter in the deep sea. *Science* **171**, 672-675.

Jonasson, K. E., C. J. Schroderadams and R. T. Patterson (1995): Benthic foraminiferal distribution at Middle Valle, Juan-de-Fuca Ridge, a Northeast Pacific hydrothermal venting site. *Mar. Micropal.* **25**, 151-167.

Keeling, C. D. and T. P. Whorf (1998): Atmospheric CO_2 records from sites in the SIO air sampling network. In: *Trends: A Compendium of Data on Global Change*. Information Analysis Center, Oakridge National Laboratory.

Lambshead, P. J. D. (1993): Recent developments in marine benthic biodiversity research. *Oceanis* **19**, 5-24.

Lotufo, G. R. and J. W. Fleeger (1995): Description of *Amphiascoides atopus*, a new species (Copepods: Harpacticoida) from a mass culture system. *Proc. Biol. Soc. Wash*. **108**, 117-124.

Meadows, P. S., A. C. Reichelt and A. Meadows (1994): Microbial and meiofaunal abundance, redox potential, pH, and shear-strength profiles in deep-sea sediments. *J. Geol. Soc*. **151**, 377-390.

Ormerod, W. G. (1996): *Ocean Storage of Carbon Dioxide. Workshop 3 – International Links and Concerns*. IEA Greenhouse Gas R&D Programme, Gloucestershire, UK, 138 pp.

Omori, M., C. P. Maeda, M. Maeda, B. Kimura and M. Takahashi (1996): Some considerations on the environmental impact of oceanic disposal of CO_2: Workshop 2, Environmental Impacts. Stoke Orchard. Gloucestershire, pp. 83-98.

Paula, J., P. F. E. Costa, A. Martins and D. Gove (2001): Patterns of abundance of seagrasses and associated infaunal communities at Inhaca Island, Mozambique. *Estuar. Coast. Sh. Sci*. **53**, 307-318.

Reichle, D., J. Houghton, R. Kane, J. Ekmann, S. Benson, J. Clarke, R. Dahlman, G. Hendrey, H. Herzog, J. Hunter-Cevera, G. Jacobs, R. Judkins, J. Ogden, A. Palmisano, R. Socolow, J. Stringer, T. Surles, A. Wolsky, N. Woodward and M. York (1999): *Carbon Sequestration Research and Development*. Office of Science, Office of Fossil Energy, US Department of Energy.

Schimel, D., I. G. Enting, M. Heimann, T. M. L. Widley, D. Raynaud, D. Alves and U. Siegenthaler (1995): CO_2 and the carbon cycle. p. 35-71. In: *Climate Change*

1994. ed. by J. Y. Houghton, L. G. M. Filho, J. Bruce, H. Lee, B. A. Callander, E. Haites, N. Harris and K. Maskell, Cambridge University Press, Cambridge.

Seibel, B. A. and P. J. Walsh (2001): Potential impacts of CO2 injection on deep-sea biota. *Science* **294**, 319-320.

Seibel, B. A. and P. J. Walsh (2003): Biological impacts of deep-sea carbon dioxide injection inferred from indices of physiological performance. *J. Exp. Biol.* **206**, 641-650

Shirayama, Y. (1995): Current status of deep-sea biology in relation to CO_2 disposal. p. 253-264 In: *Direct Ocean Disposal of Carbon Dioxide*. ed. by N. Handa, T. Ohsumi, Tera Scientific Publishing, Tokyo.

Siemens R.A., S. M. Mudge and J. M Cancino (2001): The effect of physical and chemical parameters on the macroinfaunal community structure of San Vicente Bay, Chile. *Revista Chilena de Historia Natural* **74**, 429-444.

Tamburri, M. N., E. T. Peltzer, G. E. Friederich, I. Aya, K. Yamane and P. G. Brewer (2000): A field study of the effects of CO_2 ocean disposal on mobile deep-sea animals. *Mar. Chem*. **72**, 95-101.

Thiel, H. (1979): Structural aspects of deep-sea benthos. *Ambio Spec. Rep*. **6**, 25-31

Thiermann, F., I. Akoumianaki, J. A. Hughes and O. Giere (1997): Benthic fauna of a shallow-water gaseohydrothermal vent area in the Aegean Sea (Milos, Greece). *Mar. Biol*. **128**, 149-159.

Thistle, D., K. R. Carman, L. Sedlacek, P. G. Brewer, J. W. Fleeger and J. P Barry (submitted): Experimental disposal of CO_2 on the deep-sea floor kills some sediment-dwelling animals.

Thistle, D. and L. A. Levin (1998): The effect of experimentally increased near-bottom flow on metazoan meiofauna at a deep-sea site, with comparison data on macrofauna. *Deep-Sea Res. I* **45**, 625-638.

Tyler, P. A. (2003): Disposal in the deep sea: analogue of nature or faux ami? *Environ. Conserv*. **30**, 26-39.

Vopel, K., J. Dehmlow and G. Artl (1996): Vertical distribution of *Cletocamptus confluens* (Copepoda, Harpacticoida) in relation to oxygen and sulphide microprofiles of a brackish water sulphuretum. *Mar. Eco. Prog. Ser*. **141**, 129-137.

Walters, K. (1991): Influences of abundance, behavior, species composition, and ontogenetic stage on active emergence of meiobenthic copepods in subtropical habitats. *Mar. Biol*. **108**, 207-215.

Yamasaki, A. (2003): An overview of CO_2 mitigation options for global warming - Emphasizing CO_2 sequestration options. *J. Chem. Engin. Japan*. **36**, 361-375.

Table 1: Analysis of variance on the effects of CO_2, sediment layer, and CO_2 x sediment-layer interaction. P-values are shown for each taxon and for total meiofaunal abundance.

	Factor		
Taxon	CO_2	Sediment layer	CO_2 x Sediment layer
Harpacticoids	0.13	<0.001	0.85
Nematodes	0.71	<0.001	0.32
Nauplii	0.16	0.0057	0.74
Kinorhynchs	0.16	0.018	0.54
Polychaetes	0.67	0.0023	0.55
Total Meiofauna	0.97	<0.001	0.46

Figure Legends

Figure 1. The study site off northern California. Depth contours are in meters.

Figure 2. The CO_2 treatment area. Corrals are arranged in a triangular array. The white object near the center of the triangle is an emergence trap. A corral being filled with CO_2 is shown in the inset.

Figure 3. Average abundances of meiofaunal taxa and total meiofauna in control and CO_2-treatment areas (N = 5), as well as within corrals (N =2), as a function of sediment layer. Samples were collected 30 days after addition of CO_2 to corrals. Error bars show ± 1 SD.

Fig. 1

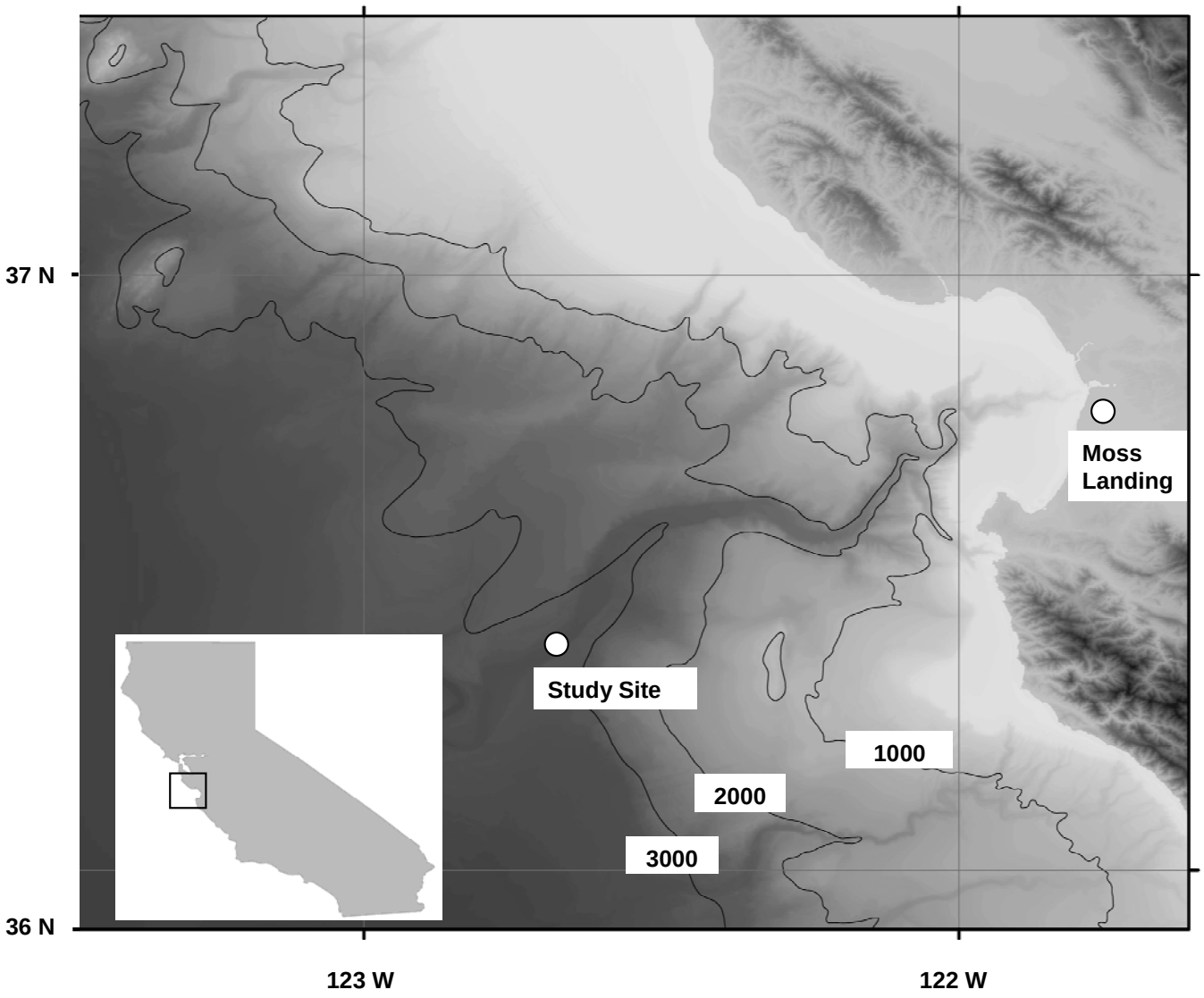

Fig. 2

Fig. 3

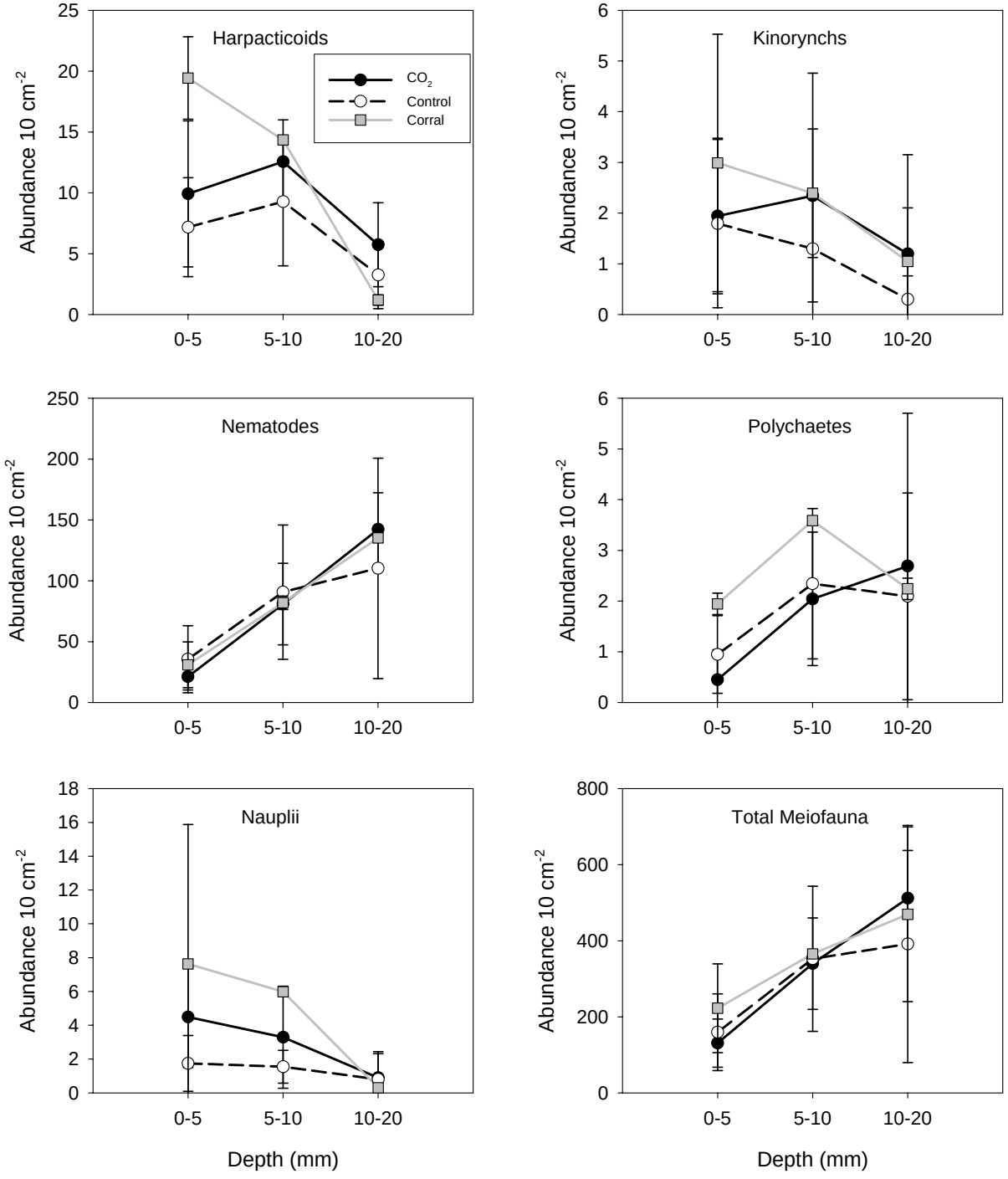
Harpacticoids
Kinorynchs
Nematodes
Polychaetes
Nauplii
Total Meiofauna
CO2
Control
Corral
Abundance 10 cm-2
0-5
5-10
10-20
Depth (mm)

Dear Jeff,

Appended below is the most recent progress report from our award by NETL concerning the same research project funded by MBARI, NETL, and Office of Science.

M B A R I MONTEREY BAY AQUARIUM RESEARCH INSTITUTE

February 3, 2004

NETL
AAD DOC Control Bldg. 921
US Dept of Energy
PO Box 10940
Pittsburgh, PA 15236-0940

RE: RESUBMISSION: ANNUAL TECHNICAL PROGRESS REPORT
Award No. DE-FC26-00NT40929 *"Feasibility of Large-Scale Ocean CO2 Sequestration"*

To Whom It May Concern:

Per your letter regarding our Technical Progress Report rejected on 1/21/2004, enclosed is the following resubmission:

1. Executive Summary
2. Technical Progress Report
3. Electronic file (CD) reformatted to integrate all files into one complete report

We will also email a "pdf" copy of this revised submission as required on the Federal Assistance Reporting Checklist, and will mail an original hard copy to Dr. Heino Beckert.

If you have any questions or if we can be of further assistance to you, please contact the Grants Office at (Tel.) 831-775-1788/1803, (FAX) 831-775-1620, or (email) grants@mbari.org.

Sincerely,

Susan Lantis

Susan Lantis
Grants and Accounting Specialist

Enclosures: As stated above

cc:
Dr. Heino Beckert
NETL
3610 Collins Ferry Road
PO Box 880, MS C04
Morgantown, WV 26507-0880

December 16, 2003

NETL
AAD DOC Control Bldg. 921
US Dept of Energy
PO Box 10940
Pittsburgh, PA 15236-0940

RE: ANNUAL TECHNICAL PROGRESS REPORT
Award No. DE-FC26-00NT40929 *"Feasibility of Large-Scale Ocean CO2 Sequestration"*

Per Department of Energy Assistance Regulations, we are providing you with several articles published or in press resulting directly from the DOE award DE-FC26-00NT40929. This set of articles constitutes the ANNUAL TECHNICAL PROGRESS REPORT for Award No. DE-FC26-00NT40929 in hardcopy and electronic (diskett) format as required.

We will also email a "pdf" copy of this report as required on the Federal Assistance Reporting Checklist to Mr. Heino Beckert as well as submitting the above documents.

If you have any questions or if we can be of any further assistance to you, please contact the Grants Office at (Tel.) 831-775-1803/1788, (FAX) 831-775-1620, or (email) grants@mbari.org.

Sincerely,

Tayeko Yamada
Grants and Accounting Specialist

cc:
Dr. Heino Berkert
NETL
3610 Collins Ferry Road
PO Box 880 , MS C04
Morgantown, WV 26507-0880

Executive Summary

Feasibility of Large-Scale Ocean CO_2 Sequestration

In this annual report we detail progress made on the project. The format is the collection of six scholarly papers resulting from partial support of our work by this DoE NETL award. In each case we have taken important critical steps to take work from the laboratory bench to the open ocean, and test our tools and ideas against the real world. Three of the papers relate to the novel development of the *in situ* Raman spectrometric technique, pioneered under this award in collaboration with the research group of Prof. Jill Pasteris (Washington University). This allows us to interrogate directly the formation of CO_2 hydrates, and the chemistry of the CO_2-water boundary layer in ways simply not accessible with other tools.

In keeping with this theme we have also collaborated with colleagues from Oak Ridge National Laboratory (C. Tsouris) in field-testing the development of a hydrate-forming nozzle. This forces droplets of sea water and CO_2 together to produce a hydrate composite, or paste like material, that is either neutrally buoyant, or sinking. This greatly aids the desirable goal of avoiding a rising plume of CO_2 droplets. The fieldwork required considerable advances in technique; the paper is now in press.

We collaborate also with Dr. James Barry (MBARI) on the biological consequences of ocean CO_2 sequestration. Enclosed here is a copy of our paper presented at the DoE NETL National Conference on Carbon Sequestration. The techniques developed under this award allow for the first time the exposure of marine animals to pools of CO_2 and the low pH field resulting from this, on the sea floor. This work is at an early stage, and is fundamentally important. So far as we are aware there are no other field studies to compare.

Our early observations force us to raise very basic questions as to experimental design, the present state of knowledge of animal respiration and behavior in the deep sea, and the kinetics of the reaction between CO_2 molecules and sea water at low temperature and high pressure. We are now making very rapid progress in this latter area.

TITLE PAGE

Report Title:	Feasibility of Large-Scale Ocean CO_2 Sequestration
Type of Report:	Annual
Reporting Period Start Date:	October 01, 2002
Reporting Period End Date:	September 30, 2003
Principal Authors:	Dr. Peter Brewer, Dr. James Barry
Date Report was Issued:	December 16, 2003
DOE Award Number:	DE-FC26-00NT40929

Name and Address of Submitting Organization:

Monterey Bay Aquarium Research Institute
7700 Sandholdt Road
Moss Landing, CA 95039-9644

Washington University at St. Louis **(Subcontract)**
Dept of Earth and Planetary Sciences
Campus Box 1169
One Brookings Drive
St. Louis, MO 631031

TABLE OF CONTENTS

Development of a Laser Raman Spectrometer for Deep-Ocean Science

Peter G. Brewer*[1], George Malby[1], Jill D. Pasteris[2], Sheri N. White[1], Edward T. Peltzer[1], B. Wopenka[2], J. Freeman[2], and Mark O. Brown[1]

1. Monterey Bay Aquarium Research Institute, 7700 Sandholdt Road, Moss Landing, CA 95039
2. Dept. of Earth and Planetary Sciences, Washington University, Campus Box 1169, St. Louis MO 63130-4899

* Corresponding author. Tel. 001-831-775-1706; Fax: 001-831-775-1620.
E-mail address: brpe@mbari.org

Development of a Laser Raman Spectrometer for Deep-Ocean Science

ABSTRACT

We have extensively modified and successfully used a laser Raman spectrometer (DORISS, Deep-Ocean Raman In Situ Spectrometer) for geochemical studies in the deep ocean. The initial instrument from Kaiser Optical, was separated into 3 components: an optical head, a laser-power supply-telemetry unit, and the spectrometer. These components were modified to fit into custom designed pressure housings, and connected by deep-sea cables and optical penetrators designed to minimize signal loss. The instrument ensemble has been field deployed on remotely operated vehicles (ROVs) for a variety of experiments and observations, with successful operation at 1.6°C, 3600m depth. Power supply, instrument control, and signal telemetry are provided through the ROV tether, which contains copper conductors and single mode optical fibers. The optical head is deployable by the ROV robotic arm for sample analysis; the remaining components are fixed within the vehicle tool-sled. Challenges of system calibration at depth, temperature and pressure artifacts, and system control through over 4 km of cable were successfully overcome. We present exemplary spectra obtained *in situ* of gas, liquid, and solid specimens, and of the ubiquitous signal of sea water itself. Future challenges include weight and size reduction, and advances in precise beam positioning on mineral targets on the sea floor.

INTRODUCTION

Geochemical studies in the deep ocean have traditionally relied upon sample recovery by bottles, cores, and dredges deployed from surface ships, or collected by manned submersibles and remotely operated vehicles (ROVs), to provide specimens for ship or shore based analysis. And while this remains the principal technique, there is a compelling case to be made for advances in *in situ* detection and analysis. Advances in measurement technique have been greatly aided by the development and increasing use of deep-ocean submersibles and ROVs. These vehicles now provide sophisticated carrying platforms with the power, telemetry and data handling, and precise manipulation capabilities (Brewer et al., 1999) to support advanced geochemical measurement systems (Kleinberg et al., 2003). In this paper we describe the adaptation of a laser Raman spectrometer (LRS) for *in situ* measurements in the deep ocean, and its successful deployment from ROVs operated by the Monterey Bay Aquarium Research Institute (MBARI). In principle the system we describe here could be adapted for use on a variety of ROVs and research submersibles available worldwide. We present exemplary spectra of sea water itself, and of selected geochemical targets examined in a carefully constructed set of controlled field experiments during the development phase, and we briefly describe some important calibration protocols. The verification of these spectra through companion laboratory studies, and detailed discussion of the spectra obtained, is reported by Pasteris et al. (submitted).

A unique advantage of Raman spectroscopy for the field geochemist (Pasteris, 1998) lies in its ability to measure solid, liquid, and gas phases, thereby greatly extending the range of possible targets. The Raman technique can measure very small samples and can

provide geochemical traverses across a heterogeneous sample. However the instrument we describe here has not yet achieved scanning capability.

Sensors typically used (Varney, 2000) for oceanic geochemical research are either electrodes and optrodes, or small-scale pumped fluid devices, for dissolved species detection. These have become sophisticated and are used for mapping geochemical fields and probing seafloor sediment fluids. However, they are typically single species detection systems, not broadly applicable, and the *in situ* measurement of solid and gaseous phases, has so far not been possible. It is ironic that a prototype Raman spectrometer has been developed for possible exploration of planetary surfaces (Wang et al., 1998; Wang et al., 1999) such as Mars, yet the >70% of Earth's surface that is ocean has until now not been made accessible to this important tool.

There are many examples of important targets in the deep ocean potentially accessible by Raman spectroscopy. These include the *in situ* identification of rocks and minerals on the sea floor and the determination chemical composition of pore water, gas seeps, and sea floor hydrothermal vents. Other interests include biologically (including microbially) precipitated solids such as the polymorphs of elemental sulfur produced by bacteria such as *Thioploca* and *Beggiatoa* (Pasteris et al., 2001). It has been reported that Raman spectroscopy can "characterize *in situ* the molecular components of pigments and other significant organic and inorganic constituents of a microbial community within its lithic habitat" (Wynn-Williams et al., 2002), although achieving this goal on the ocean floor would seem to be a significant challenge.

It is possible to distinguish between the biologically produced $CaCO_3$ polymorphs aragonite and calcite, and to investigate phosphate minerals and barite deposits on the seafloor. Other Raman active solids of interest on the seafloor include the silicates quartz and feldspar, the iron oxides magnetite and hematite, and the various manganese oxide precipitates. Clathrate hydrate phases (Sloan, 1998; Buffett, 2000; Max, 2000), which incorporate methane and many other gas species into their structure offer a compelling case for measurement in place. These hydrates are not stable at atmospheric pressure and room temperature, but exist in vast quantities in ocean margin sediments where the stability conditions are met. While hydrate specimens may be liberated from the sea floor (Brewer et al., 2002a), they are exceptionally difficult to recover in an unaltered state, and *in situ* analysis would provide unique information. The Raman spectrum of both CH_4 and CO_2 hydrates has been elegantly investigated in the laboratory (Sum et al., 1997; Subramanian and Sloan, 1999), and in situ analysis would permit the determination of the unaltered state, cage structures, and compositions.

Materials experimentally introduced into the ocean for research purposes may also be Raman active, such as in experiments to investigate the feasibility of fossil fuel CO_2 disposal (Brewer et al., 1999). Finally, possibly toxic material associated with deep ocean waste sites or accidents, where sample recovery may be hazardous, will require non-invasive analysis methods, such as may be provided by laser interrogation.

Nonetheless the challenges of carrying out Raman spectroscopy in the deep ocean are formidable. The Raman signal is notoriously weak, although possibilities for signal enhancement do exist (e.g. Altkorn et al., 2001). The vast majority of dissolved chemical species in sea water are not Raman active, or are present at micro-molar concentrations or less, and thus do not present useful Raman analytes. Water itself has a subdued Raman signature, unlike the overwhelming IR signature of water. Thus the ubiquitous signal of sea water is not likely to produce spectrally complex interferences in the Raman optical path. Fluorescence, on the other hand, is the bane of Raman spectroscopy, and there are many fluorescent oceanic species, including chlorophyll and related pigments. These are abundant in ocean surface waters, but are also rapidly transported to depth by sinking particles. It was unknown at the outset of our work how significant a problem for obtaining oceanic Raman spectra this might be.

Raman instrumentation has been typically fragile, requiring thermal stability, and a vibration free environment. Modern developments in opto-electronics have only now reached the point where these limitations may be overcome. Nonetheless, ships expose the instrumentation to significant physical motions, days of vibration during transit, and physical shock during loading and unloading. Deep ocean water is cold, and during a single lowering to the sea floor the instrumentation may be exposed to temperature changes from 20°C to 2°C in an hour. The pressure casings that house the instrument must provide protection for a 40 MPa increase in pressure without distorting the encased optical configuration. During expedition work it is very common for instrument reconfiguration to be required, often on a daily basis, and so the system must be capable of open access under often trying field conditions.

Finally, weight and size limitations, power requirements, remote instrument control and positioning, and data telemetry through over 4 km of ROV tether, also provide significant challenges. Signal loss associated with the optical connectors required for pressure housings, and electrical and optical noise that may be introduced by the vehicle, are also issues to be faced. In Figure 1 we show MBARI's ROV "Tiburon" used for several of our experiments, with the DORISS spectrometer system installed in the vehicle tool sled.

EXPERIMENTAL

Selection of an Instrument

The research team is comprised of groups from both MBARI and Washington University, St. Louis. The primary laboratory work was based at Washington University; the primary ocean program was based at MBARI. Each team acquired an initially identical instrument for research compatibility. The MBARI instrument has been very significantly modified in conversion to the DORISS unit; the Washington University instrument remains in its original configuration. The field experiments for system development were carried out jointly by both teams in the deep waters of Monterey Bay, California.

The DORISS system we have developed is based on a laboratory model laser Raman spectroscopic system from Kaiser Optical Systems, Inc. (KOSI). A schematic diagram of the various components is given in Figure 2. The requirement for robust handling

demanded that the core instrument have as few moving parts as possible, and that the laser give a stable output over a wide temperature range. A frequency-doubled Nd:YAG laser operating at 532 nm was chosen (model DPSS532 by Coherent) because of its stability and its ability to be cooled simply by thermal conduction through the walls of the high-pressure housing. The 532-nm excitation wavelength was selected for its relatively efficient propagation through sea water. The Raman shift is not a function of the exciting wavelength, but the efficiency of Raman scattering from a substance decreases as a function of λ^4, and thus a shorter wavelength laser offers significant advantages. Wavelengths shorter than 532-nm also excite greater fluorescence, and thus the laser selected represents an optimal choice.

The requirement for analysis of such a wide range of materials and processes of scientific interest requires a core Raman spectrometer that measures the full spectral range of 100 to 4000 Δcm^{-1}. The wide spectral coverage is required so that data can be collected in the low-wavenumber range (on sulfur and sulfur containing minerals), mid-range (on most minerals and on volatiles such as CO_2, O_2, N_2), and high range (for organic compounds and for the OH-groups of clathrate hydrates and hydroxylated minerals such as zeolites and clays). Appropriate resolution is required to distinguish mixtures of phases with similar band positions, such as carbonates and experimentally introduced materials with contrasting isotopic shifts (e.g., ^{12}C and ^{13}C).

The selected instrument was a Kaiser HoloSpec f/1.8i spectrometer (Owen et al., 1998) with a holographic transmissive grating and a front-illuminated cooled CCD camera with 2048 x 512 pixels by Andor Technology. The spectrum is split into two stripes on the face of the camera, thus providing a mapping of 1 cm^{-1} per pixel. This is coupled by fiber optics to Kaiser's Mark II holographic filtered probe head with two interchangeable sampling optics: a "stand-off" optic, and an immersion probe (Figure 3). We adapted the stand-off optic for housing behind a hemi-spherical deep-sea camera glass dome. It provided a ~10X objective lens with a focal length in air of ~ 6.4 cm. When immersed in sea water the dome-shielded optic provided a 10 cm working distance for target placement from the outer face of the glass dome. The immersion probe consists of a 2 mm focal length lens integrated into a 25.4-cm long metal tube with a plane sapphire end window and a working distance that is variable over a range of 1-7 mm from the probe tip. The two sampling optics require different pressure housing end caps. The stand-off optic is used by behind the glass dome window (shown assembled in Figure 3). When the immersion optic is used, the dome window is replaced by a flat titanium end cap with a gland seal that seals around the protruding optic with the plane sapphire window. The probe extends directly into the water ~20 cm.

DORISS Development

Modification of the original Instrument

Communication and control capability for the instrument via Ethernet was added by KOSI at our request at the time of purchase. This is now a standard feature for KOSI instruments. Our need for frequent field adjustment made it necessary to modify two of the original instrument alignment mechanisms. First, the laser-fiber alignment mechanism was replaced with a lockable precision three-axis micrometer stage to

facilitate the alignment of the 62.5 μm diameter excitation fiber optic cable to the laser output port. This alignment is critical for delivering and maintaining the maximum laser power to the sample of interest, and correspondingly to obtaining the maximum instrument sensitivity.

Second, the alignment of the lens that focuses the collected Raman signal on the spectrometer slit, which in part determines the spectrometer resolution, is also critical. We found that slight mechanical shock, temperature changes, or orientation deviations could cause the lens-to-slit alignment to shift, degrading the signal. The original KOSI slit alignment mechanism, designed for use in fixed installations on land, used a manual knob to translate the spot across the slit. We have replaced this mechanism with a remotely controllable motor driven stage. The stage translates the scattered-light spot across the slit in 0.5 μm increments. This translation allows a field scientist to optimize the optical throughput of the instrument in real time while at full ocean depth on an individual measurement basis to compensate for changes in the lens/slit alignment that may have occurred during deployment.

Encapsulation

The spectrometer components (schematically shown in Figure 2) are packaged in three separate pressure vessels capable of withstanding 41 MPa with a 25 percent safety margin. The probe head is contained within a 35.5 cm long by 14 cm diameter titanium pressure vessel (Figure 3) that has a removable end cap to facilitate the change between different optical configurations. Each probe head configuration weighs 18 kg including supporting frame and manipulator handle. High-pressure tolerant fiber optic cables carry the laser excitation beam to the probe head, and return the Raman scattered signals from the probe head to the spectrometer pressure vessel. The excitation fiber is 62.5 μm diameter; the collection fiber is 100 μm diameter. Signal loss was found to be unacceptably high in standard optical fiber connectors needed to penetrate the pressure housings. The cables we are now using are direct feed-through penetrating cables. These fiber optic cables are standard, pressure-tolerant polyurethane jacketed underwater cables purchased from Falmat, Inc. of San Marcos, CA. Pressure testing performed at MBARI found very small pressure effects on the throughput of the cables.

The electronics (power, telemetry, and laser) pressure vessel (Figure 4) is 100 cm long, 25.4 cm in diameter and weighs 62.6 kg fully assembled. The cylindrical portion of the vessel is a monofilament wound fiberglass reinforced resin 2.5 cm thick lay-up design. 4.4 cm thick removable aluminum end caps complete the assembly. All electronic units are mounted on an internal central aluminum web for support and stabilization. A wheel structure is mounted on each end of the web to position the assembly inside the pressure vessel.

One early design decision was to maintain the original KOSI optical bench layout. While this led to significant design challenges for packaging the system, it enabled us to focus efforts on fielding an instrument rather than on spectrometer redesign. The configuration posed a challenge for pressure vessel design because of the 90-degree orientation of the charged-coupled device (CCD) camera in relation to the optical components (Figure 5).

Preliminary Finite Element Analysis (FEA) of different designs showed size, weight and applied load to be the main drivers, given the load carrying capacity and space constraints of the ROV. Reviewed options for housing material included Titanium 6AL4V, Stainless 17-4PH, Composite Carbon Fiber and Aluminum 7075. The final selection of Aluminum 7075-T6 was based on its superior properties in yield strength, ease of manufacture, cost, and weight. The final design selection was a unique multi-part assembly that used classic ring stiffened design to provide stiffness for the protruding 90-degree arm where it intersects the main cylinder body (Figure 5). The hemispheric end bell provides superior performance at reduced weight as compared to a flat end cap, and also provides space for accommodating essential wiring and components. At the opposite end the truncated hemisphere provides added strength, and a housing surface that can support connector penetrations.

The main body of the housing is 76 cm long, including the hemispherical end caps, and 32 cm diameter. The camera extension is 22 cm long and 20 cm diameter. Total weight of the assembled spectrometer pressure vessel is 78.5 kg. The vessel was machined from 7075 aluminum and has been hard anodized and Teflon impregnated to retard corrosion. The optical bench is held in place inside the pressure vessel by internal jackscrew clamps. Electronic components are mounted both in the hemispherical end cap and under the optical bench.

Temperature and Humidity

The Raman spectrometer is designed to operate over an ambient temperature range from 0°C to 50°C. Temperature and relative humidity in each of the two major equipment pressure vessels is monitored and the data incorporated into the data stream sent through the single mode fiber of the vehicle umbilical via 10BASE-T Ethernet.

An early design concern was ensuring effective heat transfer from the cooled CCD camera during long dives with high duty cycles, particularly in warm water masses. Initial heat transfer calculations showed that the densely packed housing provided little air for the fan to move primarily because of the housing design requirement of a 90-degree extension arm, raising the possibility of sub-optimal operation. The end result of operating in a non-optimal temperature range means increased dark current (essentially leakage of charge into the pixel area that equates to system noise). Dark current is very dependent on temperature and halves in value for approximately every 6°C drop in temperature.

In normal laboratory operation the CCD is cooled to –40°C using an onboard thermoelectric cooling unit and fan; with the addition of water-cooling the array can be cooled to –80°C. A decision was made to design a heat exchanger that would be modular and could be added as necessary for warm water dives. A water-cooled heat transfer assembly was designed into the system that allows for water to circulate to cooling fins, which are external to the housing and cooled by ambient seawater. The water is run in a continuous loop returning to the CCD array at .75 liters per minute. Use of this additional cooling feature has so far not been necessary.

The temperature inside the spectrometer pressure vessel when it is deployed and operating in the deep ocean runs 2 to 3°C above ambient ocean temperature. At 3600 meters depth, 1.6°C, the measured ambient temperature inside the spectrometer pressure vessel was ~4°C. When operating in the laboratory with the spectrometer pressure vessel sealed the inside temperature stabilizes at 5 to 7°C above room temperature.

The temperature inside the electronics pressure vessel when it is deployed and operating in the ocean stabilizes at 5 to 10°C above ambient ocean temperature. When operating in the laboratory, with the electronics pressure vessel sealed, the inside temperature stabilizes at 7 to 13°C above laboratory ambient.

Four or five small packages of desiccant are added to both pressure vessels in preparation for a dive. With the desiccant, the internal relative humidity of both sealed pressure vessels runs at less than 10 percent (at 2°C) of internal vessel temperature and less than 20 percent at 20°C normal laboratory air. All of the above run conditions are well within the manufacturers specifications.

Accommodation on Carrying Platforms

The accommodation of the DORISS instrument into a vehicle payload poses significant demands. MBARI utilizes two ROVs (www.mbari.org/dmo/vessels/vessels.htm) on which the spectrometer can be deployed to support research in the deep ocean. Each vehicle has a tool-sled with sliders for instrumentation drawers to accommodate the payload (Figure 1). The ROV Ventana is rated to a depth of 1800 meters and has a useful science payload of 272 kg in air. The ROV Tiburon (Figure 1) is rated to a depth of 4000 meters and has a useful science payload of 220 kg in air. Ventana provides 2.5 kW at 120 VAC, and Tiburon provides 200W at 48 VDC and 5 kW at 240 VDC. Both ROVs provide instrument control through 10BASE-T Ethernet.

The electronics and spectrometer pressure vessels are mounted in an aluminum frame drawer that has a single cable interface to each ROV. The drawer and cabling can be completely installed on or removed from either ROV in less than 30 minutes. The probe head unit is carried in a location where it may be accessed by the ROV manipulator arm for signal acquisition from the target of interest. The total Raman system weight, including all interconnecting cables and the drawer is 211 kg. Plans to significantly reduce weight are in progress.

Data Acquisition and Processing

A single board computer, and several PCI expansion cards for remote control of the system, reside in the electronics housing. A standard desktop computer with 10BASE-T Ethernet is used topside to communicate with the single board computer, and to analyze, display and store the spectral data using Kaiser's Holograms software. The data can also be exported to GRAMS, Microsoft Excel, and Matlab software packages for further analysis and manipulation.

Calibration

The DORISS system is calibrated in the lab (ship or shore) prior to each deployment. The calibration is necessary because the system is routinely dismantled and reassembled into its pressure housings for each cruise. The primary cause of calibration changes is due to disassembly and reassembly of the instrument. In the present design the CCD camera must be removed from the optic bench when installing the spectrometer in its pressure housing. When the camera is remounted, the pixel positions can shift by as many as 50 pixels from their previous location (in both the vertical and horizontal directions). This is due to tolerances in the camera mounting holes. The calibration kit supplied by Kaiser Optical includes a neon source for wavelength calibration, a tungsten source for intensity calibration, and a cyclohexane standard to verify the laser wavelength (Tedesco and Davis, 1999).

Vibrations and temperature changes can also affect the calibration of the system, typically by a few pixels, which necessitate a calibration reference during deployment. The temperature changes experienced during deployment differentially contract the components, and may cause small changes in physical alignment. In order to check this, two *in situ* calibration routines were devised. Isopropanol contained in a small glass vial with pressure compensation reservoir was carried down with the ROV, and placed in the optical path by the vehicle manipulator whenever a calibration check across the entire CCD detector was desired.

The isopropanol-based calibration method was supplemented by a version of the diamond standard approach of Zheng et al. (2001). A small diamond plate was placed in the beam path within the probe head, but considerably off-focus. This placement moderated the extremely strong scattering efficiency of the diamond, and assured that a weak but readily detectable diamond 1332 Δcm^{-1} band was present in all spectra. The diamond undergoes cooling with the system, but remains at atmospheric pressure. Schiferl et al. (1999) have shown that for changes in temperature of 20°C to 2°C, typical for deep ocean deployment, the diamond band shifts by only ~0.2 Δcm^{-1}. Our laboratory tests confirm the modest spectral sensitivity of diamond to temperature changes. Thus this approach provides an effective spectral standard for peak position at all times.

Remaining Technical Challenges

There are areas that need improvement, and that are now being addressed. The present procedure uses laser spot positioning by robotic arm placement. This does not enable the precise positioning of the beam required for many operations, and thus spectra of large transparent objects are at present far easier to obtain than those of small opaque objects. Improved laser focusing will be achieved by the addition of a precise positioning unit that can be off-loaded from the vehicle on to the sea floor so as to decouple the probe head from any vehicle motion. This will allow three-dimensional positioning of the laser focal point with high precision on targets of interest.

This first generation DORISS system is sufficiently bulky and heavy that it forms a complete ROV payload, rather than one that would ideally be carried along with other observing tools. This is due in large part to our selection of a standard commercial Raman

system for the initial development. The L-configuration of the Kaiser optical bench, with the CCD camera at right angles, is responsible for much of the added size/mass since this dictated the use of a heavy and complex pressure vessel to contain it. In principle significantly smaller designs are possible (Dickensheets et al., 2000; Wang et al., 2003), although their implementation as a deep-sea instrument will pose challenges.

SPECTRAL ACQUISITION TECHNIQUES

We have now used the DORISS system successfully on more than 20 deep-ocean dives, with the emphasis of our efforts being primarily on instrument development. We report here on lessons learned from four *in situ* case studies, in which we examine materials with known Raman characteristics, and demonstrate successful spectral recovery from the deep ocean. We provide a brief rationale of the criteria for material selection; further discussion of spectroscopic issues is given in Pasteris et al. (submitted).

The Raman Signal of Sea Water

The Raman spectrum of sea water is present to some degree in virtually all of our work. Fortunately the spectrum is simple, and easily characterized. Sea water is a solution (~0.5M) of 11 "major ions" (present at 1 mg/kg or greater), plus a host of other inorganic and organic species at trace concentrations. Most of the major ionic species are Raman inactive. The pH of sea water varies between 8.3 and 7.6, and it is buffered by a dissolved CO_2 system of about 1.8-2.4 mM. The principal oceanic CO_2 system component is HCO_3, and this is only weakly Raman active. The fluorescence of sea water when excited with wavelengths between 350 and 550 nm is well known (Coble, 1996; Chen, 2000), and we had early concerns that this might interfere with the Raman signal. This has not been the case with the 532-nm DORISS system developed here, and all sea water signals recorded below 200m depth are remarkably free of fluorescence interference.

Raman spectra of sea water acquired in the laboratory, near surface, and at 3600m depth, are shown in Figure 6. The Raman spectrum of water has been extensively studied (Walrafen, 1964). Three main modes are designated: the ν_1 symmetric (OH) stretch near 3450 Δcm^{-1}, the ν_2 H-O-H bending mode near 1640 Δcm^{-1}, and the ν_3 water antisymmetric (OH) stretch mode near 3615 Δcm^{-1}. Walrafen (1964) also assigned four additional modes that yield weak Raman signals at 60, 175, 450, and 760 Δcm^{-1} associated with a cluster of a central water molecule surrounded by four hydrogen-bonded water molecules. The Raman spectrum of water is thus well known.

In principle it is possible to determine the concentration of dissolved gases in aqueous solution (Berger et al., 1995) by Raman spectroscopy. The possibility of detecting the dissolved N_2 signal (~2328 Δcm^{-1}) is small due to both its low concentration and to the fact that N_2 gas in air is present in the probe head as a competing signal. In later experiments we have filled the probe head space with helium to remove this possible ambiguity. Both sulfate, and N_2 gas, are conservative properties of sea water and typically show negligible variability. The presence of purely ionic dissolved species (Na^+, Cl^-, Mg^{++} etc.) does not yield Raman bands.

The only other obvious signal is that of the S-O stretch (~981 Δcm^{-1}) of the sulfate ion. Sulfate is present at 28mM concentration in sea water of 35 salinity. Since sulfate ion is a conservative component of oxygenated sea water it may well serve as a reliable concentration reference, and as a spectral reference peak. This will be true only if the Raman signal shows no significant dependency on speciation, temperature, and pressure. There is now a very large literature on this point (Appendix 1) stimulated by questions over the pressure dependence of the anomalous sound absorption of sea water by relaxation of the solvent separated $Mg\text{-}H_2O\text{-}SO_4$ ion pair. From this literature we can assume that the sea water sulfate Raman signal we observe is indeed a reliable concentration and frequency shift marker. Only very simple applications have so far been made of the field use of the sulfate Raman signal (Murata et al., 1997), such as confirmation of the near-conservative nature of sulfate ion during estuarine mixing.

By contrast the sulfate signal in sediment pore waters can show strong gradients that contain important geochemical information (Borowski et al., 1999), and thus pore waters present important future targets for Raman profiling.

There have been efforts (Abbott et al., 1982; Masutani et al., 1995) to observe the background oceanic CO_2 signal by Raman spectroscopy; all 3 major dissolved species of the carbonate system (dissolved CO_2, HCO_3^-, and CO_3^{2-}) have Raman active modes, but we have not yet detected these signals in normal ocean waters.

An ocean Raman gas experiment – N_2+CO_2

One application where no sea water background signal occurs is in the analysis of free gas, in which the immersion probe can be fully surrounded by the phase of interest. Laboratory work has shown that Raman spectroscopy is exceptionally well suited to gas phase analyses of interest to geochemists (Diller and Chang, 1980; Seitz et al., 1993; Seitz et al., 1996). Gas vents occur on the sea floor, emitting plumes primarily of methane with traces of higher alkanes, and techniques for their *in situ* analysis are of interest. Oceanic gas injection of either CO_2 (Haugan and Drange, 1992), or N_2/CO_2 mixtures has been proposed (Saito et al., 2000) as a CO_2 disposal mechanism, where the ~ 10x higher solubility of CO_2 compared to N_2 in sea water at moderate depth (200-400m) may be used to effect a separation of the gases so that a dense, sinking CO_2 rich fluid is formed, and the N_2 gas is released. This gas system appeared to offer an *in situ* experiment with a simple optical path with well-known Raman characteristics (Nakamoto, 1997) that was suitable for exploration. In Figure 7 we illustrate an experiment in which a gas mixture was released into a small box, open to the ocean at the bottom, and with the Raman immersion probe inserted horizontally and penetrating the wall of the box so that the probe tip was fully surrounded by gas. This mimics collection procedures in which gas venting from the sea floor is collected in inverted funnels before transfer to evacuated pressure cylinders for recovery and analysis. A Raman spectrum obtained at 300m depth is shown in Figure 8. The simplicity of the optical path, and the rapid response of the system, indicate that with suitable scaling of gas-liquid ratios it should be possible to quantitatively determine *in situ* mass transfer coefficients by this method.

Liquid phase studies – CO_2

There are significant vents of fluids into the ocean that provide targets for a Raman spectroscopic probe. For example there are potent fluids at hydrothermal vents and other seeps with potentially very strong Raman signatures. Access to such sites is only available to us on an expeditionary basis, and thus we sought other experimental targets for fluid analysis in order to test the DORISS system.

We have carried out a program to study deep-ocean CO_2 injection techniques for some time now (Brewer et al., 1999; Brewer et al., 2002b), and the experimental availability in local waters of this unusual hydrate forming fluid offered a unique opportunity to spectroscopically analyze a non-aqueous liquid on the ocean floor. The relatively large experimental volume and transparent nature of liquid CO_2 provided an operationally easy target for the early stages of development of Raman procedures. We have obtained spectra (Brewer et al., 2002c) of liquid CO_2 on the sea floor (Figure 9) at 3600m depth, 1.6°C, during hydrate formation and dissolution rate experiments. We were not yet successful in obtaining unambiguous spectra of CO_2 hydrate, even though it was clearly visible in our experiments. The reason for this appeared to be that the hydrate phase was intermixed with excess liquid CO_2, and that focusing of the beam purely within the relatively thin hydrate film posed operational difficulties. Plans for more precise laser spot positioning and focusing are under development.

The spectrum shown in Figure 9 reveals only the CO_2 signal, in addition to the bands due to sea water. Equilibrium calculations show that the non-polar nature of liquid CO_2 should result in the strong partitioning of other non-polar compounds (the principal dissolved gases, and some fraction of marine dissolved organic matter) from sea water into the CO_2 phase. We have not yet detected such signals. However equilibrium also dictates that the CO_2 should react with water to form a solid hydrate, and while this has been observed as a rapid reaction (Brewer et al., 1999), the specimen here remained primarily in the liquid state throughout the observing period of several hours. We predict that the Raman spectrum of CO_2 hydrate formed in natural seawater should reveal signatures of the incorporation of N_2 and O_2 from the dissolved phase, and we plan such experiments.

Solid mineral Raman signal acquisition – calcite

Raman spectroscopy has the unique advantage of enabling *in situ* identification of mineral species in the ocean, ranging from filtered suspended particles and hydrothermal precipitates to igneous and sedimentary rocks. However achieving this poses substantial scientific and operational challenges. The principal challenge for our system at this stage of development is the precise and stable location of the laser focal point on a target of interest for the several tens of seconds it takes to acquire a spectrum. We have so far relied upon positioning by vehicle robotic arms, and these are not only insufficiently steady but may also exhibit occasional erratic motions strong enough to break the probe head. Moreover the ROV itself possesses vibrations, and is forced by local ocean velocities, so that maintaining <1 mm positioning precision is unlikely. The need for precise focusing is illustrated by a laboratory study (Figure 10) in which sampling optics identical to those used for the fieldwork were used to investigate the depth-of-focus in

obtaining the Raman spectrum of a silicon wafer. Careful adjustment of the distance between the sampling optics and the opaque sample surface showed the need for position-control to better than 1 mm for the stand-off optic and better than 0.2 mm for the immersion optic in order to acquire a signal at least as strong as one-half the signal at optimum focus. Such precise beam positioning poses challenges for obtaining spectra from opaque targets on the sea floor. This problem is being addressed by the creation of a small off-loadable positioning unit, controllable from the ROV, which will decouple the probe head from vehicle motions and permit precise and steady beam location on targets of interest.

As one example of the potential of this technique we elected to measure a semi-transparent solid, where the strictures on beam positioning are somewhat relaxed. We transported several mineral specimens to 663m depth, attached to a circular frame that was placed on the sea floor. The stand-off optic configuration was used, and the probe head was placed with the laser beam horizontal and gently adjusted by the vehicle manipulator until the Raman signal was maximized. In Figure 11 we show the spectrum obtained *in situ* of a calcite rhomb. There is only a very small sea water contribution to the spectrum obtained (spectral region not shown in Fig. 11). Hydrated and hydroxylated minerals tend to have O-H stretch bands that are much narrower than the O-H stretch from sea water and thus would be readily distinguishable from those of sea water.

CONCLUSIONS

The DORISS system we have described here has successfully obtained high quality Raman spectra in real time from ocean depths down to 3600m (36 MPa; 1.6°C) from gases, liquids, and mineral solids emplaced in the ocean, and of the signal of sea water itself which permeates our working environment. The integration of remote vehicle operations/ergonomics with Raman techniques is not intuitive, and this has been a significant scientist/engineer/pilot team effort. This essentially completes the testing phase of the system, and application to geochemical problems on an expeditionary basis, and on the essential correlated laboratory studies, is now proceeding.

Finally we note with pleasure that it was an ocean voyage that originally inspired C.V. Raman. A charming account of this is given in his acceptance of the 1930 Nobel prize (Raman, 1930) for physics: "*A voyage to Europe in the summer of 1921 gave me the first opportunity of observing the wonderful blue opalescence of the Mediterranean Sea. It seemed not unlikely that the phenomenon owed its origin to the scattering of sunlight by the molecules of the water*." Modern optical oceanographers now know far more about this phenomenon, and the anecdote is simply of historical interest. Raman took many sea voyages, and wrote papers while at sea, giving ships and harbors as his address (Venkataraman, 1988). It thus seems fitting that ocean scientists should now seek to take advantage of the remarkable developments in this field.

ACKNOWLEDGEMENTS

We thank the officers and crew of the RVs Point Lobos and Western Flyer, and the ROV teams of Ventana and Tiburon, for their skill and support at sea. We acknowledge the skilled work of D. Cline in implementing the software for system operation. We thank D.

Clague and R. Kleinberg for helpful comments on the manuscript. Funding was provided by a grant to MBARI from the David and Lucile Packard Foundation, and by the U.S. Dept. of Energy Ocean Carbon Sequestration Program (Grants No. DE-FC26-00NT40929 and DE-FC03-01ER6305).

APPENDIX

A vigorous debate over sulfate ion association in sea water was stimulated by the claim by Kester and Pytkowicz (1970) that the anomalous sound absorption due to relaxation of the $Mg\text{-}H_2O\text{-}SO_4$ pair should increase with depth. This was followed by a Raman spectroscopic study (Daly, Brown, and Kester, 1972) that purported to support this model. The basis for this experimental attack is that aqueous $MgSO_4$ solutions of ~ 0.5M at room temperature show the strong ν_1 stretching band at 981 Δcm^{-1}, and a weak shoulder on the peak at around 995 Δcm^{-1} resulting from $Mg\text{-}SO_4$ ionic interaction, which thus yields a slight asymmetry to the profile. Davis and Oliver (1973) challenged the work of Daly, Brown and Kester (1973), and reported that "it is not possible to distinguish the two types of solvent separated ion pairs from each other, or the sulfate in solvent separated ion pairs from the solvated sulfate ion." Further high-pressure work by Chatterjee, Adams, and Davis (1974) supported the conclusions of Davis and Oliver (1973). This rebuttal of the claims of Kester and Pytkowicz (1970) was strongly supported by Fisher (1978). Recent work (Rull and Sobron, 1994; Frantz, Dubessy, and Mysen, 1994) confirms by both experiment and models that such weak pairing is reflected only as a shoulder on the principal peak, and that this is only detectable at high solution strengths, and at temperatures higher than the deep ocean. We therefore conclude that the small fraction (~4%) of $Mg\text{-}SO_4$ contact ion pairs in sea water, does not affect our observed signal.

REFERENCES

Abbott, T., Buchanan, G.W., Kruus, P, Lee, K.C., 1982. ^{13}C nuclear magnetic resonance and Raman investigations of aqueous carbon dioxide systems. Canadian Journal of Chemistry, 60, 1000-1006.

Altkorn, R., Malinsky, M.D., Van Duyne, R.P., Koev, I., 2001. Intensity considerations in liquid core optical fiber Raman spectroscopy. Applied Spectroscopy, 55, 373-381.

Berger, A.J., Wang, Y., Sammeth, D.M., Itzkan, I., Kneipp, K., and Feld, M.S., 1995. Aqueous dissolved-gas measurements using near-infrared Raman spectroscopy. Applied Spectroscopy 49, 1164-1169.

Borowski, W.S., Paull, C.K., Ussler, W. (1999). Global and local variations of interstitial sulfate gradients in deep-water, continental margin sediments: Sensitivity to underlying methane and gas hydrates. Marine Geology, 159, 131-154.

Brewer, P.G., Friederich, G., Peltzer, E.T., Orr, F.M Jr., 1999. Direct experiments on the ocean disposal of fossil fuel CO_2. Science 284, 943-945.

Brewer, P.G., Paull, C., Peltzer, E.T., Ussler, W., Rehder, G., Friederich, G., 2002a. Measurements of the fate of gas hydrates during transit through the ocean water column. Geophysical Research Letters, 29, doi: 10.1029/2002GL014727.

Brewer, P.G., Peltzer, E.T., Friederich, G., Rehder, G., 2002b. Experimental determination of the fate of rising CO_2 droplets in seawater. Environmental Science and Technology, 36, 5441-5446.

Brewer, P.G., Pasteris, J., Malby, G., Peltzer, E.T., White, S., Freeman, J., Wopenka, B., Brown, M., Cline, D., 2002c. Laser Raman spectroscopy used to study the ocean at 3600-m depth. EOS, 83, 469-470.

Buffett B. A., 2000. Clathrate hydrates. Annual Review of Earth and Planetary Sciences 28, 477-507.

Chatterjee, R.M., Adams, W.A., Davis, A.R., 1974. A high-pressure laser Raman spectroscopic investigation of aqueous magnesium sulfate solutions. The Journal of Physical Chemistry, 78, 246-250.

Chen, R.F., 2000. A laser-based fiber-optic fluorometer for *in situ* seawater measurements. In *Chemical Sensors in Oceanography*, M.S. Varney, Ed. Gordon and Breach, pp.189-209.

Coble, P.G., 1996. Characterization of marine and terrestrial DOM in sea water by rising excitation-emission spectroscopy. Marine Chemistry, 51, 325-346.

Daly, F.P., Brown, C.W., Kester, D.R., 1972. Sodium and magnesium sulfate ion pairing: Evidence from Raman spectroscopy. The Journal of Physical Chemistry, 76, 3664-3668.

Davis, A.R., Oliver, B.G., 1973. Raman spectroscopic evidence for contact ion pairing in aqueous magnesium sulfate solutions. The Journal of Physical Chemistry, 77, 1315-1316.

Dickensheets, D.L., Wynn-Williams, D.D., Edwards, H.G. M., Schoen, C., Crowder, C., Newton, E.M., 2000. A novel miniature confocal microscope/Raman spectrometer system for biomolecular analysis on future Mars missions after Antarctic trials. Journal of Raman Spectroscopy, 31, 633-635.

Dickson, A., 2001. Reference Materials for Oceanic Measurements. Oceanography 14(4), 21-22.

Diller, D.E., Chang, R. F., 1980. Composition of mixtures of natural gas conponents determined by Raman spectrometry. Applied Spectroscopy, 34, 411-414.

Fisher, F., 1978. Comment on "A high-pressure laser Raman spectroscopic investigation of aqueous magnesium sulfate solutions." The Journal of Physical Chemistry, 82, 495-496.

Frantz, J.D., Dubessy, J., Mysen, B.O., 1994. Ion-pairing in aqueous MgSO4 solutions along an isochore to 500°C and 11 kbar using Raman spectroscopy in conjunction with the diamond-anvil cell. Chemical Geology, 116, 181-188.

Haugan, P.M., Drange, H.,1992. Sequestration of CO_2 in the deep ocean by shallow injection. Nature, 357, 318-320.

Kester, D.R., Pytkowicz, R.M., 1970. Effect of temperature and pressure on sulfate ion association in sea water. Geochimica et Cosmochimica Acta, 34, 1039-1051.

Kleinberg, R.L., Flaum, C. Straley, C., Brewer, P.G., Malby, G.E., Peltzer, E.T., Friederich, G., Yesinowski, J.P., 2003. Seafloor nuclear magnetic resonance assay of methane hydrate in sediment and rock. Journal of Geophysical Research, 108, doi:10.1029/2001JB000919.

Masutani, S.M. Kinoshita, C.M. Nihous, G.C., Teng, H., Vega, L.A., Sharma, S.K., 1995. Laboratory experiments of CO_2 injection into the ocean. In : Handa, N., Ohsumi, T. (Eds.), Direct ocean disposal of carbon dioxide, Terra Scientific Publishing, Tokyo, pp.239-152.

Max, M.D., 2000. *Natural Gas Hydrate in Oceanic and Permafrost Environments.* Kluwer, 414 pp.

Murata, K., Kawakami, K., Matsunaga, Y., Yamashita, S., 1997. Determination of sulfate in brackish waters by laser Raman spectrocopy. Analytica Chimica Acta, 344, 153-157.

Nakamoto, K. 1997. Infrared and Raman Spectra of Inorganic and Coordination Compounds. Part A: Theory and Applications in Inorganic Chemistry. Wiley, 387 pp.

Owen, H., Battery, D.E., Pelletier, M.J., Slater, J., 1998. New spectroscopic instrument based on volume holographic optical elements. Proceedings SPIE, 2406, 260.

Pasteris, J., 1998 The laser Raman microprobe as a tool for the economic geologist, *in* M. A. McKibben, W. C. Shanks, and W. I. Ridley, eds., Applications of Microanalytical Techniques to Understanding Mineralizing Processes, Littleton, CO, Society of Economic Geologists, p. 233-250.

Pasteris, J. D., Freeman, J. J., Goffredi, S. K., K. R. Buck, S. K., 2001. Raman spectroscopic and laser scanning confocal microscopic analysis of sulfur-precipitating marine bacteria. Chemical Geology 180, 3 -18.

Pasteris, J.D., Wopenka, B., Freeman, J.J., Brewer, P.G., White, S.N., Peltzer, E.T., George E. Malby, G.E., Spectroscopic Successes and Challenges: Raman Spectroscopy at 3.6 Km Depth in the Ocean. Applied Spectroscopy. Submitted.

Raman, C.V., 1930. The molecular scattering of light. Nobel Prize Lecture.

Rull, F., Sobron, F., 1994. Band profile analysis of the Raman spectra of sulfate ions in aqueous solutions. Journal of Raman Spectroscopy, 25, 693-698.

Saito, T., Kajishima, and R. Naguosa, 2000. CO_2 sequestration at sea by gas-lift system of shallow injection and deep releasing. Environmental Science and Technology, 34, 4140-4145.

Schiferl, D., Nicol, M., Zaug, J.M., Sharma, S.K., Cooney, T.F., Wang, S.Y., Anthony, T.R., Fleischer, J.F. (1997) The diamond $^{13}C/^{12}C$ isotope Raman pressure sensor system for high-temperature/pressure diamond-anvil cells with reactive samples. Journal of Applied Physics, 82, 3256-3265.

Seitz, J. C., Pasteris, J. D., Chou, I.-M.,1993. Raman spectroscopic characterization of gas mixtures. I. Quantitative composition and pressure determinations of CH_4, N_2, and their mixtures. American Journal of Science, 293, 297-321.

Seitz, J. C., Pasteris, J. D., Chou, I.-M.,1996. Raman spectroscopic characterization of gas mixtures. II. Quantitative composition and pressure determination of the CO_2-CH_4 system. American Journal of Science, 296, 577-600.

Sloan E. D.1998 *Clathrate Hydrates of Natural Gases*. New York: Marcel Dekker, Inc, 705 pp.

Subramanian, S. and E.D. Sloan, Jr., 1999. Molecular measurements of methane hydrate formation. Fluid Phase Equilibria, 158-160, 813-820.

Sum, A.K., Burruss, R.C., Sloan, E.D., Jr., 1997. Measurement of clathrate hydrates via Raman spectroscopy. Journal of Physical Chemistry, 101, 7371-7377.

Tedesco, J.M., Davis, K.L., 1999. Calibration of dispersive Raman process analyzers. Proceedings of SPIE, 3537,

Varney, M.S., 2000. Ed. *Chemical Sensors in Oceanography* (Gordon and Breach, The Netherlands), pp. 333.

Venkataraman, G., 1988. *Journey into Light: Life and Science of C.V. Raman.* Indian Academy of Sciences.

Walrafen, G.E., 1964. Raman spectral studies of water structure. The Journal of Chemical Physics, 40, 3249-3256.

Wang, A., Haskin, L.A., Cortez, E., 1998. Prototype Raman Spectroscopic sensor for in situ mineral characterization on planetary surfaces. Applied Spectroscopy 52, 477- 487.

Wang, A. Jolliff, B.J., Haskin, L.A. 1999. Raman spectroscopic characterization of a highly weathered basalt: Igneous mineralogy, alteration products, and a microorganism. Journal of Geophysical Research 104, 27,067-27,077.

Wang, A., Haskin, L.A., Lane, A.L., Wdowiak, T.J., Squyres, S.W., Wilson, R.J., Hovland, L.E., Manatt, K. S., Raouf, N., Smith, C.D., 2003. Development of the Mars microbeam Raman spectrometer (MMRS). Journal of Geophysical Research, 108, doi: 10.1029/2002JE001902.

Wynn-Williams, D.D., Edwards, H.G.M., Newton, E.M., Holder, J.M., 2002. Pigmentation as a survival strategy for ancient and modern photosynthetic microbes under high ultraviolet stress on planetary surfaces. International Journal of Astrobiology, 1, 39-49.

Zheng, X., Fu, W., Albin, S., Wise, K. L., A. Javey, K. L., Cooper, J. B., 2001. Self-referencing Raman probes for quantitative analysis. Applied Spectroscopy, 55, 382-388.

FIGURES

Figure 1. MBARI's remotely operated vehicle "Tiburon", in side view. The base vehicle weight is 3,084 kg. Front, with manipulators and cameras not shown, is to the right of the image. The syntactic foam pack that provides buoyancy is on top, the core vehicle power, thrust, telemetry, and computing, systems are housed in the middle. Below is the tool sled with the drawer used to house the Deep Ocean Raman In-Situ Spectrometer (DORISS) system seen at bottom left.

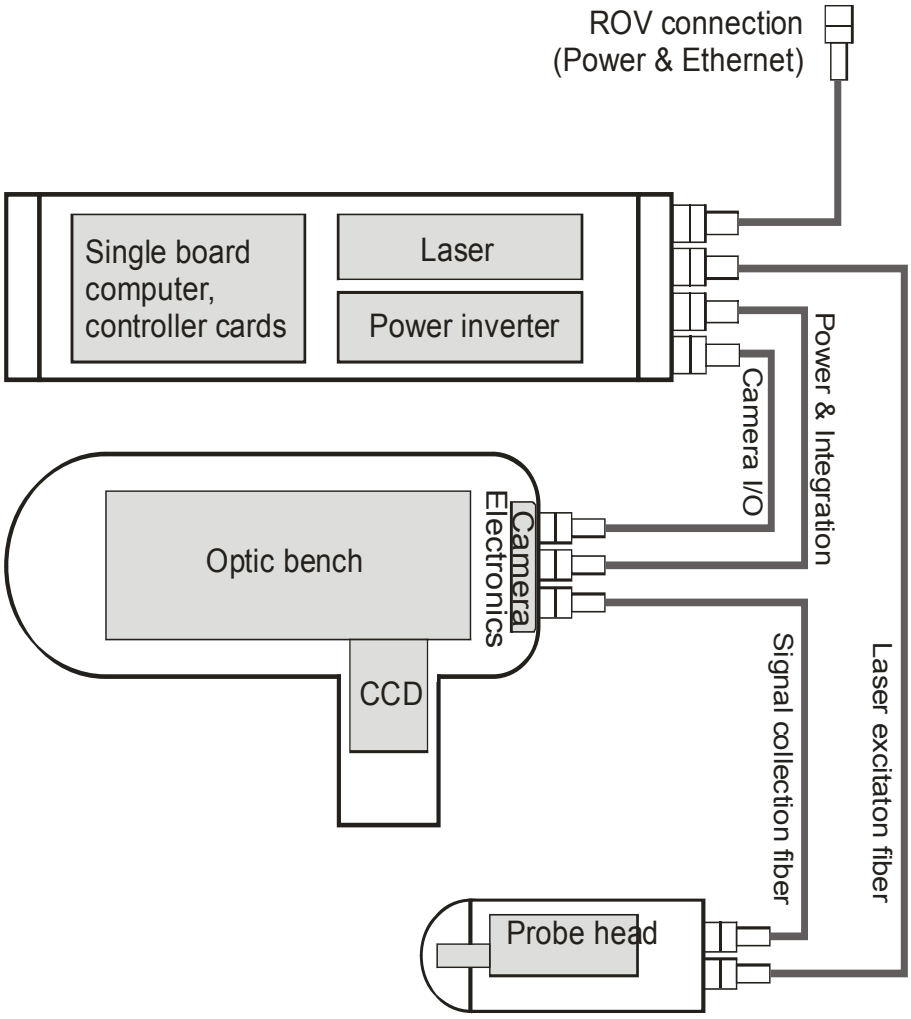

Figure 2. Schematic of the DORISS system, showing the two pressure housings for the power/laser/computer, and the optical bench. These are carried in the vehicle tool-sled, and are connected to the probe head by pressure tolerant optical fiber cables. The probe head used for sample interrogation is carried on the front of the vehicle so as to be accessible by the vehicle robotic arm.

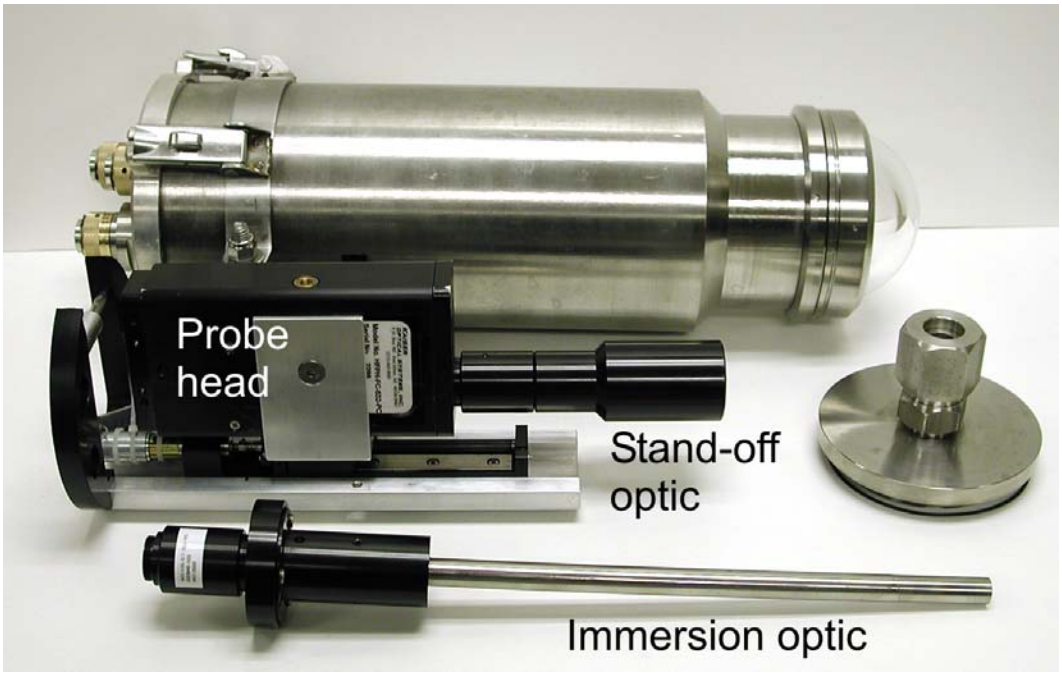

Figure 3. The probe head, showing the pressure housing (above), and both the stand-off optic, in which the laser beam projects through the glass dome, and the immersion probe with a planar sapphire window at the tip. When the immersion optic is used the dome window is replaced with the flat end cap (seen on the right side of the picture) and a gland seal is used to seal around the probe. We determine ahead of the dive which optic will be appropriate for the target we anticipate. Since the range of focus is far greater for the standoff optic this offers more flexibility, albeit with somewhat lower sensitivity. The time taken for optic exchange is a few (3-4) hours, mostly for fine scale adjustment to achieve maximum laser output.

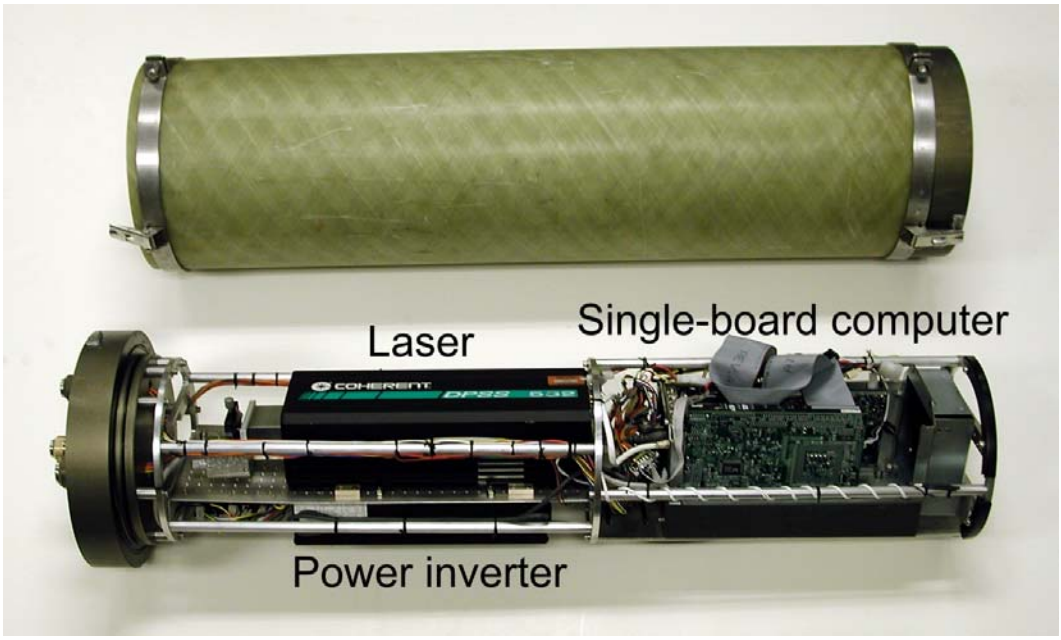

Figure 4. The fiberglass pressure housing used for the power/laser/computer system, and the incorporated components. The housing is 100 cm long, 25.4 cm diameter.

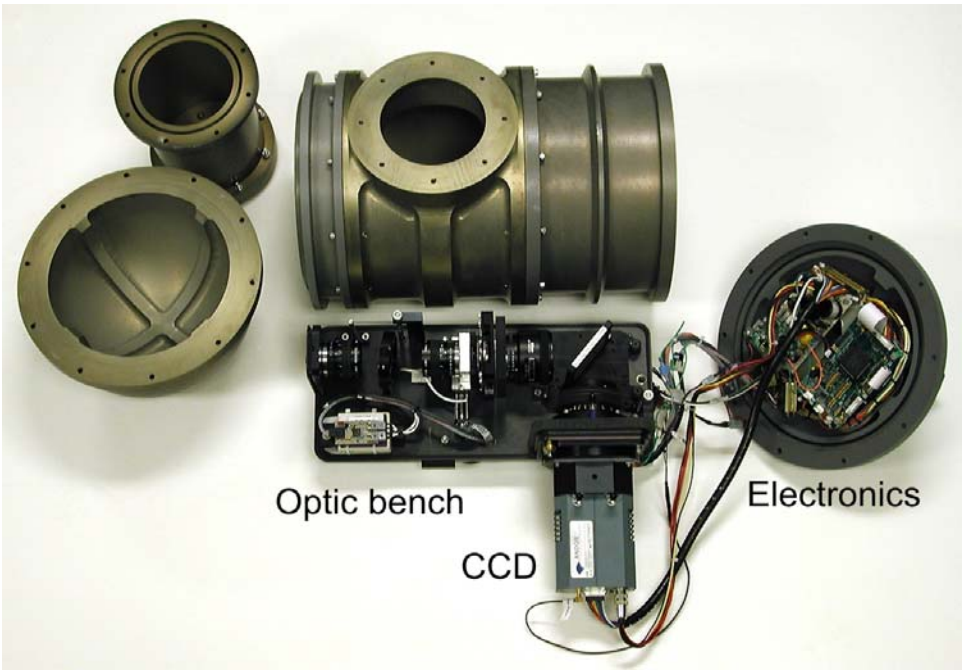

Figure 5. The pressure housing used to contain the optical bench/spectrometer. The housing end cap incorporates required electronics and the environmental sensors for detecting temperature and humidity.

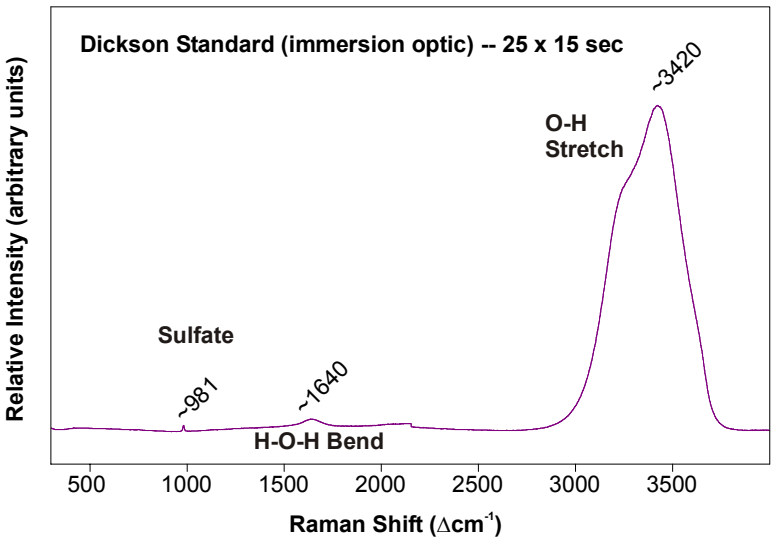
Dickson Standard (immersion optic) -- 25 x 15 sec
~3420
O-H
Stretch
Sulfate
~981
~1640
H-O-H Bend
Relative Intensity (arbitrary units)
500
1000
1500
2000
2500
3000
3500
Raman Shift (Δcm-1)

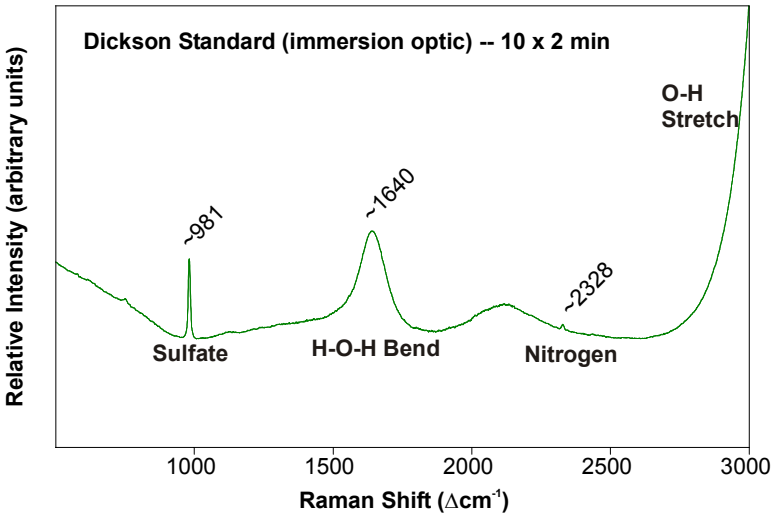
Dickson Standard (immersion optic) -- 10 x 2 min
O-H
Stretch
~981
~1640
~2328
Sulfate
H-O-H Bend
Nitrogen
Relative Intensity (arbitrary units)
1000
1500
2000
2500
3000
Raman Shift (Δcm-1)

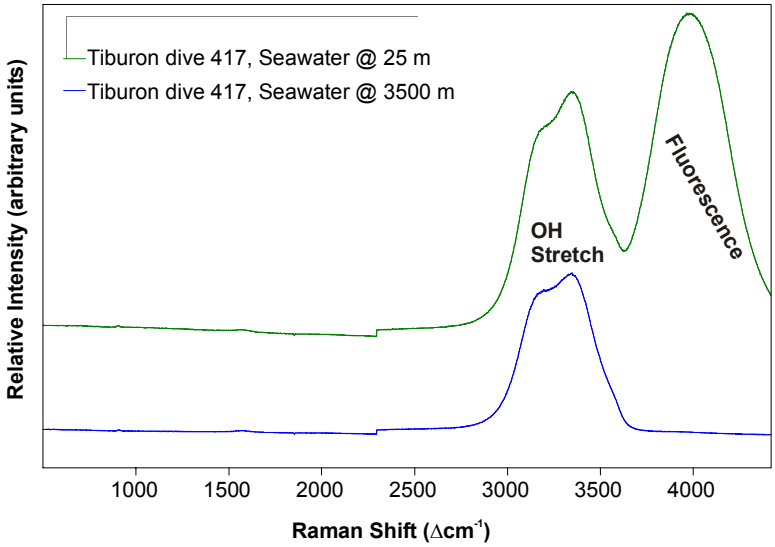
Tiburon dive 417, Seawater @ 25 m
Tiburon dive 417, Seawater @ 3500 m
OH
Stretch
Fluorescence
Relative Intensity (arbitrary units)
1000
1500
2000
2500
3000
3500
4000
Raman Shift (Δcm-1)

Figure 6. Comparative spectra of sea water. Upper two panels show spectra of standard sea water (Dickson, 2001) obtained with the immersion optic in the laboratory. The upper panel shows the full spectrum; the center panel focuses on the sulfate and nitrogen peaks. The nitrogen signal has not been corrected for the air contained in the immersion probe itself. The lower panel shows two spectra taken *in situ* of natural sea water: upper trace from 25m depth, showing the fluorescence from phytoplankton pigments; and lower trace obtained at 3500m depth with fluorescence absent.

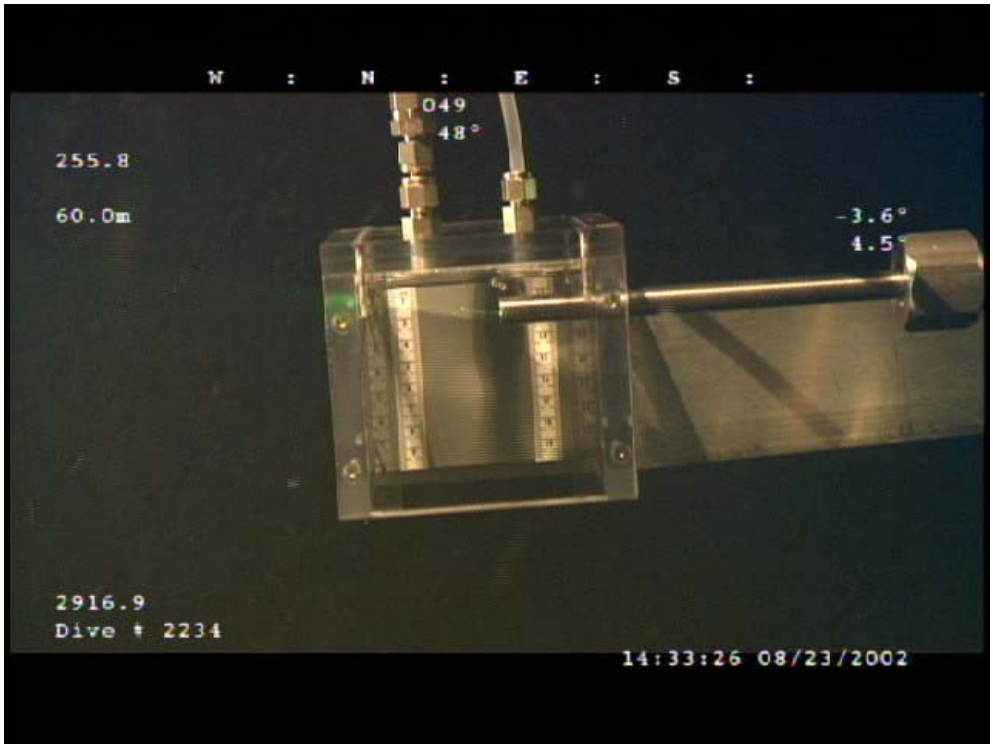

Figure 7. Image of the *in situ* gas phase experiment at 255m depth, showing the immersion probe optic installed in a 10 x 10 x 10 cm gas cube. The gas handling lines and connectors are visible on top of the cube. In this image the vehicle lights, normally turned off for acquisition of spectra, have been turned on, and the gas is being vented so that the gas/water interface now lies above the probe tip.

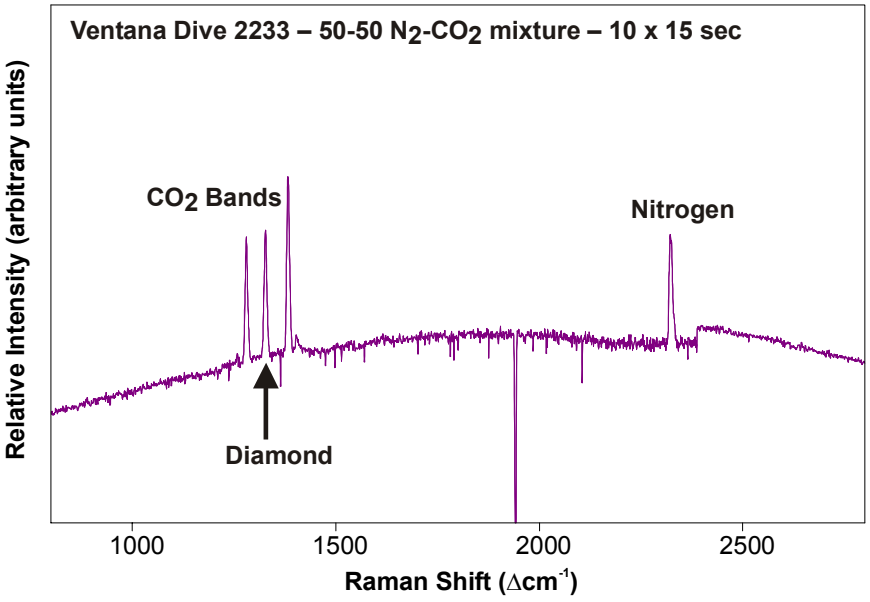

Figure 8. Spectrum of a 50-50 N_2-CO_2 gas mixture at 300 m depth. The DORISS immersion optic was inserted into a 10 x 10 x 10 cm bottomless cube (Figure 7) in which the gas mixture was contained. The diamond reference band (1332 Δcm^{-1}) is seen between the Fermi diad of the gaseous CO_2. The signal drop-out at ~1940 Δcm^{-1} is due to a flaw on the CCD chip.

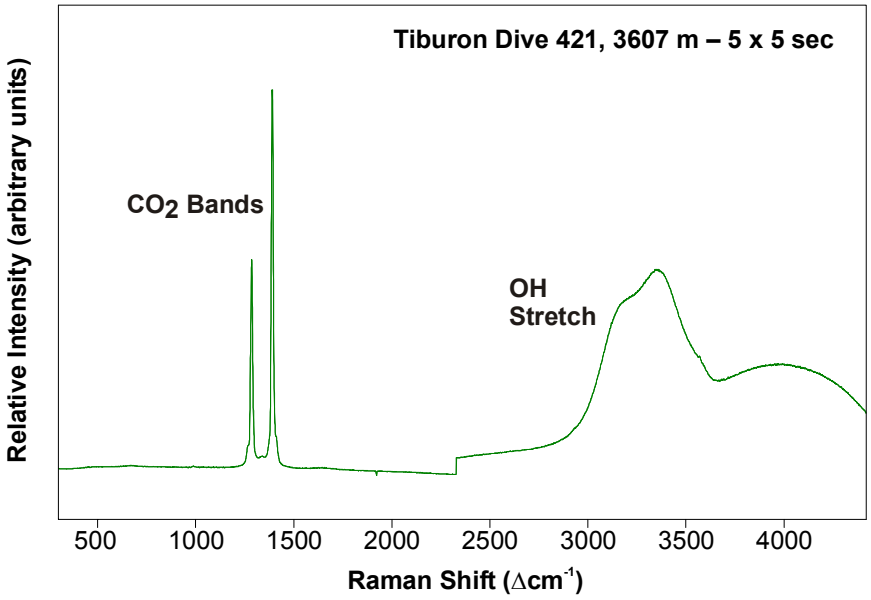

Figure 9. Raman spectrum of a pool of liquid CO_2 on the sea floor at 3607m depth, obtained with the stand-off optic. The Fermi diad peaks define the CO_2 signal; the O-H stretch signal results from sea water in the optical path, although not within the focal volume of the lens. The broad hump beyond the O-H stretch band results from fluorescence from organic matter in the surficial marine sediments.

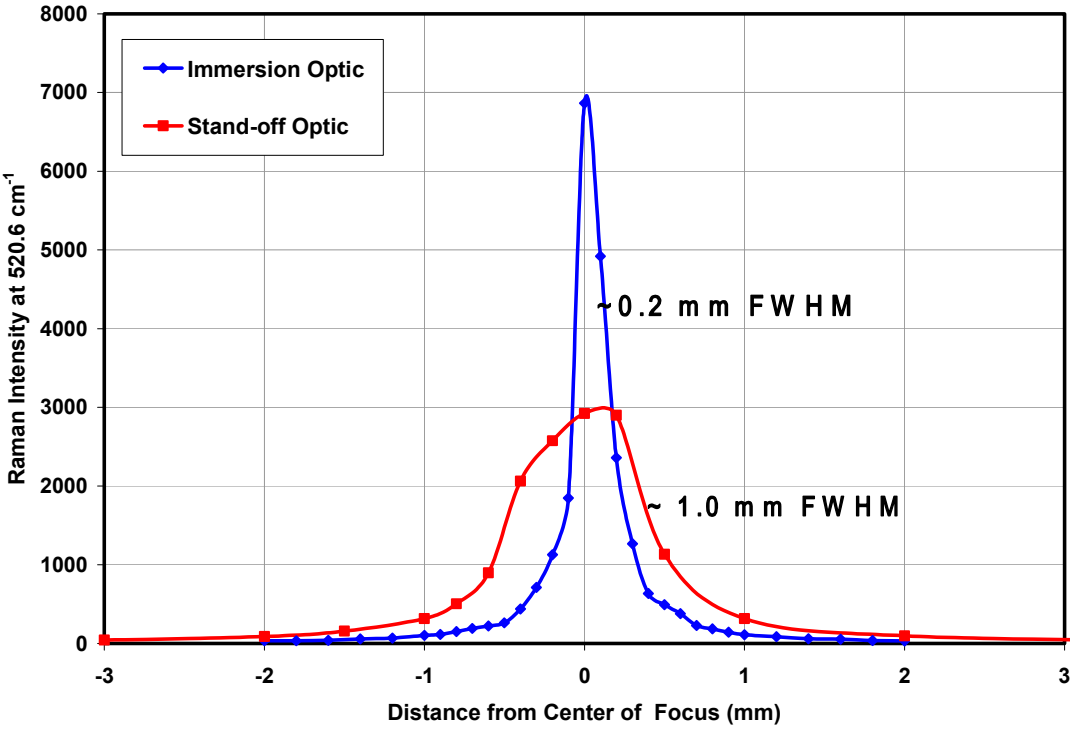

Figure 10. Example of the beam focusing requirement for an opaque solid for the two probe heads illustrated in Figure 3. The specimen selected was a silicon wafer. The signal intensity of the 520.6Δcm^{-1} band of silicon was monitored as the probe was moved incrementally closer to the sample, ultimately reaching the optimum focal position (maximum count rate on Y-axis, 0-point position on X-axis) and then residing at a distance less than the focal distance. The reported FWHM (full width at half maximum) values indicate the range of movement possible in order to still acquire at least half the count rate obtained at the actual focal distance. The results indicate that the immersion optic is much more sensitive to focus than is the stand-off optic.

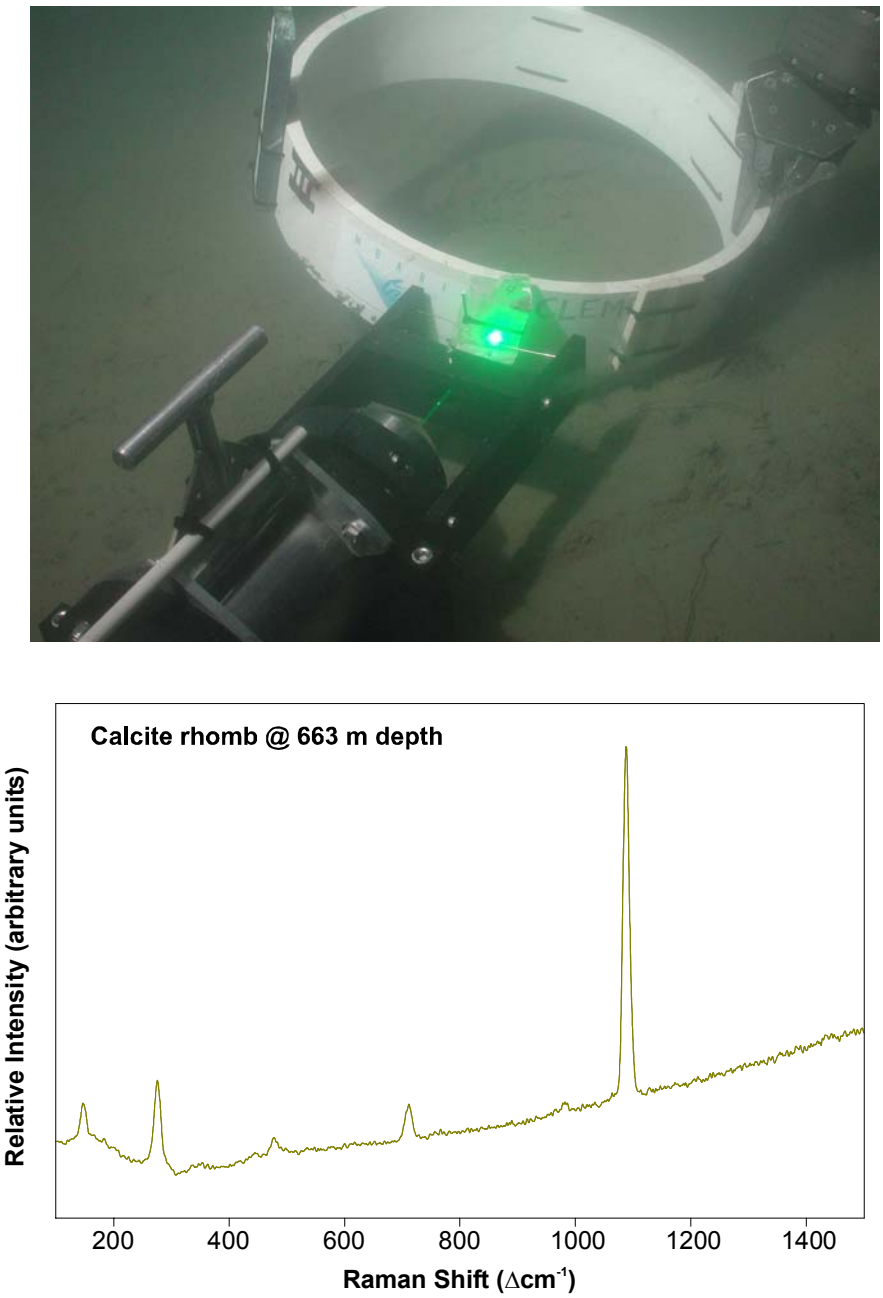

Figure 11. Upper Panel. An image showing ROV arm placement of the DORISS probe head on the sea floor (663m depth), so as to decouple it from vehicle motions. This allowed adjustment by the vehicle arm to locate the laser focal point within the volume of a rhomb of calcite. The calcite specimen is attached to a circular mount of ~ 45 cm diameter.
Lower Panel. The Raman spectrum obtained by the procedure illustrated above.

D:\MBARI\Papers\ApplSpect\FINALSpecSuccessChallengeNUMBERS.wpd 11/19/03

To Be Submitted to *Applied Spectroscopy*

Spectroscopic Successes and Challenges:

Raman Spectroscopy at 3.6 Km Depth in the Ocean

Jill Dill Pasteris [1], Brigitte Wopenka [1], John J. Freeman [1], Peter G. Brewer [2], Sheri N. White [2], Edward T. Peltzer [2], George E. Malby

[1] Department of Earth and Planetary Sciences, Washington University, Campus Box 1169, St. Louis, MO 63132-4899

[2] Monterey Bay Aquarium Research Institute, 7700 Sandholdt Road, Moss Landing, CA 95039

ABSTRACT

We report on the successful deployment by Remotely Operated Vehicle (ROV) at depths up to 3600 m of a Deep-Ocean Raman *In-Situ* Spectrometer (DORISS) system. Raman spectroscopy is a technique capable of characterizing the mineralogy of the ocean floor and analyzing the chemistry of pore water, gas seeps, and sea-floor vents. The selection and modification of the core Raman instrument are described. In a series of over 20 dives in Monterey Bay and the Gulf of California, we have deployed DORISS to analyze solid, liquid, and gas samples of synthetic and natural origin using spectral acquisition times typically ranging from one second to several tens of seconds. The intensity and resolution of these spectra compare very well with similar analyses made with a matching, but unmodified instrument in the laboratory. In an underwater, small-scale experiment, we recorded the expected shifts in Raman peak positions for CO_2 as a function of changing density as the sample was lowered to the ocean bottom and then raised. Biologically induced fluorescence in the ocean water could be monitored at shallow depths, but it caused minimal interference with the collection of Raman spectra. The major instrumental challenges in the near future are the development of a precision positioning system to better guide the probe head into focus on the sample and a reduction in weight and size of the DORISS system.

INTRODUCTION

The deep ocean is a demanding environment to the analyst, one that contains fine particles of degraded organic matter and is characterized by high pressures (about 360 atmospheres at 3.6 km depth), low temperatures (down to ~ 2° C), and a high concentration (3.5 wt. %) of corrosive salts. Such conditions make it difficult to analyze *in situ* interesting and important geologic materials and dynamic processes on the ocean floor, such as the fluids and solids that issue

from hydrothermal vents, the rocks that are formed by undersea lava eruptions, the skeletons and shells of calcareous animals such as corals and clams, and ice-like clathrates that form when natural gas seeps upward through the ocean-floor sediments and into the water column above. Because some of the phases of interest are not stable once they are brought to the surface and exposed to ambient pressure, temperature, and high oxygen concentration, only an *in-situ* analytical technique can enable detailed investigation of the ocean environment.

Raman spectroscopy is well suited to meet some of the challenges of analysis on the ocean floor: the technique is very amenable to materials that reside in an aqueous environment (in contrast to IR spectroscopy[1]); analysis is possible on solids, liquids, gases, and dissolved species; and modern Raman instrumentation has fiber-optically-coupled components that can be encapsulated in pressure-resistant housings for operation underwater.

In the present paper we report on the development, modification, calibration, deployment, and first successful applications of the Deep-Ocean Raman *In-Situ* Spectrometer (DORISS), which is based on a laboratory-model laser Raman spectroscopic system from Kaiser Optical Systems, Inc. (KOSI). This paper documents some of the analytical successes to date and discusses some of the challenges that lie ahead.

SCIENTIFIC INTERESTS IN THE SEA FLOOR AMENABLE TO RAMAN SPECTROSCOPY

The selection of the components for the deep-ocean Raman system was determined by the anticipated analytical requirements and challenges posed by our scientific interests. Those interests include the mineralogy of the sea floor and the chemistry of pore water, gas seeps, and sea floor vents. We would like to monitor gas vents for such species as CH_4, CO_2, CO, H_2S, and H_2 and to distinguish speciations that are sensitive to oxygen concentration (e.g., CH_4 vs. CO_2, sulfate vs. sulfide) and pH (e.g., HCO_3^- vs. CO_3^{2-}). We also want to make time- and spatially-resolved measurements of the ocean chemistry, e.g., investigate gradients in dissolved

gases, such as CO_2, and dissolved aqueous complexes, such as sulfate and carbonate. The concentrations of such species typically are homogeneous and unchanging in the deep ocean. When there are compositional variations and concentration gradients, however, such as may exist around a hydrothermal vent, they often are transient. They need to be recorded quickly by an *in-situ* technique, such as Raman spectroscopy, that does not disturb the compositional distribution.

Other interests include the identification of biologically precipitated solids such as elemental sulfur produced by bacteria such as *Thioploca* and *Beggiatoa*,[2] the distinction between the biologically produced $CaCO_3$ polymorphs aragonite and calcite, the identification of various Mn-oxide phases, and the investigation of phosphate minerals and deposits on the sea floor. Other solids of interest on the sea floor include the silicates quartz and feldspar, as well as the iron oxides magnetite and hematite.

Another oceanographic interest amenable to Raman spectroscopy revolves around clathrate hydrate phases, which incorporate methane and/or carbon dioxide into their structure. For the past several years, researchers at the Monterey Bay Aquarium Research Institute (MBARI) in Moss Landing, California, have been carrying out experiments related to the ocean sequestration of carbon dioxide.[3-6] The latter research addresses the attempt to develop large-scale strategies to limit the growth of greenhouse gas in the atmosphere by placing it in geochemically stable environments.[7-9] The ocean already absorbs over 7 gigatons of fossil-fuel-derived CO_2 per year by uptake from the atmosphere. It is well known that at sufficient pressure (i.e., depth, in the ocean) and at temperatures above (but approaching) the freezing point of water, both natural gas (methane) and CO_2 will interact with seawater to form clathrate hydrate, which is an ice-like phase in which gas molecules are trapped in crystalline cages formed by the H_2O molecules.[10-12] Therefore, for the past several years, researchers at MBARI have been using remotely operated vehicles (ROVs) to release liter-scale amounts of liquid carbon dioxide

into the deep ocean, where they have monitored its dissolution, downward percolation into sediments, and formation of clathrate hydrates[3-4] with ROV imaging technology. In future experiments, the newly developed DORISS system will be used to make specific geochemical measurements on the liquid CO_2, the seawater surrounding the CO_2, the nature of CO_2 clathrate hydrates, and the sediments that potentially interact with the CO_2.

THE CHALLENGES

Deployment of the DORISS down to 3.6 km Depth. The encapsulation of a Raman spectrometer in a pressure-resistant, water-tight housing and its successful deployment by a remotely operated vehicle (ROV) on the ocean floor are challenging tasks. An ROV is an integrated, unmanned submersible that is connected to the research ship on the ocean surface via a tether containing copper power conductors and fiber-optic cables. An ROV can be lowered through the water column (at a speed of 20-30 m/minute) to a depth as great as 10 km, and then landed on the deep ocean floor (Fig. 1). The ROV is equipped with lights and video cameras, and its position can be determined to within a few meters via acoustic navigation systems on the research ship. MBARI operates two research ships *(R/V Western Flyer* and *R/V Point Lobos*), which are equipped with two different ROVs (*Tiburon* and *Ventana*). The ROV *Tiburon* measures 3.0 m L x 2.4 m H x 1.8 m W and has a maximum weight of 3356.6 kg, including a payload of 499 kg.

The lower part of the ROV consists of a modular tool sled with drawers that carry mission-specific, pressure-resistant, and water-tight payloads and instrumentation, such as the DORISS, described here. The ROV has robotically controlled manipulators that are operated by specially trained pilots from the control room in the research ship. These robotic arms, which have a range up to 2 m from the ROV, can be used to precisely move mission-specific equipment (e.g., animal cages) or an instrument (e.g., the probe head of the DORISS) on the

sea floor. The position of the DORISS probe head can be manipulated with an accuracy of a few centimeters via the ROV's robotic arm and the skills of the human pilot in the control room of the research ship. Video imaging of the lighted underwater scene enables selection of the sample of interest followed by the proper positioning of the probe head near the sample's surface in order to make an analysis. The video cameras are mounted on the ROV, and images are monitored live by both the ROV pilots and scientists in the ship's control room. The dynamic display of the Raman spectrum also can be observed live on a dedicated computer in the ship's control room. This real-time feedback helps guide the optimum positioning of the Raman probe head with respect to the target sample. The number of spectral acquisitions and the collection times can be controlled in real time, exactly as in the laboratory, via a 10 Base-T Ethernet link. Raman spectra can be acquired not only while the instrument is stationary on the sea floor, but also during descent and ascent of the ROV.

In April 2002, the DORISS was deployed to the deep ocean for the first time, in the tool sled of the ROV *Tiburon*. Since then, both of MBARI's ROVs have been involved in more than twenty additional successful deep-ocean deployments, most of them in Monterey Bay off the coast of California and several of them in the Gulf of California, in Mexico.

Our research team consists of two groups. The engineering development and the oceanographic program were carried out by the group at MBARI; most of the laboratory work was carried out by the group at Washington University in St. Louis. Both groups participated in the initial field experiments in the deep ocean of Monterey Bay.

Specification and Selection of the Core Instrument. DORISS is based on a laboratory-model, laser Raman spectroscopic system from Kaiser Optical Systems, Inc. (KOSI), which is the core instrument. The need for the DORISS to be placed repeatedly at different sites on the sea floor demanded the core instrument to have as few moving parts as possible and the

laser to give a stable output under the thermal conditions pertinent to the ocean.

A frequency-doubled Nd:YAG laser operating at 532 nm was chosen (Coherent model DPSS532) because of its stability and its ability to be cooled simply by thermal conduction through the high-pressure housing and via its contained air. In addition, the 532-nm excitation wavelength was selected for its relatively efficient propagation through sea water.

The analysis of the wide range of materials and processes of scientific interest on the sea floor requires a core Raman spectrometer that is physically robust, measures the full spectral range of 100 to 4000 Δcm^{-1}, and has a resolution on the order of 3 cm^{-1}. A wide spectral coverage is required so that data can be collected in the low-wavenumber range (on sulfur and typical minerals, which incorporate inorganic complexes), mid-range (on volatiles such as CO_2 and O_2), and high range (for organic compounds, CH_4, and the OH-groups of clathrate hydrates and hydroxylated minerals such as zeolites and clays). Appropriate resolution is needed to distinguish mixtures of phases with similar band positions, such as carbonate minerals, and experimentally introduced or natural materials with contrasting isotopic signatures (e.g., ^{12}C and ^{13}C).

Our requirements were met by the following base instrument: Kaiser's HoloSpec f/1.8i spectrometer with a holographic transmissive grating; a front-illuminated CCD camera with 2048 x 512 pixels, by Andor Technology; and Kaiser's Mark II holographic filtered probe head with two interchangeable optical elements: a "dry" stand-off optic (i.e., an ~10X objective lens with a focal length in air of ~ 6.4 cm, which resulted in a maximum working distance of 15 cm when projected through a protective glass dome into seawater); and a short-focal-length, immersible optic that consists of an f/2.0 lens integrated into the tip of a 25.4-cm-long metal cylinder that is rated for temperatures of -40 to 280° C and pressures of 0-204 atm.

Making the Core Instrument Seaworthy. The core Raman instrument was re-

configured to permit its deployment in the deep ocean to depths as great as 4000 m.[13] The as-received laboratory spectrometer, plus a single-board computer and power inverter, were re-packaged into three pressure-tight housings: the electronics housing, the spectrometer housing, and the probe-head housing (Fig. 2). The electronics housing holds the Nd-YAG laser, a power inverter (48 VDC to 110 VAC), and a single-board computer with the CCD controller card and flash memory. The spectrometer housing holds the spectrometer, the CCD detector, and the associated electronics. The probe head is contained in a pressure housing with a handle that allows the ROV's robotic arm to hold and move it, thereby bringing the laser into focus on prospective targets. In the case of the dry optic, a ~1.3-cm-thick protective glass dome is used (Fig. 2), through which the exciting laser emerges. This protected dry optic can be used at several kilometers depth. For deployment of the DORISS to depths as great as 2000 m, the immersion optic also can be used. The tip of the immersion optic projects directly into the water (this optic not shown in Fig. 2).

An electrical cable connects the DORISS electronics housing to the ROV to provide power and communications via Ethernet protocol through the ROV tether to the surface. For our application, Kaiser and MBARI software engineers developed a remote protocol for controlling the instrument on the sea floor via a computer in the research ship's control room. Two additional electrical cables connect the electronics housing to the spectrometer housing: one connecting the CCD detector to its controller card on the single-board computer, the second providing power and other communications. The probe head is connected to both the laser (in the electronics housing) and the spectrometer via pressure-tolerant, fiber-optic cables.

The electronics and spectrometer housings remain in the ROV's tool sled during the entire dive (see Fig. 1). The probe-head housing is carried in a tool-sled drawer during descent and ascent of the ROV, but once the vehicle is on the sea floor, the probe-head housing can be picked up and manipulated by the ROV's robotic arm. The translation distance (about 2 m) is

limited by the “arm’s reach” and the lengths of the fiber optic cables that connect the probe head to the DORISS spectrometer and electronics housings.

The difficulties of cold temperatures and a corrosive, conductive, seawater environment also pose challenges that need to be addressed. Temperature, humidity, and water sensors were installed in the electronics housing and the spectrometer housing to alert the researcher to leaks before serious water damage can occur. Knowledge of the instrument’s temperature and other possible instrumental effects is very important for proper interpretation of the spectral data. Packs of desiccant are installed in both the electronics and spectrometer housings to prevent condensation of water vapor onto critical components.

Seagoing instruments are often subjected to significant jostling and vibrations, unlike in a laboratory environment. In addition, between ocean dives, the DORISS typically is removed from its pressure housings and taken apart for inspection, repair, and cleaning. For these reasons, a few components in the original core instrument were removed and replaced with more robust components. These parts included the laser injector and the slit-optimization mechanism. In the latter case, a motorized single-axis stage was installed such that the slit position can be optimized via remote control while the spectrometer is enclosed in its pressure-tight housing.

EXPERIMENTAL PROTOCOLS

Laboratory Simulations. Many comparison measurements were made with a duplicate KOSI Raman instrument (not enclosed in pressure housings, but with the same laser, gratings, and CCD detector as the MBARI instrument) in the laboratory at Washington University in St. Louis. Simulation experiments were conducted at atmospheric pressure in glass containers. In some studies, we used a 38-liter aquarium tank filled with artificial sea water. The probe-head optics were identical to the two types deployed on the DORISS (dry, stand-off optic and immersion probe optic), except for the lack of a protective glass dome in front of the dry optic.

We analyzed synthetic sea water solutions at temperatures between 2 and 25 °C, mineral samples submersed in water, and gas mixtures contained in glass vessels at ambient pressure and temperature. Even though we were able to simulate the low temperatures appropriate to the ocean floor using a laboratory coolant system, we did not simulate in our laboratory the high pressure that is encountered on the deep ocean floor, i.e., hydrostatic pressures approaching 400 atm at ocean depths of about 4 km.

Calibration Routines. The Kaiser Raman system, like many modern Raman systems, can be purchased with spectral calibration standards (He-Ne lamp and white light for wavelength and intensity calibrations, respectively) and appropriate software to allow automatic correction of each spectral acquisition for both wavelength and intensity. Such a system works very well under laboratory conditions: the two calibration lamps are used and then a known spectral standard (such as cyclohexane or isopropanol) is analyzed as a so-called “Raman-shift standard” to complete the calibration protocol. The unknown samples are run at the same conditions, and the calibration factors (position of the laser line, i.e., 0 Δ cm^{-1} on the CCD detector; dispersion of the wavelengths across the pixels of the detector; pixel number vs. intensity response) automatically are applied to the resultant spectra.

Effective calibration in deep-ocean spectroscopy, however, is more complicated. Although it is still possible to carry out a calibration shipboard immediately before the DORISS is lowered into the ocean (procedure we have been following), the calibration is affected as the instrument moves downward: The decreasing water temperature cools and differentially contracts the components of the laser, spectrometer, and CCD detector. Moreover, the pressure-tight housings flex slightly, thereby affecting the physical alignment of the components. Our results suggest that the above factors shift the recorded band positions by several wavenumbers and probably affect the recorded band intensities differently across the spectral

window.

For the DORISS instrument, absolute wavelength calibration with a Ne lamp standard is performed shipboard immediately before each dive, which establishes the dispersion function. This is followed by a shipboard "Raman shift calibration" (i.e., relative wavenumber calibration) using both a liquid standard (such as isopropanol in a glass vial) and a solid standard (such as diamond). Raman shift standards are used for shipboard calibration immediately before and immediately after each dive.

As an additional aid to monitor and evaluate dive-induced changes in the DORISS instrument's response while submerged, we have placed a small, polished diamond chip within the probe head, but considerably away from the focal point of the laser.[14] The extremely strong Raman-scattering efficiency of diamond assures that the positioning of a small diamond in the probe head provides continuous monitoring of the diamond's band position as a Raman shift standard, because the 1332 Δcm^{-1} band is superimposed on each spectrum. Because the diamond is within the pressure-tight housing, its Raman peak position is affected only by temperature changes during the dive. In our laboratory, a change in sample temperature from 20°C (as on shipboard) to 2°C (as on the sea floor) results in a change of less than 0.2 cm^{-1} in the position of the 1332 Δcm^{-1} Raman band of diamond, as predicted in the literature.[15] The continuous monitoring of the diamond band during a dive therefore provides information on the dive's effect on the spectrometer and aids the post-dive correction of the wavenumber calibration.

In some of our earliest dives, both isopropanol and diamond standards were taken down and measured about once an hour at ambient *in situ* sea floor conditions (Figs. 3 and 4). The isopropanol standard was contained in a pressure-compensated glass vial connected to a deformable, plastic reservoir, and the diamond chip was mounted on the outside of the glass vial. On those dives, depth-induced shifts in the band positions were recorded not only for

isopropanol and diamond, but also for seawater as a function of its pressure and temperature, and thus its density. The spectra for seawater as a function of depth were obtained by directing the laser as it exits the probe head (which is in the ROV's tool sled) into ambient seawater as the ROV descended and ascended.

For the DORISS ocean deployments conducted during 2002-2003, we determined that the wavenumber calibration is displaced by up to +3.2 cm^{-1} at 3600 m depth and 1.6° C ocean temperature, with the exact value slightly different for each dive. The spectra shown in the present paper (with the exception of those in Fig. 6) thus have an uncertainty of ± 3 cm^{-1} in accuracy of peak position. Nevertheless, the precision (i.e., reproducibility) of peak positions as measured *in situ* on the sea floor is excellent (± 0.4 cm^{-1}). In the dives during the years 2002 and 2003, the DORISS was calibrated for wavelength only; a sea-floor intensity calibration has not yet been attempted.

Typical Analytical Conditions. The analytical conditions varied somewhat between dives depending upon the laser output power, the Raman scattering efficiency of the sample, the transparency of the water, and the degree of focus of the laser on the sample. The conditions of a typical *in-situ* analysis are: 10-25 mW laser power (measured output from the probe head while DORISS is still on deck; subsequent adoption of improved laser injector component permits more constant laser power); 1-15 scans of 1-15 seconds duration are averaged; spectral resolution is 6-8 cm^{-1} when no slit is used (resolution determined by the 100-μm diameter of the collection optical fiber), but 3-4 cm^{-1} when a 50-μm slit is employed.

The laser typically remains on for the full duration of the dive, i.e., during descent and ascent, as well as while the ROV is residing on the sea floor. The laser appears as a focused green light beam exiting the probe head, and can be captured live by the ROV's video cameras and watched by the scientists in the ship's control room (Fig. 5). During acquisition of Raman spectra, the ROV's high-intensity lights typically are turned off so as not to interfere with the

acquisition of the Raman signal.

EARLY SUCCESSES OF THE DEEP OCEAN RAMAN SYSTEM

Fluids. *Raman Spectra of Sea Water*. Among the first spectra obtained with the DORISS were those of seawater. An early concern that did not materialize into a problem was the possibility of a laser-induced high fluorescence background in Raman spectra taken in the deep ocean due to either dissolved organic matter or particulate organic debris ("marine snow") that constantly rains down through the ocean water column.[16] In practice, however, we found that the fluorescence signal of sea water was not overwhelming and rarely approached in intensity that of the Raman OH-stretching bands of water at about 3400 Δ cm^{-1}**.**

The Raman spectrum of (ocean) water (Fig. 6) is characterized by the OH-bend and -stretch, centered at ~1640 and ~3400 Δcm^{-1}, together with the v_1 sulfate band (~984 Δcm^{-1}), as has been reported for *ex situ* analysis of natural and synthetic seawater.[17-18] The covalently bonded anionic complex, SO_4^{2-}, which has an average concentration of 28 mM in seawater, is readily recorded (Fig. 6). In fact, our laboratory Raman instrument can detect sulfate in seawater diluted to 0.057 times its normal salinity, i.e., 1.6 mM sulfate or 150 ppm sulfate. Although the purely ionic species such as Na^+ and Cl^- do not yield explicit Raman bands, the nature and concentration of dissolved salts have a measurable effect on the band-structure of water.[19-21] This effect is illustrated by the difference in the OH bands of pure water and ocean water, which has 35 g/kg dissolved salts, as shown in Fig. 6.

Raman spectra of Carbon Dioxide Introduced into the Deep Ocean. Raman spectroscopy offers one important means of monitoring the composition of a CO_2 stream that may be introduced into the ocean, e.g., in connection with studies of ocean sequestration of CO_2. In the past, we have done Raman analyses in the laboratory[22] on pure CO_2 enclosed in a glass capillary under controlled conditions of temperature (23°C) and pressure (up to 700 bars). In April, 2002, we

used DORISS to make comparable pressure- and temperature-dependent measurements on 500-600 ml (measured in liquid state) of essentially pure CO_2, which were injected underwater into an inverted clear, soft-glass jam jar. (The choice of container was forced upon us by the exigencies of field work.) The jar was mounted within the tool sled of the ROV. The open-ended, inverted jar permitted the CO_2 to equilibrate with both the pressure and temperature of the surrounding seawater as the ROV descended to 664 m depth at 5.2 °C and then returned to the surface. The jar underwent video monitoring during the entire experiment. During the initial descent of the ROV, CO_2 was introduced in several aliquots (beginning at 200 m depth) at increasing depths, as the increasing pressure caused compression of the CO_2 sample. At depths less than 400 m, two phases were observed in the jar: the higher one was a vapor mixture consisting of entrapped air and gaseous CO_2, and the lower one was sea water. At depths of 400 m and greater, there were three phases separated by two interfaces: an upper phase dominated by entrapped air, a middle phase of liquid CO_2, and a lower phase of sea water. Although the density of the CO_2 increased as the ROV moved deeper into the ocean, for the maximum depth of this dive (664 m) and the temperature range of this experiment, the CO_2 phase always was less dense than the seawater and thus remained trapped in the inverted jar.

During the entire descent and ascent, the laser beam was focused into the same small volume within the interior of the jar. At shallower depths, the irradiation volume was at the level of the gas phase; at greater dive depths, the focus was at the level of the liquid CO_2 phase. Raman spectra were taken at a total of 13 intervals (spaced by 40-100 m) along the descent and ascent paths of the ROV. A marked increase in signal intensity and a downshift in Raman band positions for CO_2 accompanied the phase change in CO_2 from the vapor to the liquid state (Fig. 7).

It is well known that the physical parameters of CO_2, such as density and solubility in (sea)water, are a function of temperature and pressure. The ability to monitor changes in these fundamental parameters with the DORISS is important in experiments that test the feasibility of

sequestering CO_2 on the ocean floor. The Raman spectrum of CO_2, in turn, is a moderately accurate monitor of its density,[22-30] and Raman spectroscopy can be used to determine the concentration and speciation (e.g., into CO_3^{2-} and $H_2CO_3^{2-}$) of CO_2 dissolved in water.[31-33]

Our laboratory work[22] and that of others has shown that, as CO_2 density increases, the Raman band positions of both the v_1 and $2v_2$ bands of the Fermi diad[34] downshift, whereas the spectral separation increases between these two bands.[23,25-26] We used the equation of state of Span and Wagner[35] as implemented with the program CO2Tab from ChemicaLogic Corporation[36] to calculate the density of the CO_2 in our previous laboratory experiments[22] and in the ocean experiment. Figure 8 compares the spectral separation between the bands of the Fermi diad as a function of calculated CO_2 density for both our laboratory data and ocean data. The laboratory and DORISS curves are, for the most part, parallel but offset by more than a wavenumber, suggesting that the calibration (specifically the spectrometer dispersion function) applied to the DORISS was not optimal for the conditions during this dive. The marked non-parallelism in the low-density (i.e., low-pressure, shallow-ocean) data suggests that the CO_2 had not come to thermal equilibrium with the surrounding sea water when the spectra were acquired. In such cases, our assumption that the temperature of the CO_2 sample was the same as that of the ambient sea water would have lead to a miscalculation of the density of the CO_2.

In other experiments testing the possibility of ocean sequestration of CO_2, liquid CO_2 was analyzed where it had been deposited at 3600 m depth on the sea floor. At these depths, the density of CO_2 exceeds that of sea water, and the liquid CO_2 remains essentially where it was deposited. The Raman probe head was focused into liter-scale immiscible blobs of CO_2, using several different observation geometries (Fig. 5). In some experiments, the laser was projected through the side wall of or directly down onto an open-topped glass vessel into which CO_2 had been injected from the delivery system on the ROV. In other experiments, the laser was projected onto a CO_2 blob placed directly on the sediments of the ocean floor, contained inside of a 50-cm-

diameter PVC “corral.” Figure 9 shows a typical spectrum acquired on a CO_2 blob deposited directly onto the ocean floor. The CO_2 bands are superimposed on the background seawater spectrum.

Gases and Their Detection Limits. For our laboratory instrument, we evaluated the detection limits for gas species, based on the use of a stand-off optic with 60 mW of laser power exiting from it. Samples of 1 atm CO_2, 0.7 atm N_2, 0.2 atm O_2, or 0.01 atm of H_2O vapor were contained in an Erlenmeyer flask, and the laser was focused through the wall of the glass vessel. We collected 64 acquisitions of 10 seconds each and determined the following detection limits: 0.2 bar CO_2, 0.1 bar N_2, 0.1 bar O_2, 0.01 bar CH_4, and 0.01 bar H_2O vapor. These results are consistent with the well-documented fact that the Raman scattering cross-sections for CO_2, N_2, and O_2 are very similar, whereas the scattering cross-section for CH_4 is almost an order of magnitude greater.[24,37-38] The detection limit for CH_4 is therefore about 10X better than that for CO_2, N_2, and O_2.

The DORISS instrument, enclosed in its pressure-resistant housings, probably has somewhat less sensitivity than the laboratory instrument due to additional signal losses through the pressure-resistant fiber-optic cables, the penetrators through the pressure-resistant housings, and the protective glass dome in front of the stand-off optic. However, even on the maiden voyage of DORISS, operating at a laser output from the head of only 10 mW, we were able to acquire a reasonable spectrum of gaseous CO_2 at 31.33 bars pressure (CO_2 density of 0.077 g/cm^3) in one acquisition of 5 seconds duration (Fig. 10). As will be detailed in a subsequent paper, we also have measured natural occurrences of CH_4 and artificially introduced samples of gaseous CO_2 and N_2 at hundreds of meters depth in the ocean. Moreover, the peak positions of the gases were seen to change with gas density, as predicted theoretically and as determined in laboratory experiments.

Solids. To test our capability in manipulating the probe head into focus on a rock or mineral sample fully immersed in seawater, we strapped several samples of carbonate rocks and carbonate minerals to the outside of a 50-cm-diameter PVC ring and took them to the ocean floor (Fig. 11)**.** In one geometrical configuration, the DORISS probe head projected the laser perpendicular to the approximately 7 x 10 cm face of a translucent, yellow, cleaved rhomb of calcite ($CaCO_3$) affixed to the PVC ring. The ROV operator adjusted the focus of the laser on the calcite by using the robotic arm of the ROV to move the PVC ring. This configuration readily produced a strong Raman spectrum of calcite (Fig. 11b) superimposed on the background spectrum of seawater (not shown).

The superposition of the seawater spectrum does not appreciably degrade the signal:noise ratio of spectra taken of minerals on the ocean floor: The positions and strengths of the Raman bands of sea water are such that they do not interfere significantly with the bands of most minerals. The OH-stretch bands of many hydrated and hydroxylated minerals tend to be much narrower than and readily distinguished from those of water. In minerals with weak OH bands, however, the latter could be buried in the strong bands for water.

To date, there has been only one instance in which very high fluorescence precluded useful Raman measurements. This effect occurred when the laser was directed onto clay-rich, organic-rich sediments of the ocean floor, in this case, in Monterey Canyon west of Moss Landing, CA. Such fluorescence occurred both during *in situ* measurements and in measurements made in the laboratory on core samples recovered from the same region of the sea floor.

ADDITIONAL CHALLENGES

Selection of Better Calibration Standards. The results of the initial dives in 2002-2003 show that the deep-ocean environment changes not only the position of the 0 Δ cm^{-1} on the CCD

detector, but also the dispersion of the spectrometer and the intensity response of the integrated system. An *in-situ* full calibration protocol is therefore needed during deployment of the DORISS. One possible solution is to incorporate all three calibration sources (Ne lamp, white-light standard, and Raman-shift standard) into the pressure-resistant housing of the probe head. This configuration would necessitate additional electronic controls and electro-mechanical devices to bring the calibration sources into and out of the optical path. An alternative and simpler solution in the future might be to use as a wavelength standard the ROV's lights, which typically have been turned off during spectral acquisition. First, however, the Raman band positions and intensities of these lights need to be determined at the temperatures encountered during the deep-ocean calibration.

The selection of Raman-shift standards for *in-situ* calibration also has been difficult. Such standards: 1) should have numerous, narrow bands distributed across the entire 100-4000 Δcm^{-1} region, 2) should be stable and transportable to depth in seawater (if a container is required, it must be transparent to the laser), and 3) either should not be spectrally sensitive to changes in temperature and pressure, i.e., density, or should have a very well-known spectral response to changes in density. Some liquids that are commonly used in the laboratory as Raman-shift standards, such as isopropanol (which we did take to the ocean floor in our first deep ocean dives), are much more compressible than water; this means that they undergo significant changes in density, which can be assumed to be accompanied by significant changes in band positions, making them unreliable calibration standards.

Solid samples such as minerals, in principle, should be better calibration standards than liquids, provided that they exhibit a sufficient number of strong, narrow Raman bands over the spectral range of interest. The diamond standard has been extremely useful in our experiments thus far because the temperature and pressure sensitivity of its Raman band is fully known and because this band lies between those of the Fermi diad of CO_2. We currently are investigating

the use of hydrous silicate minerals or polystyrene as a standard. It would be particularly useful if the standard were placed within the housing of the probe head so that only thermal effects would need to be considered.

Improvement of Control on Laser Focus. Laser Raman spectroscopy is a scattering phenomenon that calls for the laser to be focused on a relatively small volume of material in order to create sufficient power density. The same optics used to focus the laser also permit the spatial isolation of the scattering signal. With appropriate optics, one selectively can retrieve the back-scattered radiation and thereby isolate the signal of the desired target from that of its background/matrix.

Whether the Raman spectrometer is configured with a probe head fixed within an optical microscope (in the laboratory) or with a mobile probe head (for sea-floor operation), there are three important issues to consider in the selection of a focusing lens: power-density at the sample, focal length (more specifically, working distance), and depth-of-field. These parameters, of course, are not independent of each other.[39-40] For instance, the power-density of the laser irradiation, which is inversely proportional to the size of the focused beam spot, is controlled by the magnification and numerical aperture of the lens.

In our first year of deployments of the DORISS in the deep ocean, the ROV pilot controlled the position of the Raman probe head with respect to the target object through manipulation of the probe head, the sample, or both by the robotic arm of the ROV. A combination of visual observation of the laser on the sample via the HDTV cameras and the continuous, real-time display of the Raman spectrum recorded by the DORISS system were used when adjusting the sample to improve its focus within the laser irradiation volume (Fig. 12). This type of sample positioning, which can be precise to within several millimeters, depends mostly on the fine-motor skills of the individual pilot who maneuvers the robotic arm of the ROV and the functioning of the

arm mechanics at that time. Under these conditions, it is better for the Raman probe head to have a focusing lens that offers a working distance of 5 cm or more to reduce the potential of a collision between the sample and the protective glass dome of the Raman probe head. Large working distances (or focal lengths), however, typically correlate with a large depth-of-field. The latter permits reasonable laser-focusing and recovery of the Raman signal even if the distance between the probe head and the sample is difficult to control at the sub-millimeter level. Thus, the f/2 lens of the dry optic permitted focus through sea water onto an immiscible blob of carbon dioxide on the ocean floor (Figs. 9, 12), through a glass beaker into the liquid CO_2 within it, as well as through sea water into a transparent fragment of the mineral calcite (Fig. 11).

Studying samples immersed in the ocean, however, demonstrated two drawbacks to the large working distance (focal length) of the focusing lens that we predominantly have used so far. Firstly, the laser has a long path length through the ambient medium (sea water) before it reaches the target at the laser focal point. Although this surrounding medium is not at the point of laser focus, the sea water does scatter the beam (thereby decreasing the laser intensity on the intended target), and some of that back-scattered light is accepted by the lens. This means that the spectrum of the sample is always superimposed on that of the background (Figs. 3, 9, 12). Secondly, this spectral superposition eliminates the ability of the Raman probe to spatially resolve compositional differences that occur along the laser beam path, e.g., changes in concentration of dissolved components.

For the above reasons, we have begun testing the use of a high-pressure immersion tip, also with an f/2 lens, but with only a 7-mm working distance in water and a small depth of field. For purposes of the present discussion, however, we find it more useful to define a parameter called the “Raman depth of focus,” which is the distance over which the sample-to-lens distance can be varied while maintaining an intensity of Raman-scattering from an opaque sample that is within 50% of the maximum recorded Raman intensity from that sample. By this definition, the

immersion lens has a Raman depth of focus about 0.2 mm in air as compared to about 1.0 mm Raman depth of focus in air for the dry lens. The smaller beam spot (greater focusing) of the immersion lens produces higher signal:noise ratios, and its shorter focal length produces better rejection of a background sea-water signature than does the dry optic. The small Raman depth of focus of the immersion probe is not a problem when the tip is immersed in a gaseous or liquid sample. However, for analysis of an opaque or semi-opaque sample, the immersion lens's smaller Raman depth of focus requires finer control of the sample positioning than is possible with the robotic arm alone.

Another challenge to the focusing capability of the DORISS instrument comes from optical interfaces. Because Raman spectroscopy is a scattering phenomenon, the retrieved signal is affected by all aspects of optical scattering within the sample and on the sample's surface. The case of two transparent liquids with a smooth (although curved) shared interface, as between immiscible liquid CO_2 and water, creates no strong optical problem, as long as the laser is aimed perpendicular to the interface (see Fig. 12). Samples that are milky translucent or extremely fine-grained (whether as powders or consolidated solid masses), however, cause almost the same optical responses as opaque phases. This non-penetration of the interface is due to light scattering, whose intensity tracks with the difference in refractive index between the two (admixed) substances. Thus, even with the relatively large depth of field of the dry optic in its pressure housing, we were unable with the DORISS to obtain a good Raman signal from the fine-grained, milky translucent limestone and marble samples (both rocks are calcium carbonate, i.e., calcite) fixed onto the PVC corral, although the signal from the transparent calcite was very strong (Fig.11). The same scattering phenomenon apparently prevented us from collecting Raman spectra from the CO_2 clathrate-hydrate polycrystalline mush that formed in some of our experiments.

These optical challenges provided the impetus for additional engineering upgrades to the instrument. We are in the process of developing a precision underwater positioner, as a separate, portable platform that can be carried and deployed by an ROV. It will be off-loadable onto the sea floor, so as to decouple the probe head from ROV-induced motion or vibration. The positioner will be able to place the probe head with an accuracy and reproducibility on the order of 0.1 mm.

Reduction in Weight and Size. The large size and weight of the current version of DORISS make it difficult to transport any additional equipment to the ocean floor when Raman measurements are planned. We therefore are considering both how to reduce the weight of the current base instrument (e.g., by linearizing the optical bench) and whether a different base instrument might be re-configured to a DORISS instrument. The goal is to make DORISS so small and lightweight that it can be used routinely in conjunction with other types of geochemical and geophysical instruments carried down by the ROV and deployed on the ocean floor.

SUMMARY AND CONCLUSION

We have demonstrated that it is possible to obtain on the sea floor at 3600 m depth Raman spectra that have a high signal:noise ratio and very good spectral resolution. The main reason that Raman spectroscopy has not been used previously in this environment is that only recently have the following essentials become available: 1) Sophisticated carrying platforms such as research ROVs; 2) small, light-weight, portable Raman instruments; and 3) small stable solid-state lasers. Third-generation Raman spectrometers are now available with holographic gratings, high throughput, and very sensitive CCD detectors that provide the small size and the stability that permitted us to construct the DORISS system.

During construction and implementation of the DORISS, there were many difficulties that needed to be overcome: limitation of size and weight, elimination of fragile optical components, building of housings resistant to pressure and temperature and water, and the establishment of electronic communication and control over a 4-km-long tether from the ship to the remotely operated vehicle and the deep ocean Raman system.[13]

We have accomplished the first feasibility tests, but we are still in the early stages of solving problems. We have been able to carry out some aspects of calibration (with a diamond chip in the optical path), but we need to improve our methods of both wavelength and intensity calibration. The challenges of precise positioning and focus of the laser have limited our successful analyses to large, transparent objects on the first dives. In response to the needs for accurate laser positioning, focus, and manipulation in the Raman analysis of solid phases (rocks, precipitates, etc.), we are designing a precision underwater positioning system for measurement of solids in the deep ocean. We also plan to add “through-the-lens visualization” to guide our positioning of the laser beam onto the target of interest.

ACKNOWLEDGMENTS

This research was supported by the David and Lucile Packard Foundation and the United States Department of Energy Ocean Carbon Sequestration Program (grants no. DE-FC26-00NT40929 and DE-FC03-01ER6305). We gratefully acknowledge MBARI's Mark Brown for his engineering and design help and Danelle Cline for her skilled work in implementing the software for system operation. The staff of Kaiser Optical, Inc. are thanked for their willingness to provide information necessary to the re-configuring of the spectrometer and its software. We thank the following people for providing carbonate samples that were taken to the sea floor: Bob Cradock, Cheryl Seeger, Jere Cadoret, and Larry Nuelle. We thank the officers and crew of the RVs Point Lobos and Western Flyer, and the ROV pilot teams of Ventana and Tiburon, for their skill and support at sea.

Figure Captions

Fig. 1. Schematic overview (not to scale) of the sampling and data-communication systems of the deep-ocean Raman *in-situ* spectrometer (DORISS) system. The remotely operated vehicle (ROV) is tethered by copper wiring (electrical) and fiber-optic bundles (communication) to the research vessel. DORISS' electronics and spectrometer housings remain in the tool sled of the ROV, whereas the probe head is held by the robotic arm and moved to the sampling site.

Fig. 2. Schematic view of the distribution of DORISS' components among three pressure-resistant housings: A) electronics, B) spectrometer, and C) probe head. (The handle on the probe head housing and the fiber-optic cables connecting the three housings are not shown here.)

Fig. 3. Comparison of isopropanol spectra acquired with DORISS onboard the research ship in the Pacific Ocean (DORISS Deck), with DORISS at 3600 m ocean depth on the ROV Tiburon (DORISS 3600 m), and with the duplicate laboratory Raman system at Washington University (Laboratory). Data for both the low-wavenumber (a) and high-wavenumber (b) spectral regions. For these spectra, a 100-μm spectral slit was used on the laboratory instrument, but no slit was used on the DORISS. The broad double-band feature at 3200-3500 Δcm^{-1} arises from the intervening sea water.

Fig. 4. Comparison of spectral quality and peak positions measured with DORISS and with the well-calibrated duplicate laboratory Raman system at Washington University. (a) Blow-up of one of the many Raman peaks for isopropanol (b) Blow-up of the only Raman-active peak for

diamond. The spectra were acquired with DORISS onboard the research ship in the Pacific Ocean (DORISS Deck), with DORISS at 3600 m ocean depth on the ROV Tiburon (DORISS 3600 m), and at Washington University (Laboratory). The laboratory instrument had a 100-μm spectral slit, whereas the DORISS had no slit for the acquisition of these spectra.

Fig. 5. Laser-sample interaction in three types of experimental configurations during Raman analysis on the deep ocean floor: a) CO_2-water-hydrate "slush" in a beaker on sea floor; probe head focused horizontally into beaker; b) probe head focused vertically down onto large, clear blob of CO_2 that almost completely covers bottom of corral; c) robotic arm (vertical, black) holds probe head and brings the laser into focus on (and through) CO_2-water-hydrate slush in graduated cylinder; large beaker of similar slush lies on its side on ocean floor (bottom, left). The whitish glow, sparkle, and beam seen in Figs. 5a,b, and c, respectively, appear as an intense green color on the ship's monitors.

Fig. 6: Comparison of the Raman spectra of deionized water (acquired with the laboratory system at Washington University at room temperature) and ocean water (acquired with the MBARI Deep Ocean Raman System at 3600 m depth and 4° C). Inset shows enlargement of 800 to 1900 Δcm^{-1} spectral region. The laboratory system had a 100-μm spectral slit, whereas the DORISS had no slit (resolution imposed by 100-μm collection fiber).

Fig. 7. Raman spectra of liquid and gaseous CO_2 collected during small-scale CO_2 injection experiments on the ROV Tiburon. Raman spectra were acquired during ascent from the ocean floor while DORISS was sitting in the ROV's toolsled. Difference in phase is recognized by strong increase in intensity and spectral downshift in the liquid compared to the gas. In this figure, the peak positions are uncorrected for depth-induced wavenumber shifts. The spectral separation

between the two CO_2 peaks (more accurately measurable than the absolute peak positions) is shown in Fig. 8.

Fig. 8. Plot of the Raman spectral separation between the two peaks of Fermi diad of CO_2 versus CO_2 density (see text). Laboratory data were collected at 23 °C at well calibrated pressures; Raman peak positions were corrected based on gas emission lines from calibration lamps.[22] DORISS data (uncorrected peak positions) were collected in ascent from 664 m depth in the ocean. Parallelism of laboratory and DORISS data indicates appropriate spectral response to changes in density. Offset between the two curves suggests that the dispersion function that was applied to the DORISS was inappropriate under the specific dive conditions.

Fig. 9. Raman spectrum taken by DORISS on a large liquid CO_2 blob artificially introduced directly onto the sea floor at 3600 m depth. Although only CO_2 was within the focal volume of the probe head, Raman scattering also was detected from the intervening sea water due to the long focal length of the probe optics.

Fig. 10. Raman spectra of CO_2 gas contained at 1 atm in an Erlenmeyer flask in the laboratory (upper trace) and contained in an inverted jam jar in the ocean at 300 m depth (lower trace). Laboratory spectrum also shows signature of air (O_2 and N_2) between flask and probe. Lab spectrum is the average of 64 10-second scans acquired with a 100-μm slit. DORISS spectrum is one 5-second scan acquired without a slit. Small peaks to the low- and high-wavenumber side of the CO_2 Fermi diad are hot bands.[34]

Fig. 11. a) Several sawn slabs of calcite and carbonate rocks (indicated by arrows) are strapped to a PVC corral at 663 m depth on sea floor. Probe head has been guided into focus on the large

calcite rhomb painted with a white vertical stripe. b) Raman spectrum of that calcite rhomb (1-second acquisition).

Fig. 12. Series of Raman spectra (each with 1-second acquisition time) as the probe head is moved away from optimal focus of the laser on a CO_2 liquid blob on the ocean floor. As explained in Fig. 9, both sea water and CO_2 are in the laser beam's path. Spectra of both phases are recorded, but the CO_2:H_2O band ratios vary with position of the probe head. The CO_2 blob is in best focus in spectrum a).

References

[1] M. Kraft, M. Jakusch, M. Karlowatz, A. Katzir, and B. Mizaikoff, Appl. Spec. **57**, 591 (2003).

[2] J.D. Pasteris, J.J. Freeman, S.K. Goffredi, and K.R. Buck, Chemical Geology **180**, 3 (2001).

[3] P.G. Brewer, G. Friederich, E.T. Pe.tzer, and F.M. Orr, Jr., Science **284**, 943 (1999).

[4] P.G. Brewer, E.T. Peltzer, G. Friederich, I. Aya, and K. Yamane, Marine Chemistry **72**, 83 (2000).

[5] M. Tamburri, E.T. Peltzer, G. Friederich, I. Aya, K. Yamane, and P.G. Brewer, Marine Chemistry **72**, 95 (2000).

[6] J.P. Barry, B.A. Seibel, J.C. Drazen, M.N. Tamburri, K.R. Buck, C. Lovera, L. Kuhnz, E.T. Peltzer, K. Osborn, P.J. Whaling, P. Walz, and P.G. Brewer, Proc. of the Second Annual Conference on Carbon Sequestration (May 5-8, 2003).

[7] C. Marchetti, Climatic Change 1, **59** (1977).

[8] N. Handa and T. Ohsumi, *Direct Ocean Disposal of Carbon Dioxide* (Terra Scientific Publishing, Tokyo, 1995).

[9] E.A. Parson and D.W. Keith, Science **282**, 1054 (1998).

[10] E.D. Sloan, *Clathrate Hydrates of Natural Gases* (Marcel Dekker, Inc., New York, 1998).

[11] B.A. Buffett, Ann. Rev. Earth Planet. Sci. **28**, 477 (2000) .

[12] M.D. Max, Ed. *Natural Gas Hydrate in Oceanic and Permafrost Environments* (Kluwer Academic Publishers, Dordrecht, The Netherlands, 2000).

[13] P.G. Brewer, G. Malby, J.D. Pasteris, S.N. White, E.T. Peltzer, B. Wopenka, J. Freeman, and M. O. Brown, Deep-Sea Research, in revision.

[14] X. Zheng, W. Fu, S. Albin, K.L. Wise, A. Javey, J.B. Cooper, Appl. Spectros. **55**, 382 (2001).

[15] D. Schiferl, M. Nicol, J.M. Zaug, S.K. Sharma, T.F. Cooney, S.-Y. Wang, T.R. Anthony, and J.F. Fleischer, J. Appl. Phys. **82**, 3256 (1997).

[16] F. Azam and R.A. Long, Nature **414**, 495 (2001).

[17] J.S. Bartlett, K.J. Voss, S. Sathyendranath, and A. Vodacek, Appl. Optics **37**, 3324 (1998).

[18] M. Becucci, S. Cavalieri, R. Eramo, L. Fini, and M. Materazzi, Appl. Optics **38**, 928 (1999).

[19] T. P. Mernagh and A.R. Wilde, Geochim. Cosmochim. Acta **53**, 765 (1989).

[20] K. Furić, I.Ciglenečki, and B. Ćosović, J. Molec. Struc. **550-551**, 225 (2000).

[21] J. Dubessy, T. Lhomme, M.-C. Boiron, and F. Rull, Appl. Spec. **56**, 99 (2002).

[22] J.C. Seitz, J.D. Pasteris, and I-M. Chou, American Journal of Science **296**, 577 (1996).

[23] R. B. Wright and C.H. Wang, J. Chem. Phys. **58**, 2893 (1973).

[24] H.W. Schrötter and H.W. Klöckner, in *Raman Spectroscopy of Gases and Liquids*, A. Weber, Ed. (Springer-Verlag, New York, 1979) pp. 123-166.

[25] Y. Garrabos, R. Tufe, and R. Le Neindre, J. Chem. Phys. **72**, 4637 (1980).

[26] Y. Garrabos, M.A. Echargui, and F. Marsault-Herail, J. Chem. Phys. **91**, 5869 (1989).

[27] A. Hacura, Physics Letters A **227**, 237(1997).

[28] B. Maté, G. Tejeda, and S. Montero, J. Chem. Phys. **108**, 2676 (1998).

[29] Y. Gu, Y. Zhou, H. Tang, E.W. Rothe, and G.P. Reck, Appl. Phys. B, **71**, 865.

[30] M.A. Blatchford and S.L. Wallen, S.L., Anal. Chem. **74**, 1922 (2002).

[31] A.R. Davis, J. Solution Chemistry **1**, 329 (1972).

[32] T.M. Abbott, G.W. Buchanan, P. Kruus, and K.C. Lee, Canad. J. Chem. **60**, 1000 (1982).

[33] A.J. Berger, Y. Wang, D.M. Sammeth, I. Itzkan, K. Kneipp, and M.S. Feld, Appl. Spectrosc. **49**, 1164 (1995)

[34] G. Herzberg, *Molecular Spectra and Molecular Structure* (Van Nostrand Reinhold Company, New York, 1945).

[35] R. Span and W. Wagner, J. Physical Chemistry Reference Data **25**, 1509 (1996).

[36] Website for ChemicaLogic Corp., Burlington, MA: http://www.chemicalogic.com/

[37] B. Wopenka and J.D. Pasteris, Anal. Chem. **59**, 2165 (1987).

[38] J. Dubessy, B. Poty, and C. Ramboz, Eur. J. Mineral. **1**, 517 (1989).

[39] I. Newton, Opticks, or, *A Treatise of the Reflections, Refractions, Inflections and Colours of Light*, based on the 4th edition London of 1730 (Dover Publications, Inc., New York, 1979).

[40] Nikon Corporation website on microscopy

http://www.microscopyu.com/articles/formulas/formulasfielddepth.html

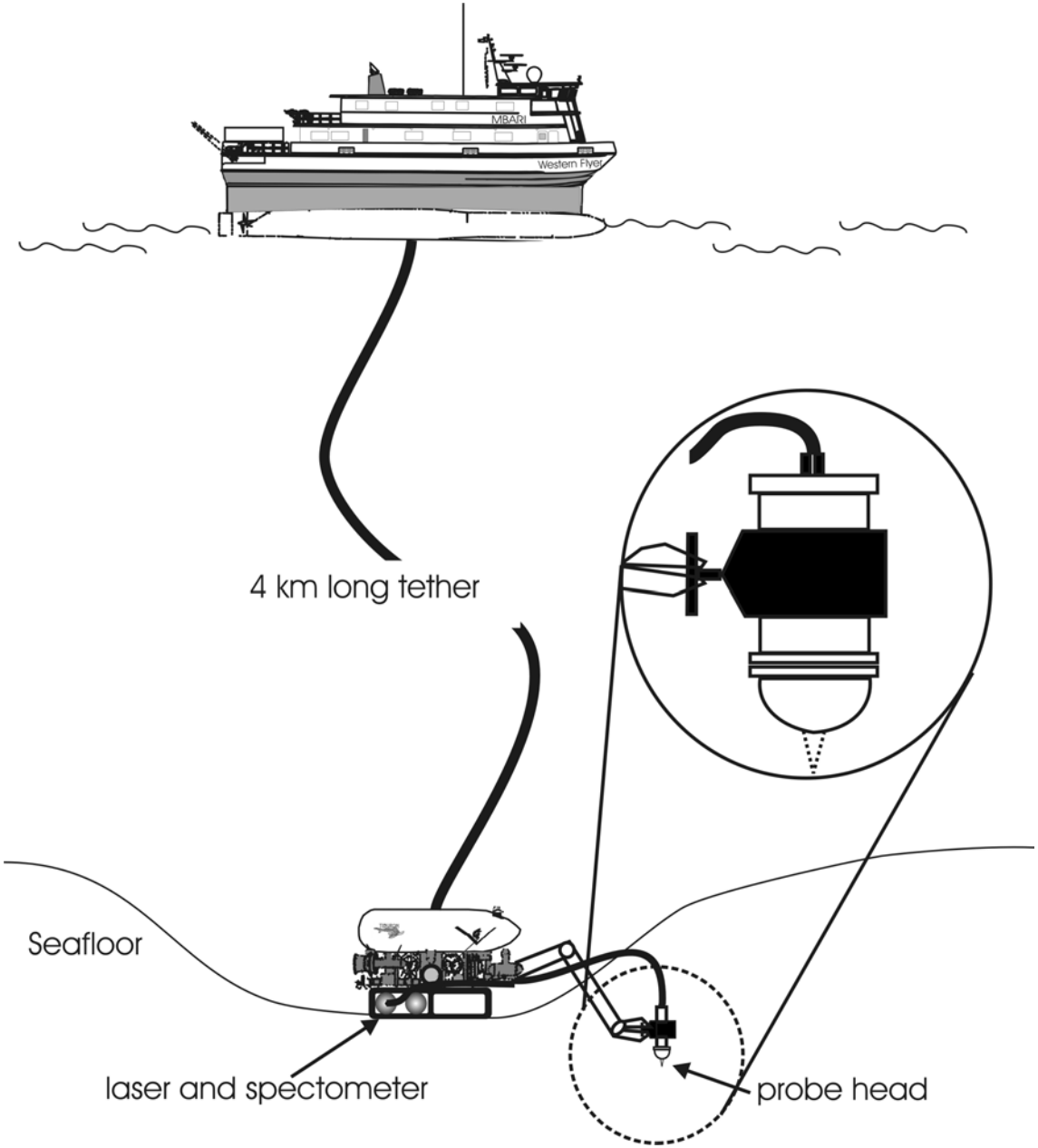

Fig. 1. Schematic overview (not to scale) of the sampling and data-communication systems of the deep-ocean Raman *in-situ* spectrometer (DORISS) system. The remotely operated vehicle (ROV) is tethered by copper wiring (electrical) and fiber-optic bundles (communication) to the research vessel. DORISS' electronics and spectrometer housings remain in the tool sled of the ROV, whereas the probe head is held by the robotic arm and moved to the sampling site.

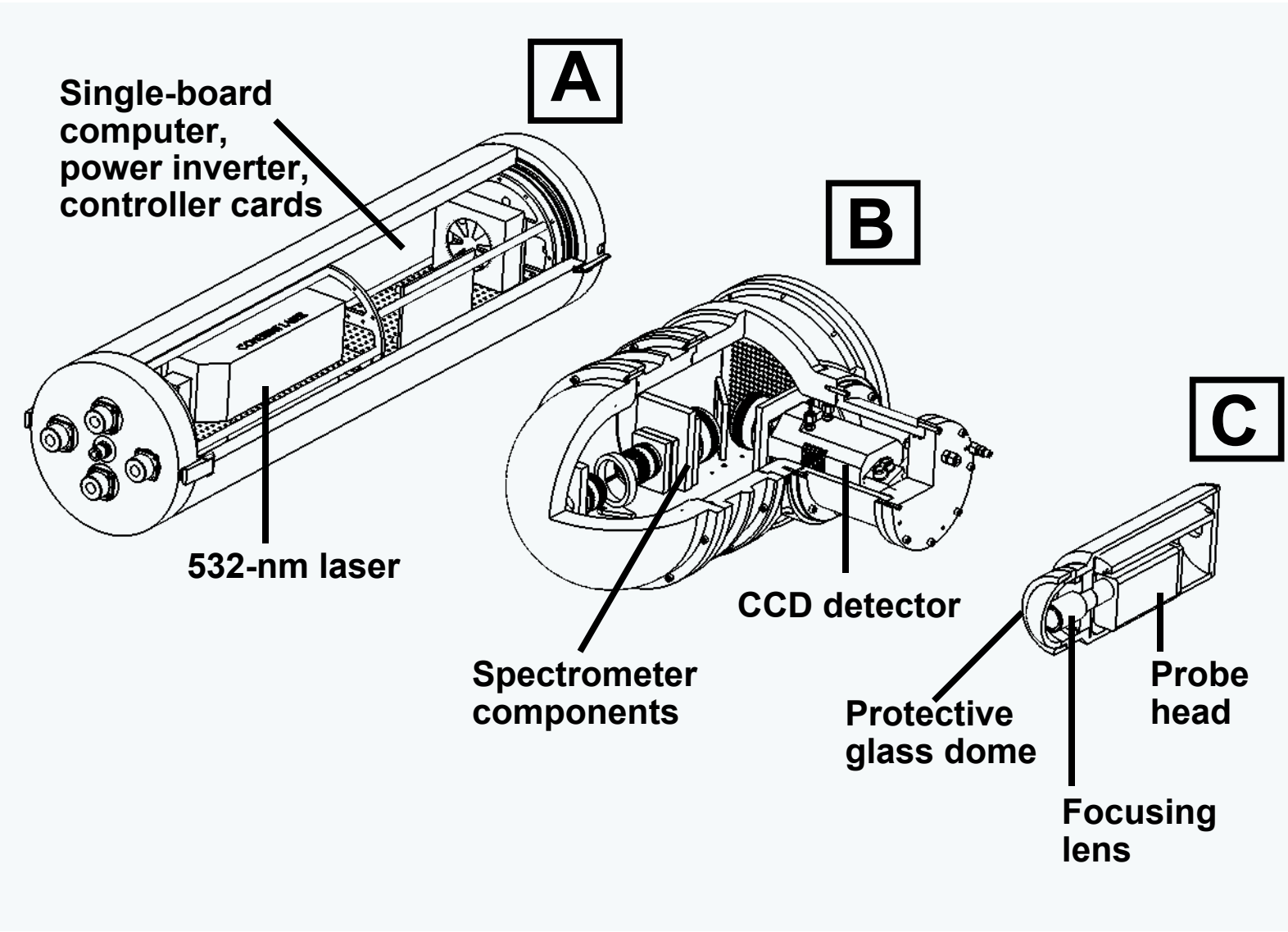

Fig. 2. Schematic view of the distribution of DORISS' components among three pressure-resistant housings: A) electronics, B) spectrometer, and C) probe head. (The handle on the probe head housing and the fiber-optic cables connecting the three housings are not shown here.)

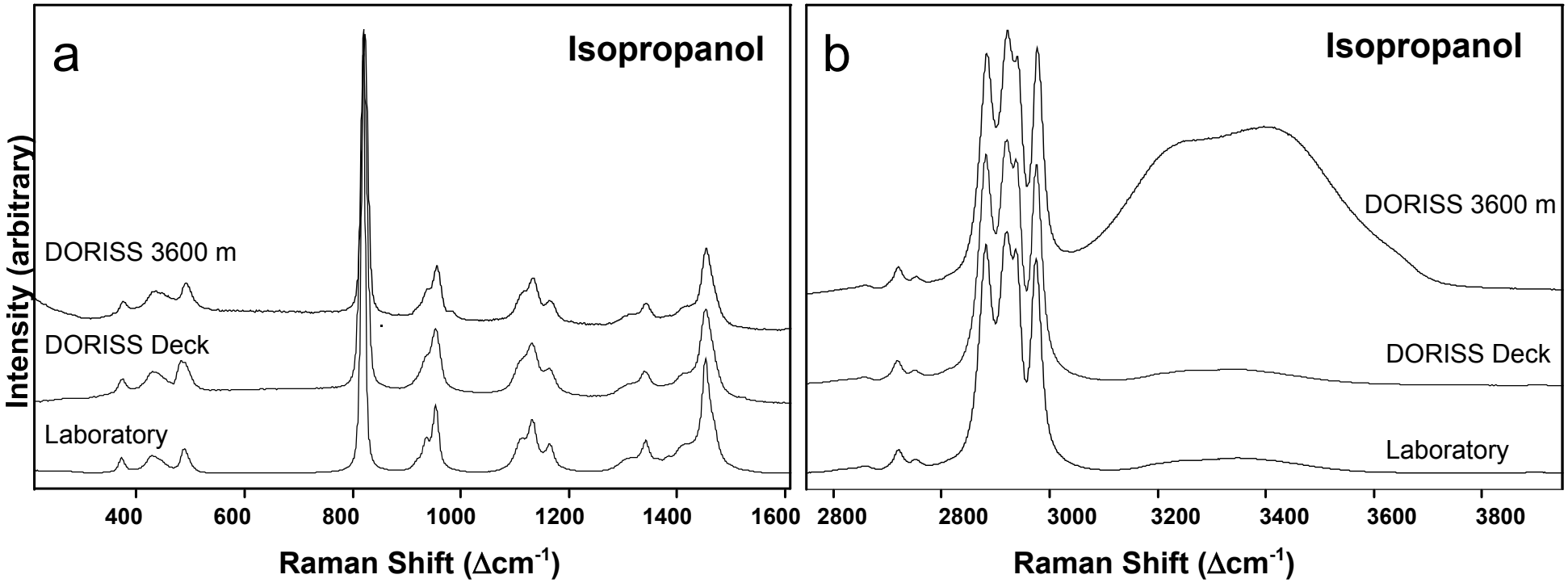

Fig. 3. Comparison of isopropanol spectra acquired with DORISS onboard the research ship in the Pacific Ocean (DORISS Deck), with DORISS at 3600 m ocean depth on the ROV Tiburon (DORISS 3600 m), and with the duplicate laboratory Raman system at Washington University (Laboratory). Data for both the low-wavenumber (a) and high-wavenumber (b) spectral regions. For these spectra, a 100-μm spectral slit was used on the laboratory instrument, but no slit was used on the DORISS. The broad double-band feature at 3200-3500 Δcm^{-1} arises from the intervening sea water.

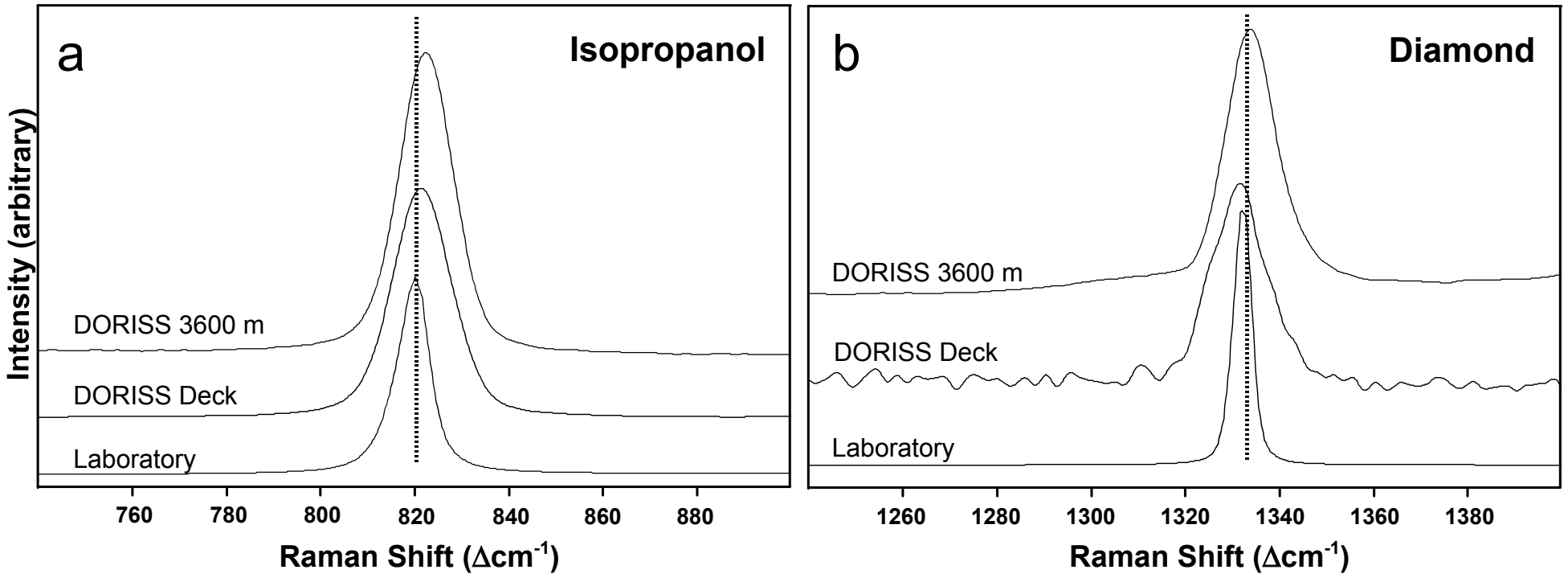

Fig. 4. Comparison of spectral quality and peak positions measured with DORISS and with the well-calibrated duplicate laboratory Raman system at Washington University. (a) Blow-up of one of the many Raman peaks for isopropanol (b) Blow-up of the only Raman-active peak for diamond. The spectra were acquired with DORISS onboard the research ship in the Pacific Ocean (DORISS Deck), with DORISS at 3600 m ocean depth on the ROV Tiburon (DORISS 3600 m), and at Washington University (Laboratory). The laboratory instrument had a 100-μm spectral slit, whereas the DORISS had no slit for the acquisition of these spectra.

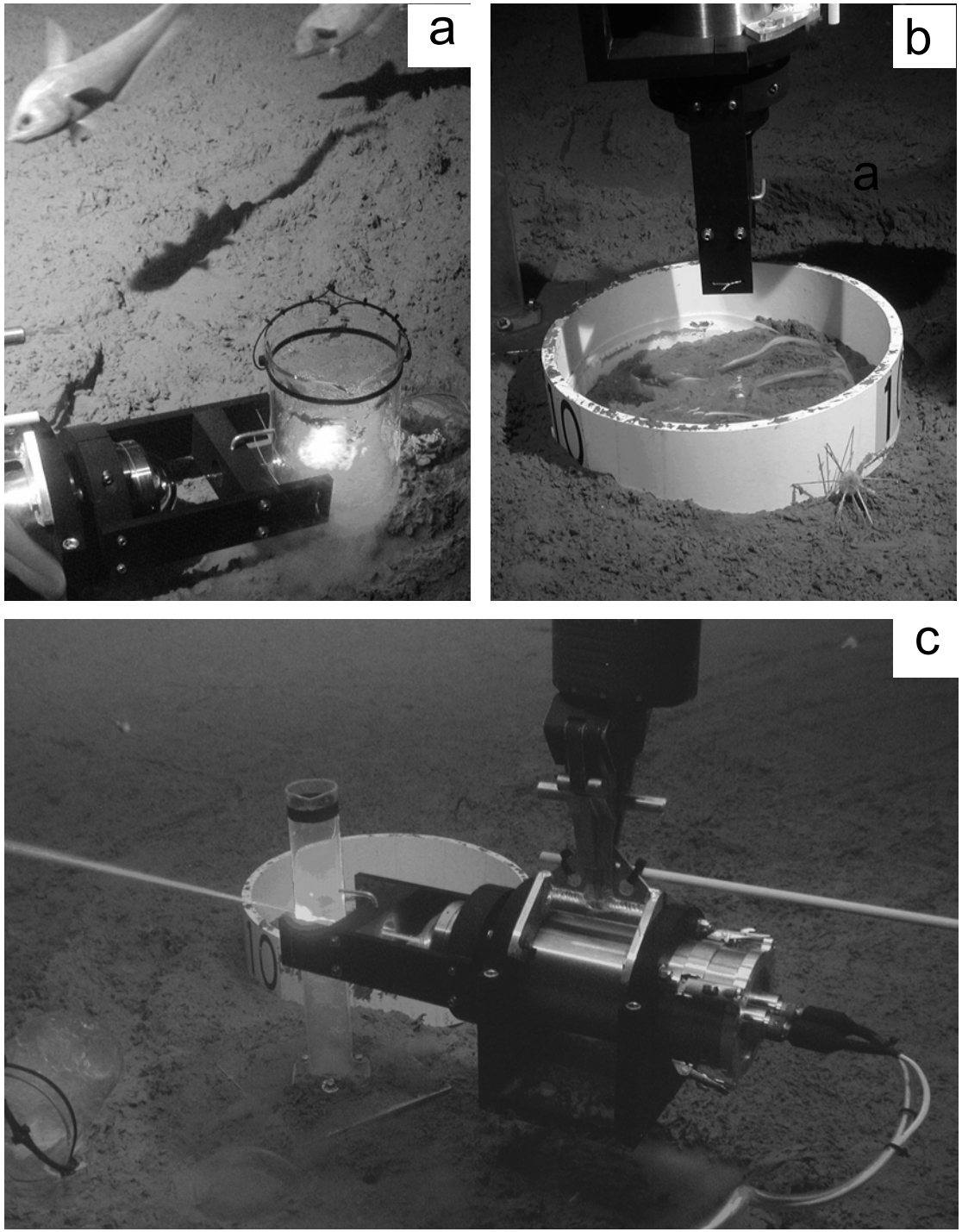

Fig. 5. Laser-sample interaction in three types of experimental configurations during Raman analysis on the deep ocean floor: a) CO_2-water-hydrate "slush" in a beaker on sea floor; probe head focused horizontally into beaker; b) probe head focused vertically down onto large, clear blob of CO_2 that almost completely covers bottom of corral; c) robotic arm (vertical, black) holds probe head and brings the laser into focus on (and through) CO_2-water-hydrate slush in graduated cylinder; large beaker of similar slush lies on its side on ocean floor (bottom, left). The whitish glow, sparkle, and beam seen in Figs. 5a,b, and c, respectively, appear as an intense green color on the ship's monitors.

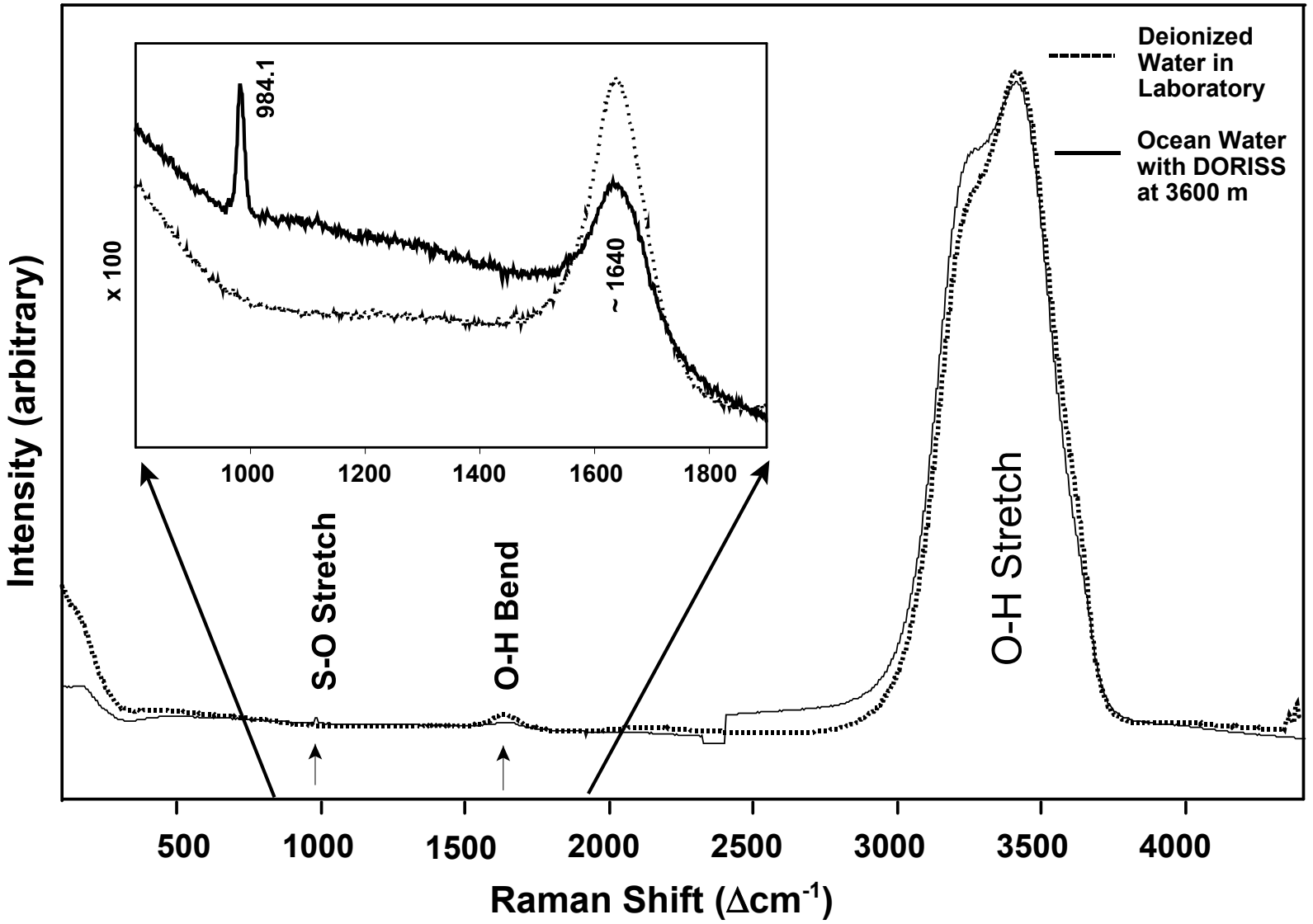

Fig. 6: Comparison of the Raman spectra of deionized water (acquired with the laboratory system at Washington University at room temperature) and ocean water (acquired with the MBARI Deep Ocean Raman System at 3600 m depth and 4 ° C). Inset shows enlargement of 800 to 1900 Δcm^{-1} spectral region. The laboratory system had a 100-μm spectral slit, whereas the DORISS had no slit (resolution imposed by 100-μm collection fiber).

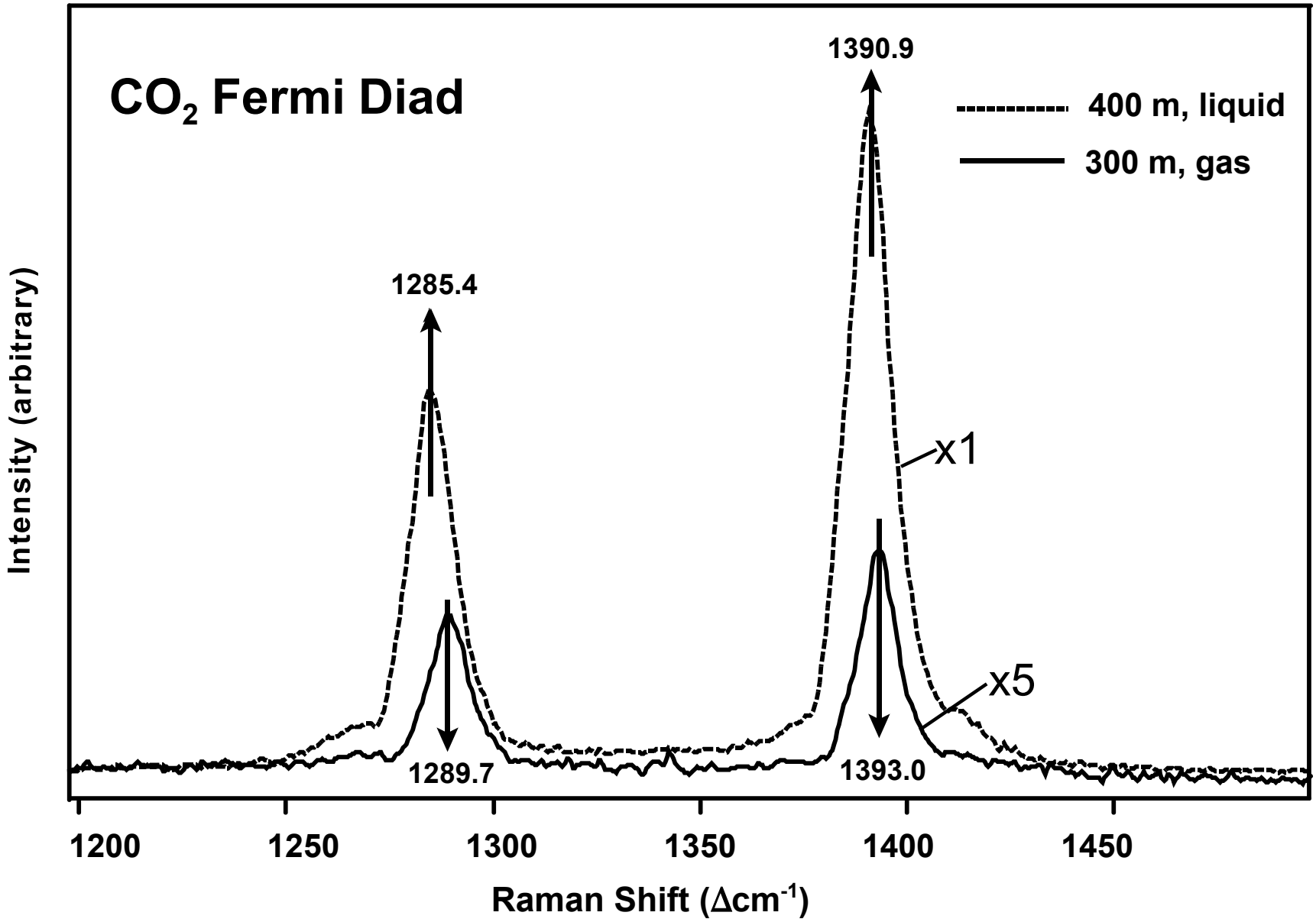

Fig. 7. Raman spectra of liquid and gaseous CO_2 collected during small-scale CO_2 injection experiments on the ROV Tiburon. Raman spectra were acquired during ascent from the ocean floor while DORISS was sitting in the ROV's toolsled. Difference in phase is recognized by strong increase in intensity and spectral downshift in the liquid compared to the gas. In this figure, the peak positions are uncorrected for depth-induced wavenumber shifts. The spectral separation between the two CO_2 peaks (more accurately measurable than the absolute peak positions) is shown in Fig. 8.

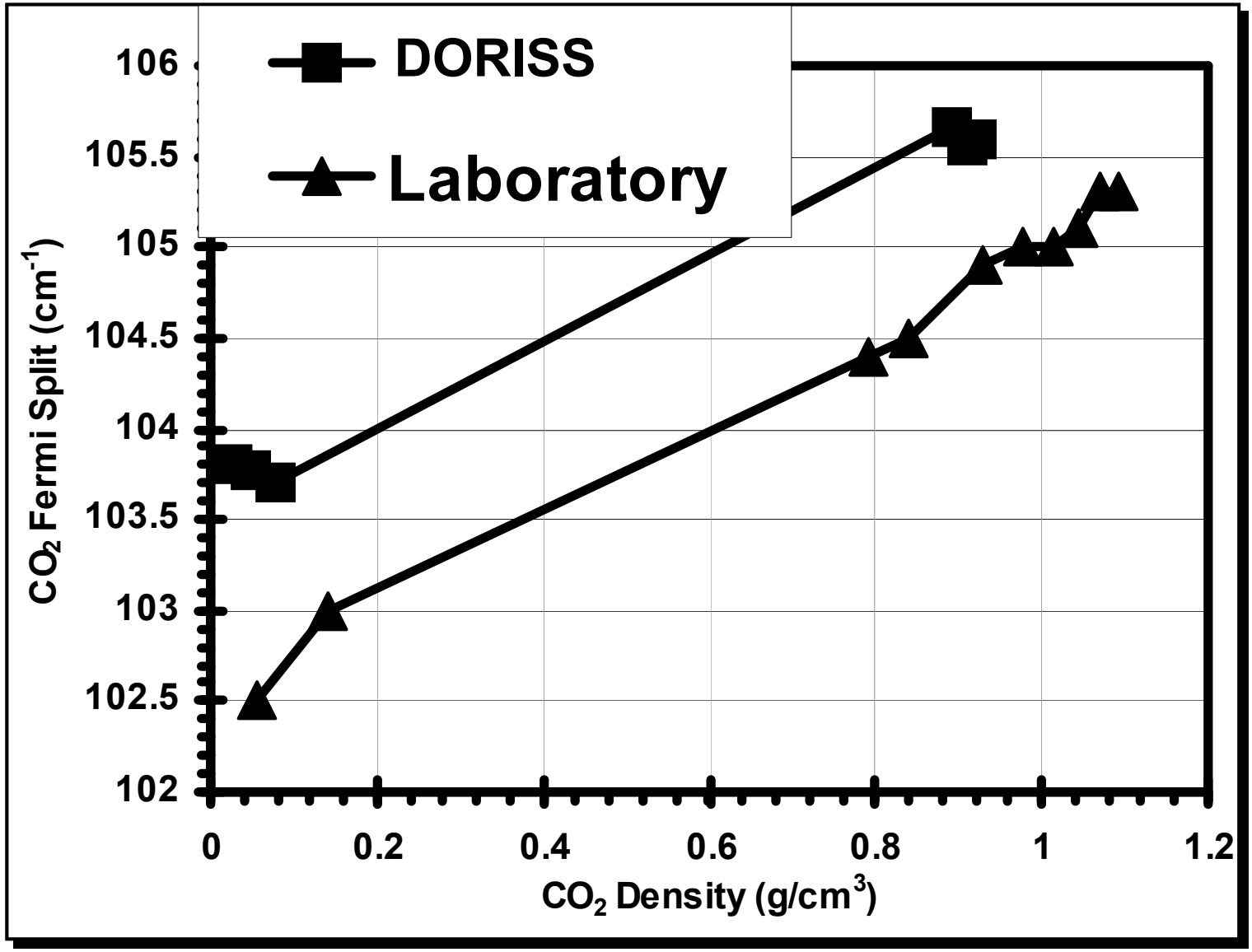

Fig. 8. Plot of the Raman spectral separation between the two peaks of Fermi diad of CO_2 versus CO_2 density (see text). Laboratory data were collected at 23 °C at well calibrated pressures; Raman peak positions were corrected based on gas emission lines from calibration lamps.[22] DORISS data (uncorrected peak positions) were collected in ascent from 664 m depth in the ocean. Parallelism of laboratory and DORISS data indicates appropriate spectral response to changes in density. Offset between the two curves suggests that the dispersion function that was applied to the DORISS was inappropriate under the specific dive conditions.

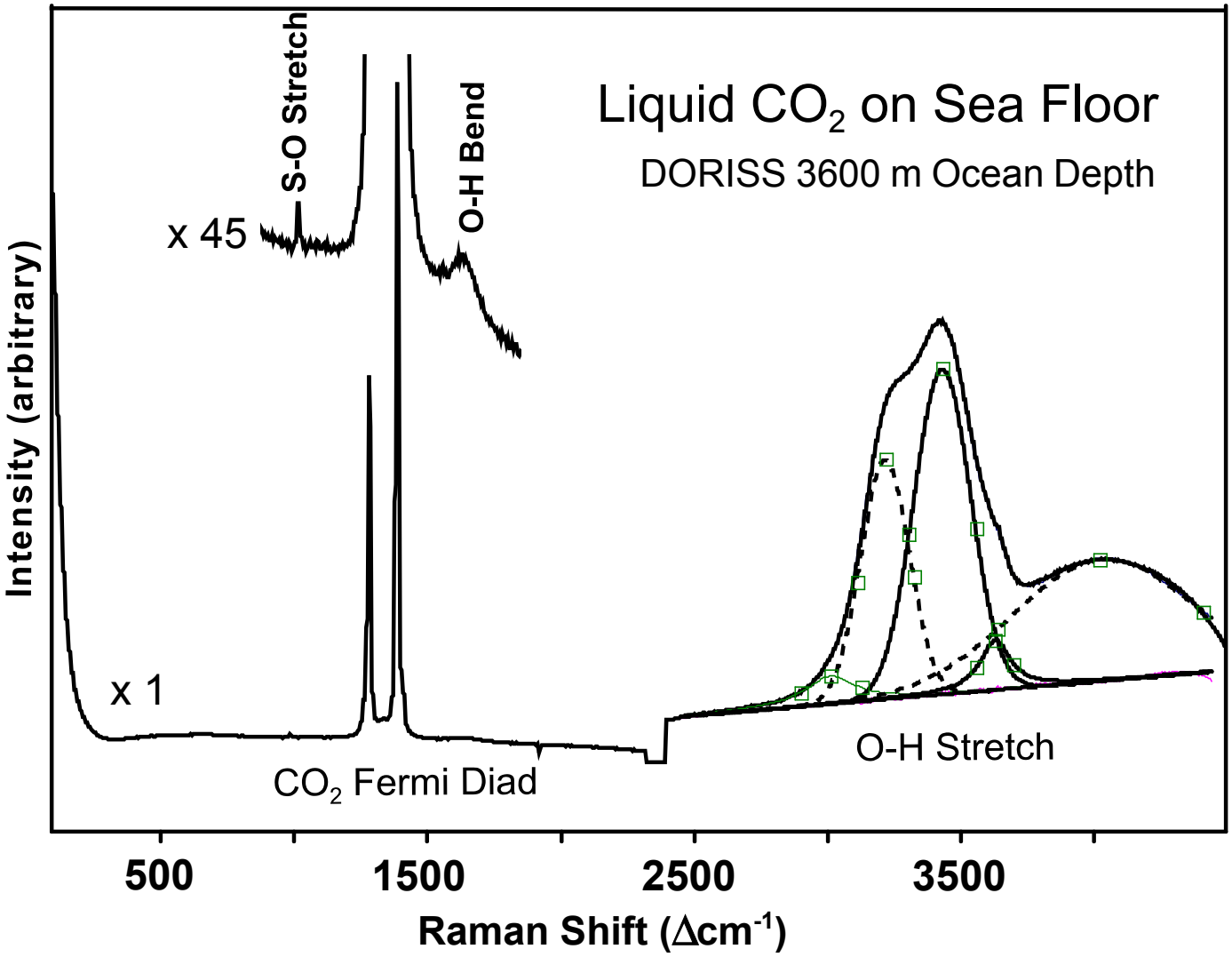

Fig. 9. Raman spectrum taken by DORISS on a large liquid CO_2 blob artificially introduced directly onto the sea floor at 3600 m depth. Although only CO_2 was within the focal volume of the probe head, Raman scattering also was detected from the intervening sea water due to the long focal length of the probe optics.

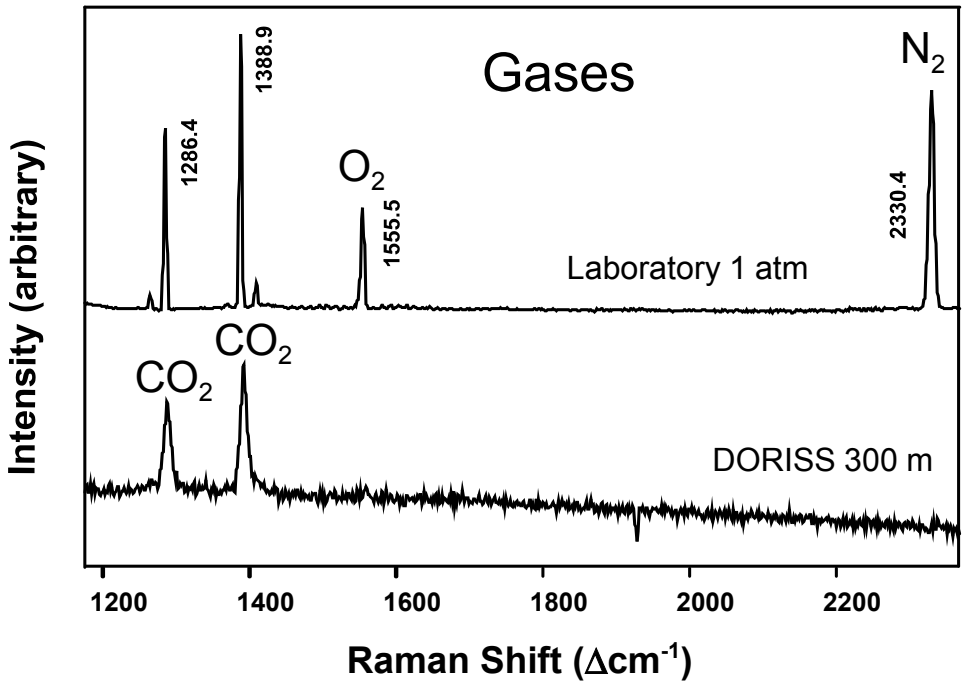

Fig. 10. Raman spectra of CO_2 gas contained at 1 atm in an Erlenmeyer flask in the laboratory (upper trace) and contained in an inverted jam jar in the ocean at 300 m depth (lower trace). Laboratory spectrum also shows signature of air (O_2 and N_2) between flask and probe. Lab spectrum is the average of 64 10-second scans acquired with a 100-μm slit. DORISS spectrum is one 5-second scan acquired without a slit. Small peaks to the low- and high-wavenumber side of the CO_2 Fermi diad are hot bands.[34]

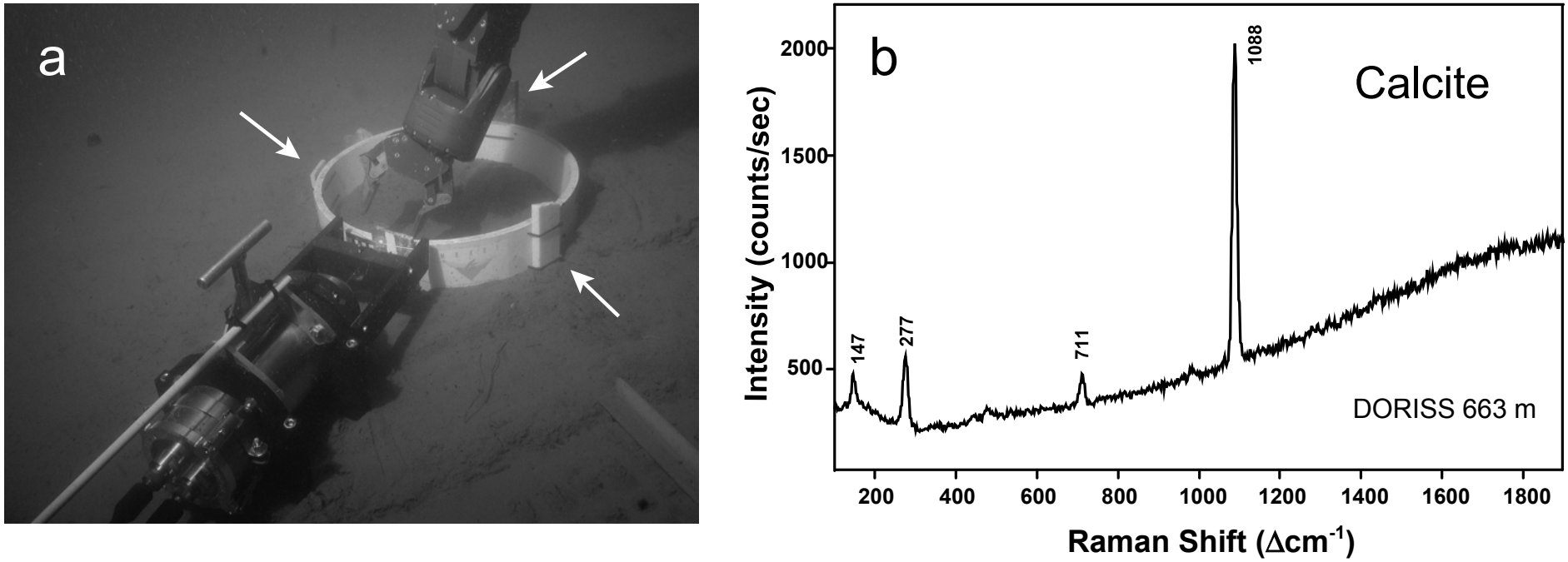

Fig. 11. a) Several sawn slabs of calcite and carbonate rocks (indicated by arrows) are strapped to a PVC corral at 663 m depth on sea floor. Probe head has been guided into focus on the large calcite rhomb painted with a white vertical stripe. b) Raman spectrum of that calcite rhomb (1-second acquisition).

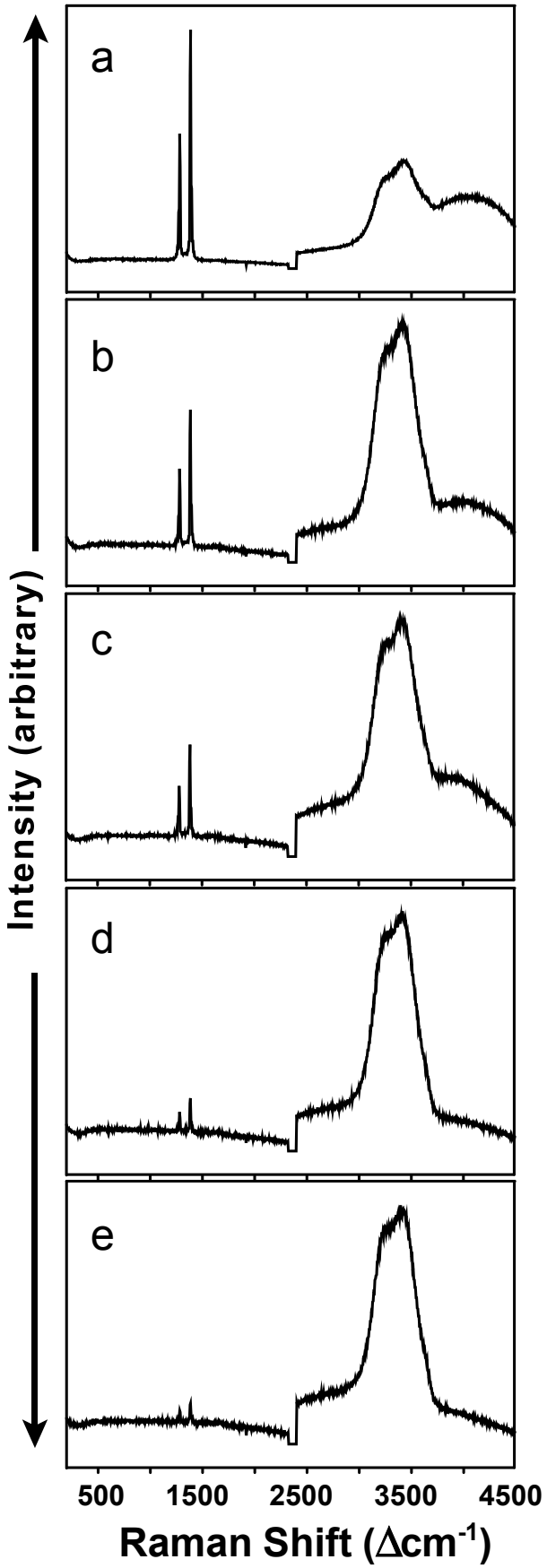

Fig. 12. Series of Raman spectra (each with 1-second acquisition time) as the probe head is moved away from optimal focus of the laser on a CO_2 liquid blob on the ocean floor. As explained in Fig. 9, both sea water and CO_2 are in the laser beam's path. Spectra of both phases are recorded, but the CO_2:H_2O band ratios vary with position of the probe head. The CO_2 blob is in best focus in spectrum a).

Hydrate Composite Particles for Ocean Carbon Sequestration: Field Verification

Costas Tsouris,[1,*] Peter Brewer,[2,*] Edward Peltzer,[2] Peter Walz,[2]
David Riestenberg,[1] Liyuan Liang,[1] Olivia R. West[1]

[1]Oak Ridge National Laboratory, P.O. Box 2008
Oak Ridge, TN 37831-6181

[2]Monterey Bay Aquarium Research Institute
7700 Sandholdt Road, Moss Landing, CA 95039-9644

Submitted to

Environmental Science & Technology

September 2003

*Corresponding authors: tsourisc@ornl.gov (865-241-3246), brpe@mbari.org (831-775-1706)

Hydrate Composite Particles for Ocean Carbon Sequestration: Field Verification

Costas Tsouris,[1,*] Peter Brewer,[2,*] Edward Peltzer,[2] Peter Walz,[2]
David Riestenberg,[1] Liyuan Liang,[1] Olivia R. West[1]

[1]Oak Ridge National Laboratory, P.O. Box 2008
Oak Ridge, TN 37831-6181

[2]Monterey Bay Aquarium Research Institute
7700 Sandholdt Road, Moss Landing, CA 95039-9644

Abstract

This article reports on the formation and dissolution of CO_2/seawater/CO_2 hydrate composite particles produced during field experiments in Monterey Bay, California using a CO_2 injector system previously developed in the laboratory. The injector consisted of a co-flow reactor wherein water was introduced as a jet into liquid CO_2, causing vigorous mixing of the two immiscible fluids to promote the formation of CO_2 hydrate that is stable at ambient pressures and temperatures typical of ocean depths greater than ~500 m. Using flow-rate ratios of water and CO_2 of 1:1 and 5:1, particulate composites of CO_2 hydrate/liquid CO_2/seawater phases were produced in seawater at depths between 1100 and 1300 m. The resultant composite particles were tracked by a remotely operated vehicle system as they freely traveled in an imaging box that had no bottom or top walls. Results from the field experiments were consistent with laboratory experiments, which were conducted in a 70-L high-pressure vessel to simulate the conditions in the ocean at intermediate depths. The particle velocity and volume histories were monitored and used to calculate the conversion of CO_2 into hydrate and its subsequent dissolution rate after release into the ocean. The dissolution rate of the composite particles was found to be higher than that reported for pure CO_2 droplets. However, when the rate was corrected to correspond to pure CO_2, the difference was very small. Results indicate that a higher conversion of liquid CO_2 to CO_2 hydrate is needed to form negatively buoyant particles in seawater when compared to freshwater, due primarily to the increased density of the liquid phase, but also due to processes involving brine rejection during hydrate formation.

Keywords: CO_2 hydrate, ocean carbon sequestration, carbon management

*Corresponding authors: tsourisc@ornl.gov (865-241-3246), brpe@mbari.org (831-775-1706)

Introduction

The world's oceans are the primary natural sink for fossil fuel CO_2 released to the atmosphere (*1*). The net uptake of CO_2 is limited, however, primarily because of the slow ventilation rate, or annual exposure of deep waters to the atmosphere *(2*). Injection of CO_2 into the oceans is being studied as a potential sequestration strategy for some fraction of the future production of fossil fuel CO_2 (*3,4*). Some 7 Gt of C, released as anthropogenic CO_2, is currently produced per year (*1*). However, any ocean CO_2 injection scenario presents economic and environmental challenges (*5, 6*). Lowering oceanic pH and increasing the CO_2 concentration near the injection point may present a biological impact (*7 - 10*). The economics of a deep injection must also be considered, because deeper injection depths inevitably lead to increased injection energy penalties and costs. Finally, any method must minimize the potential for CO_2 to reenter the atmosphere. Sequestering CO_2 in the deep waters below the main oceanic thermocline (depths of >1000–1500 m) will result in extended residence times. The average ventilation age of deep ocean waters is approximately 250 years for the Atlantic, and approximately 550 years for the Pacific (*11*).

Injection of CO_2 at depths >3500 m to form a CO_2 "lake" on the seafloor has been considered (*12*). Although this method will result in longer-term sequestration, infrastructure and implementation costs increase significantly with greater injection depth and the localized high concentration of CO_2 may cause negative biological effects. The identification of sites with suitable large-scale sea floor valleys close by a CO_2 source may also be difficult.

An alternative method is to release CO_2 as a positively buoyant plume of droplets (*13, 14*). In this approach the impact on benthic marine animals is minimized, and the release technology can be designed to minimize mid-water impacts also. However, because of the rising nature of the plume, some of the work expended to carry out the injection is undone by the rise to shallower depths. The injection point must be sufficiently deep to allow complete dissolution of the liquid CO_2 into the surrounding seawater before the droplets reach depths at which the water masses are ventilated on short time scales (*15*).

Formation of a slowly dissolving negatively buoyant plume of CO_2 at intermediate depths is another way to address these challenges. In the case of a sinking plume, the goal of energy efficient deeper injection, and thus greater oceanic retention, is more easily met. Aya and coworkers (*16*) investigated the injection of cold liquid CO_2 and slurries of cold CO_2 with dry ice, which are denser than the surrounding seawater at intermediate depths. They observed that as cold CO_2 particles sink, ice forms on their surface which lowers the density of the particles.

Another approach in producing dense CO_2 particles at intermediate depths is by promoting CO_2 hydrate formation. CO_2 hydrate is a non-stoichiometric solid phase of CO_2 and water that is thermodynamically stable at pressures equivalent to those typically found at >500-m depth (*12*), and pure CO_2 hydrate is approximately 10% denser than typical abyssal seawater (*17*). Therefore, complete conversion of CO_2 into hydrate would produce a negatively buoyant CO_2 phase at relatively shallow depths. Fully crystalline pure CO_2 hydrate is a hard solid, comparable to water ice; thus it will not easily flow, and this presents severe problems for pipe disposal schemes. However, complete conversion

of CO_2 to the hydrated phase is not necessary to create a negatively buoyant composite. For example, a composite slurry or paste consisting of water, liquid CO_2, and CO_2 hydrate will be negatively buoyant in seawater typically found at approximately 1000 m depth (*18*) with a 25% conversion of liquid CO_2 to hydrate. Such a composite also has the rheological characteristics required for flow. The hydrate also dissolves more slowly than liquid CO_2 (*19 -21*), possibly lessening the local biological impacts of injection.

A method was recently developed to partially convert a stream of liquid-phase CO_2 to CO_2 hydrate using a CO_2/water coflow jet reactor (*18, 22*). In the reactor, water was introduced as a jet and vigorously mixed into liquid CO_2, continuously forming a composite paste of liquid CO_2, CO_2 hydrate, and water. In experiments with seawater, dense brine resulting from salt rejection during hydrate formation is also included. The composite paste, deformable enough to flow, but dense enough to at least equal the surrounding fluid, was extruded from the reactor into the surrounding water. Experiments were previously performed in the laboratory to determine the flow rates of CO_2 and water in the reactor necessary for the formation of a negatively buoyant composite at pressures of 10–13 MPa (approximately equivalent to 1- to 1.3-km ocean depth) (*23*).

This article reports the results of field injection experiments that were performed in Monterey Bay, California, at 1100- to 1300-m depth using the same coflow jet reactor and varying flow rates of CO_2 and water. The velocity and changing dimensions of the composite cylindrical slugs extruded were determined by using a highly instrumented remotely operated vehicle (ROV) (*15*) to track the particles as they traveled through the water column. The density and composition of the particles were calculated, as was the

composite dissolution rate. The results are compared with those obtained in the laboratory.

Methods

The Coflow Jet Reactor. The coflow jet reactor (Figure 1A) has been developed and used to extrude a composite paste of liquid CO_2 /water/ CO_2 hydrate in the laboratory (*18, 22*). The reactor consisted of an outer tube (OD of 9.5×10^{-3} m and ID of 6.4×10^{-3} m) and a concentrically located inner capillary tube (OD of 1.6×10^{-3} m and ID of 0.254×10^{-3} m). This design permits spraying of water droplets through the capillary tube into liquid CO_2 that is continuously pumped in the reactor via the outer tube. The stainless steel capillary tube terminated approximately 0.14 m from the end of the outer tube, creating a zone in which the liquid CO_2 and water could vigorously mix, enhancing the production of CO_2 hydrate. The outer tube consists primarily of stainless steel with a 0.125-m section of Teflon at the end; this construction prevents wetting of the wall by the water phase in the mixing zone and keeps water finely dispersed in the CO_2 liquid phase. The composite particles are produced in the mixing zone before being discharged into the ambient water. In laboratory experiments using a 72-liter pressure vessel (description in *22*), water and liquid CO_2 were delivered through the inner capillary and outer tubes via syringe pumps at predetermined flow rates of 15–25 and 2–10 mL/min, respectively. In previous laboratory studies, water droplets produced via the capillary averaged 267 ± 79 μm (*23*).

Field Experiments. The coflow jet reactor was field tested in ocean waters from 1100 to 1300 m in depth in Monterey Bay, California. The ROV *Ventana* was deployed by the RV *Point Lobos* to perform the injections. The injector was mounted in a Plexiglas box (0.3-m wide, 0.25-m deep, and 0.91-m high) that was open at the top and bottom (Figure 1B), and had an illuminated translucent rear panel. A picture of the ROV Ventana carrying the injector inside the Plexiglass box is presented in Figure 2. The box allowed the injected composite particles to rise or fall freely based on their buoyancy but restricted lateral motion (*15*), thus easing the vehicle piloting requirements. The illuminated rear wall of the box served to back light the particles, and also to screen our visual clutter from the ubiquitous mid-water animals and marine snow. Carbon dioxide and ambient seawater were pumped via a piston assembly, as described earlier (*24*). Volumetric flow meters were installed to measure the flow rates of the fluids as they were introduced into the coflow jet reactor, and were arranged so that they were viewable with the primary HDTV camera system. Injections were performed using a 1:1 volumetric ratio of CO_2 to water at ~1000-m depth to produce a floating composite and with a 1:5 ratio at ~1300-m depth to produce a sinking composite. The size and velocity of the resultant particles were determined using the ROV, which traveled vertically to follow one randomly selected particle for each injection experiment through the water column, and recorded the particle using a HDTV camera as described previously (*15*). Selected video frames in which the particle appeared to be oriented parallel to the front Plexiglas plane were processed post cruise, using image analysis software (*Scion Image*) to determine the dimensions of the particle. Scales on the front and rear planes of the Plexiglas imaging box were used to measure the length and diameter of the cylindrical

composite particles. To correct for errors introduced by the 0.25-m depth of the imaged field, the dimensions of the composite particles were taken as the average of the dimensions based on the front and rear calibration scales. The seawater depth, temperature, density, and pressure were logged using the instrumentation suite installed on the ROV, and recorded in time sequence throughout the experiment from the production of the composite particles through their dissolution. These data were then used to estimate particle velocity, density, and dissolution rate.

Results

Description of Field Injection. Liquid CO_2/water/CO_2 hydrate composite particles were successfully created during field injections in Monterey Bay, California at ocean depths of 1100 to 1300 m. The composite produced in the field (Figure 3B) was similar in appearance to that produced in previous laboratory experiments (Figure 3A) at equivalent pressures and temperatures in a 3.5% NaCl solution. The diameters of both the laboratory- and field-produced composites are approximately 6.5 mm. Data from the field experiments showed that the resultant composite particles varied from 5 to 85 mm in length, with an average of length 29 ± 18 mm. The particles were observed to shrink in diameter and length over time in the ambient seawater. The direction and velocity of their motion depended on the injection depth (or pressure), as well as the ratio of CO_2 to water injected. Figure 4 shows the vertical path of three particles through the water column from three different injection runs.

In the first injection experiment, run number 163_1107, composite particles were successfully produced using flow rates of 50 mL/min for both seawater and CO_2,

respectively, in the co-flow jet reactor. The injection was performed at a depth of 1099.4 m where the temperature was 3.57 °C. The injected composite was followed by the ROV as it rose vertically to a depth of 1061.8 m (37.5 m from the release point) over a period of 10 min and 20 s (Figure 4), where the temperature was 3.69 °C. After that point, the composite became too small to follow. The positive buoyancy of these composite particles was expected based on our previous laboratory studies (*23*), which showed that a flow-rate ratio for CO_2:H_2O of less than 1:3 is needed to form a negatively buoyant composite.

Two subsequent injections were performed, runs number 164_1226 and 164_1232, in which attempts were made to produce a sinking composite. These injections were performed at a greater depth than run 163_1107 (the floating experiment). With increasing depth, the density of the highly compressible liquid CO_2 increases faster than that of the incompressible seawater, contributing to the net density contrast of the composite particles created (*14*). The water flow rate was maintained at 50 mL/min but the CO_2 flow rate was reduced to 10 mL/ min to give a 1:5 ratio for CO_2:H_2O in the injector.

Injection run 164_1226 was performed at a depth of 1251 m and temperature of 3.68 °C. A resultant composite particle was followed for 5 min and 21 s during which time it initially sank slowly and then became neutrally buoyant at a depth of 1258 m (6.8 m below the release point) and a temperature of 3.26 °C (Figure 4). Injection run 164_1232 was performed at a depth of 1297 m and a temperature of 3.24 °C. A composite particle was followed for 10 min and 46 s during which time it initially moved slowly downward, and then floated to a depth of 1286 m (11 m above the release point);

the particle was then too small to be followed and imaged by the ROV (Figure 4). A CO_2 droplet is expected to rise at roughly twice the velocity (*15*) of the particle in run 163_1107, assuming a drop diameter of 1.28 cm (twice the diameter of the injector) and neglecting the effect of any CO_2 conversion to hydrate on the surface of the droplet. This layer remains relatively thin (~10^{-5} m) based on previous experiments (*25*). This illustrates the benefits of pre-mixing water into the CO_2 stream to promote hydrate formation prior to injection; CO_2 ocean sequestration techniques can thus be improved even for positively buoyant particles.

The length and diameter of one randomly selected composite particle for each injection experiment were measured as they moved through the water column. In all cases, the particles were observed to decrease in length and diameter over time. The uncertainty in the location of the particles within the imaging depth of field likely resulted in errors when measuring the particle dimensions. Figure 5 shows the volume and velocity of the particle followed in injection run 163_1107 over time, with error bars to show the maximum and minimum possible volume based on the rear and front scales, respectively. Similar calculations were made for the other injection runs (not shown).

Analysis of Injections. For each experiment, the particle density (ρ_p) was estimated from the particle dimensions and velocity using the following equation

$$\rho_p = \rho_w + i\frac{3C_D\rho_w U_p^2}{4D_{ps}g} \qquad (1)$$

obtained from the balance of buoyancy and drag forces on a spherical particle having the same volume as the cylindrical particle *(26)*. In Eq. 1, C_D is the drag coefficient, ρ_w is the

density of seawater at the injection depth, U_p is the vertical velocity of the particle, i is +1 for a sinking particle and -1 for a floating particle, g is the gravity constant, and D_{ps} is the diameter of the equivalent spherical particle $(1.5D_{pc}^2 L_p)^{1/3}$, where L_p is the particle length and D_{pc} is the particle diameter. The length, diameter, and velocity for each particle immediately after it was released from the injector were used for calculating the particle densities.

The drag coefficient in Eq. 1 was obtained from a published correlation between C_D and Reynolds number (*Re*) (*26*). The Reynolds number of the equivalent spherical particle is defined as

$$Re = \frac{D_{ps} U_p \rho_w}{\mu_w} \tag{2}$$

where μ_w is the seawater viscosity (0.014 g/cm sec). The Reynolds number was determined for each particle and was found to be approximately 490, 180, and 0 for particles 163_1107, 164_1226 and 164_1232, respectively, using the particle velocity just after injection. For the sake of simplicity, the particles are considered spherical in estimating the drag coefficient (C_D). For a Reynolds number range of 1 to 1000, the relationship of R_e to C_D for a sphere has been established as (*26*):

$$C_D \cong \frac{18.5}{R_e^{3/5}} \tag{3}$$

The calculated drag coefficients for the particles were 0.45 and 0.81 for particles in runs 163_1107 and 164_1226. The particle in run 164_1232 had zero vertical velocity, in which case a drag coefficient does not apply.

The hydrate conversion factor, x_h, in the particles tracked under each experiment can be calculated from the estimated density of the composite particles. The density is also a function of the hydrate density ρ_h, CO_2 and water densities, the moles of CO_2 and water initially present in the composite particle (i.e., before hydrate formation) n_c and n_w, and the hydration number n (*23*):

$$\rho_p = \frac{44n_c + 18n_w}{44n_c(1/\rho_c - x_h(1/\rho_c - 1/\rho_h)) - 18(nx_h n_c(1/\rho_w - 1/\rho_h) - n_w/\rho_w)} \quad (4)$$

For a given volumetric flow rate ratio between CO_2 and water, λ, the ratio between n_c and n_w is as follows:

$$\frac{n_c}{n_w} = \frac{18\rho_c\lambda}{44\rho_w} \quad (5)$$

Substituting Eq. 5 into Eq. 4 and re-arranging, the hydrate conversion x_h can be calculated from the flow rate ratio λ, the composite density ρ_p estimated from Eq. 1, and phase densities:

$$x_h = \frac{(1/\rho_c - 1/\rho_p) + (\rho_w/\rho_c)(1/\lambda)(1/\rho_w - 1/\rho_p)}{(1/\rho_c - 1/\rho_h) + 18n(1/\rho_w - 1/\rho_h)/44} \quad (6)$$

The estimated hydrate conversion for each injection experiment is shown in Table 1, and compared with the minimum CO_2 hydrate conversion necessary to produce a neutrally buoyant particle x_{h_min} (where $\rho_p = \rho_w$ in Eq. 4) for a particular depth (*23*):

$$x_{h\_\min} = \frac{1/\rho_c - 1/\rho_w}{(1/\rho_c - 1/\rho_h) + 18n(1/\rho_w - 1/\rho_h)/44} \quad (7)$$

Consistent with previous laboratory experiments, the hydrate conversion in *163_1107* is lower than in the other experiments due to a higher flow rate ratio between CO_2 and water.

The rate of particle shrinkage over time allows a comparison of the dissolution rates of composite particles with those observed for hydrate-covered CO_2 droplets by others. Figure 6 shows the equivalent spherical diameter D_{ps} for each particle after injection as a function of time. The overall particle shrinkage rates calculated for the injection runs 164_1226 and 164_1232 were 10.5×10^{-6} and 8.5×10^{-6} m/s, respectively, while that for injection run 163_1107 was 8.6×10^{-6} m/s. The error in the dissolution rates was calculated based on the error in the measurement of the dimensions of the particles and was approximately $\pm 1 \times 10^{-6}$ m/s. Radhakrishnan et al. (*21*) recently reviewed the dissolution rates of hydrate-covered CO_2 droplets and reported them to range between 10^{-6} and 10^{-8} m/s. Brewer et al. (*15*) recently performed injections of CO_2 droplets at 800-m depth in Monterey Bay and reported a dissolution rate of approximately 3×10^{-6} m/s. The composite particles investigated in this work appear to have a higher shrinkage rate than those observed for droplets covered with hydrate. Because the composite particles contain considerable amounts of water, it is reasonable to correct for the presence of water in order to convert the shrinkage rate to an equivalent CO_2 dissolution rate. If we assume that the CO_2 fraction is less than 1/3 of the initial mixture, then the dissolution rate corresponding to pure CO_2 averaged between 3×10^{-6} m/s and 3.5×10^{-6} m/s, which is similar to the values reported by Brewer and coworkers (*15*).

Comparison of Field and Laboratory Data. Laboratory experiments were conducted with the coflow jet reactor in simulated saltwater (3.5 % NaCl) prior to ocean injections (*18, 22*). The results of those injections showed that for a given water flow rate, there was a maximum CO_2 flow rate above which a floating composite was

produced, and below which sinking composite was produced (Figure 7). From the laboratory results it is apparent that, as the water flow rate increased, more CO_2 could be injected while the composite remained negatively buoyant. Due to pump limitations, the maximum water flow rate available for the laboratory injections was 25 mL/min. Because the water flow rate in the ocean injections was limited to 50 mL/min, a direct comparison cannot be made. However, if the laboratory results are extrapolated to higher water flow rates, the maximum flow rate of CO_2 per nozzle of this design that will produce a sinking composite with 50 mL/min water would be 17.2 mL/min at 10.3 MPa and 28.4 mL/min at 13.1 MPa (using linear extrapolation in Figure 7). Injection run 163_1107 was performed at 10.99 MPa with a CO_2 flow rate of 50 mL/min. These conditions produced a floating particle composite and lower hydrate conversion as predicted by the laboratory flow rate ratios. Injection runs 164_1226 and 164_1232, however, were performed with a CO_2 flow rate of 10 mL/min, which, according to the laboratory experiment, should give a negatively buoyant composite. Instead, the particles were neutrally buoyant. This result suggests a nonlinear behavior, which should be expected because of the complexity of the system and the dependency on mixing conditions. In terms of the capillary Reynolds number, in the laboratory experiments this parameter varied between 2200 and 2900, which is close to the transitional region from laminar to turbulent flow. In the field injections, however, the capillary Re was approximately 5900, which is in the turbulent regime. Further laboratory studies on composites produced by using higher flow rates are planned.

In conclusion, solid CO_2/water/CO_2 hydrate composite paste-like particles were successfully formed and extruded in ocean injections at depths of 1100 to 1300 m using a

coflow CO_2/water injector. Particles were tracked vertically after injection and were found to be either slightly positively buoyant or neutral, depending on the amount of CO_2 injected and the injection depth. Conversion of CO_2 to hydrate in the composite ranged from 21% to 30%. Future challenges include modifying the injection system to increase conversion and produce a slowly dissolving, negatively buoyant CO_2 phase that can be used for ocean carbon sequestration.

Acknowledgments

Gratefully acknowledged is support by the Ocean Carbon Sequestration Program, Office of Biological and Environmental Research, U.S. Department of Energy, grant no. KP120203, under contract DE-AC05-00OR22725 with UT-Battelle, LLC. Support for MBARI was provided by the David and Lucile Packard Foundation, and by the U.S. Dept. of Energy under contracts DE-FC26-00NT40929 and DE-FG03-01ER63065. We would like to thank the captain and crew of the RV *Point Lobos* and the pilots of the ROV *Ventana* for making the field experiments possible and Dr. Marsha Savage for editing the manuscript.

Literature Cited

(1) Intergovernmental Panel on Climate Change: The Science of Climate Change.1995. 572 pp. Cambridge University Press.

(2) McNeil, B.; Matear, R.J.; Key, R.M.; Bullister, J.L.; Sarmiento, J.L. *Science*, **2003**, *299*, 235-239.

(3) Medina, M-G.; Bond, G. M.; Stringer, J., *Interface* **2001**, *10* (1) 26–30.

(4) Hoffert, M. I.; Caldeira, K.; Benford, G.; Criswell, D. R.; Green, C.; Herzog, H.; Jain, A. K.; Kheshgi, H. S.; Lackner, K. S.; Lewis, J. S.; Lightfoot, H.D.; Manheimer, W.; Mankins, J. C.; Mauel, M. E; Perkins, L. J.; Schlesinger, M. E.; Volk, T.; Wigley, T. M. L. *Science* **2002**, *298*, 981-987.

(5) Golomb, D. *Energy Convers. Manage*. **1993**, *34*, 967–976.

(6) Adams, E. E.; Golomb, D. S.; Herzog, H. J. *Energy Convers. Manage*. **1995**, *36*, 447–452.

(7) Auerbach, D. I.; Caulfield, J. A.; Adams E. E.; Herzog, H. J. *Environ Model. Assess.* **1997**, 333–343.

(8) Tamburri, M. N.; Peltzer, E. T.; Friederich, G. E.; Aya, I.; Yamane, K.; Brewer, P. G. *Mar. Chem*. **2000**, *72*, 95–101.

(9) Takeuchi, K.; Fujioka, Y.; Kawasaki, Y.; Shirayama, Y. *Energy Convers. Manage*. **1997**, *38*, 5337–5341.

(10) Seibel, B. A.; Walsh P. J. *Science* **2001**, *294*, 379–380.

(11) Stuiver, M.; Quay, P.D.; Ostlund, H.G. *Science* **1983,** *219,* 849-851.

(12) Brewer, P. G.; Friederich, G.; Peltzer, E. T.; Orr, F. M., Jr. *Science* **1999**, *284*, 943–945.

(13) Liro,; C. R., Adams, E. E., Herzog, H. G. *Energy Convers. Manage.* **1992**, *33*, 667–674.

(14) Alendal, G.; Drange, H. *J. Geophys. Res.* **2001,** *106*, 1085-1096.

(15) Brewer, P. G.; Peltzer, E. T.; Friederich, G.; Rehder, G. *Envir. Sci. Technol*., **2002**, *36*, 5441-5446.

(16) Aya, I.; Kojima, R.; Yamane, K.; Shiozaki, K.; Brewer, P. G.; Peltzer, E. T. III. *Energy*, **in press**.

(17) Sloan, E. D. Jr., *Clathrate Hydrates of Natural Gases*, 2nd ed.; **1998**, Marcel Dekker, Inc.: New York.

(18) West, O. R.; Tsouris, C.; Liang, L.; Lee, S-Y.; McCallum, S. D. *AIChE J.,* **2003**, *49*, 283 - 285.

(19) Aya, I.; Yamane, K.; Nariai, H. *Energy* **1997**, *22*, 263–271.

(20) Hirai, S.; Okazaki, K.; Tabe, Y.; Hijikata, K.; and Mori, Y. *Energy* **1997**, *22*, 285–293.

(21) Radhakrishnan, R.; Demorov, A.; Herzog. H.; Trout, B. L. *Energy Convers. Manage*. **2003**, *44*, 773–782.

(22) Phelps, T. J.; Peters, D. J.; Marshall, S. L.; West, O. R.; Liang, L.; Blencoe, J. G.; Alexiades, V.; Jacobs, G. K.; Naney, M. T.; Heck, J. L., Jr. *Rev. Sci. Instrum.* **2001**, *72*, 1514–1521.

(23) Lee, S-Y.; Liang, L.; Riestenberg, D. E.; West, O. R..; Tsouris, C.; Adams, E. E. *Environ. Sci. Technol.,* **2003**, 37, 3701-3708.

(24) Brewer, P. G.; Orr, F. M., Jr.; Friederich, G.; Kvenvolden, K. A.; Orange, D. *Energy Fuels* **1998**, *12*, 183–188.

(25) Teng, H.; Yamasaki, A.; Shindo, Y. *Chem. Eng. Sci.*, **1996**, *51*, 4979-4986.

(26) Tek, M. R.; Wilkes, J. O. *Fluid Flow and Heat Transfer***;** Ann Arbor, MI; University of Michigan. 1974.

Table 1. Summary of Field Data and Calculated Results from Three Injections

	experiment no.		
	163_1107	*164_1226*	*164_1232*
Observed initial behavior	floating	sinking	neutral
Injection depth (m)	1099	1251	1297
Phase densities (Kg/m^3)			
CO_2 liquid	943	955	957
seawater	1032.60	1033.31	1033.53
CO_2 hydrate	1100	1100	1100
Particle velocity (m/s)	-0.06	+0.02	0
Initial particle length (mm)	24.6	34	26.2
Initial particle diameter (mm)	6.0	6.1	5.7
Initial volume of composite ($\times 10^{-6}\ m^3$)	0.687	0.986	0.692
Estimated composite density (kg/m^3)	1020.9	1035.4	1033.5
volumetric flow rate ratio (Q_{CO2}/Q_W)	1	0.2	0.2
CO_2 hydrate conversion (x_h)	0.21	0.30	0.26
minimum conversion for sinking composite (x_{h_min})	0.2864	0.2593	0.2551

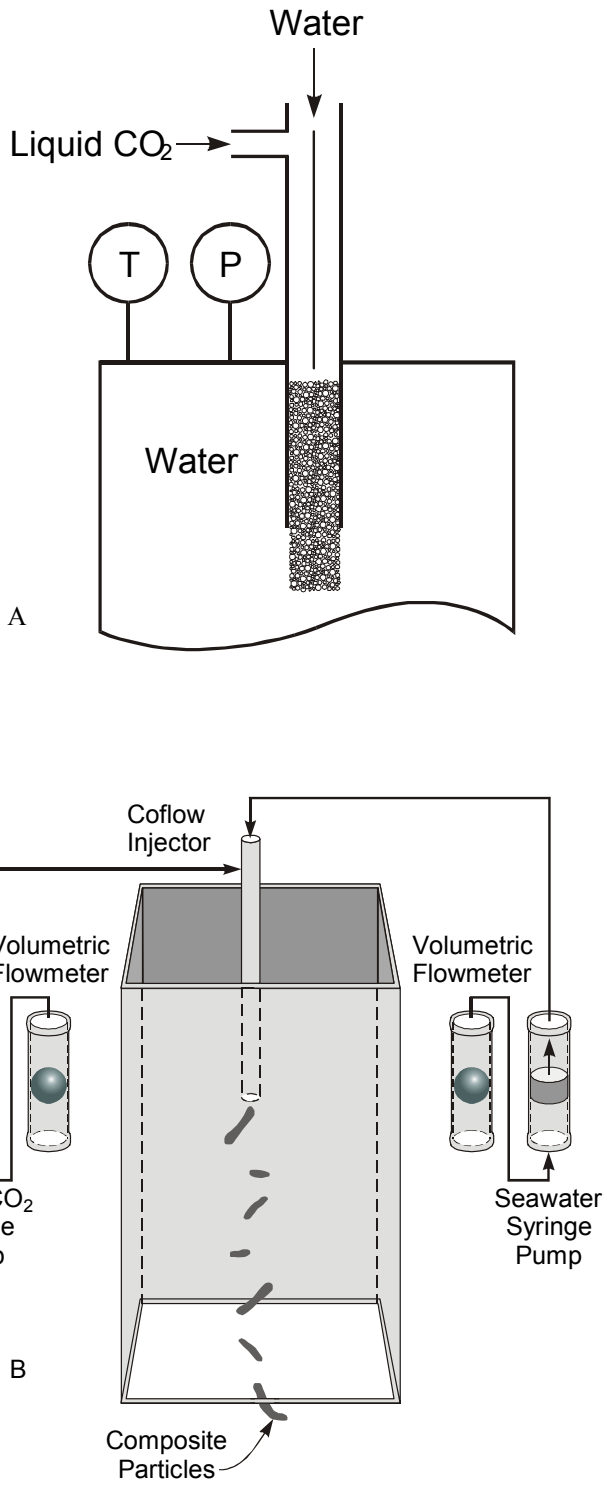
Water
Liquid CO_2
T
P
Water
A
Coflow
Injector
Volumetric
Flowmeter
Volumetric
Flowmeter
Liquid CO_2
Syringe
Pump
Seawater
Syringe
Pump
B
Composite
Particles

FIGURE 1

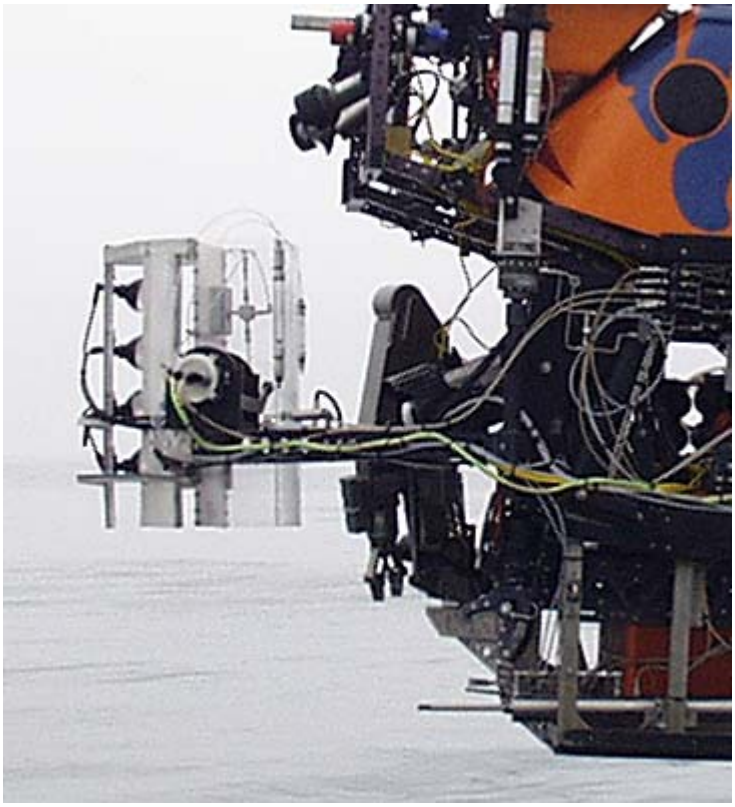

FIGURE 2

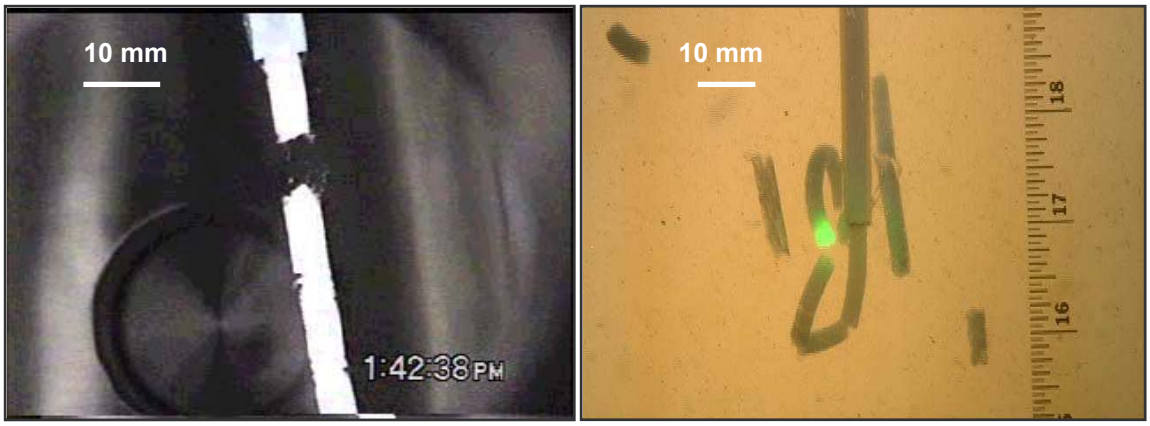

A B

FIGURE 3

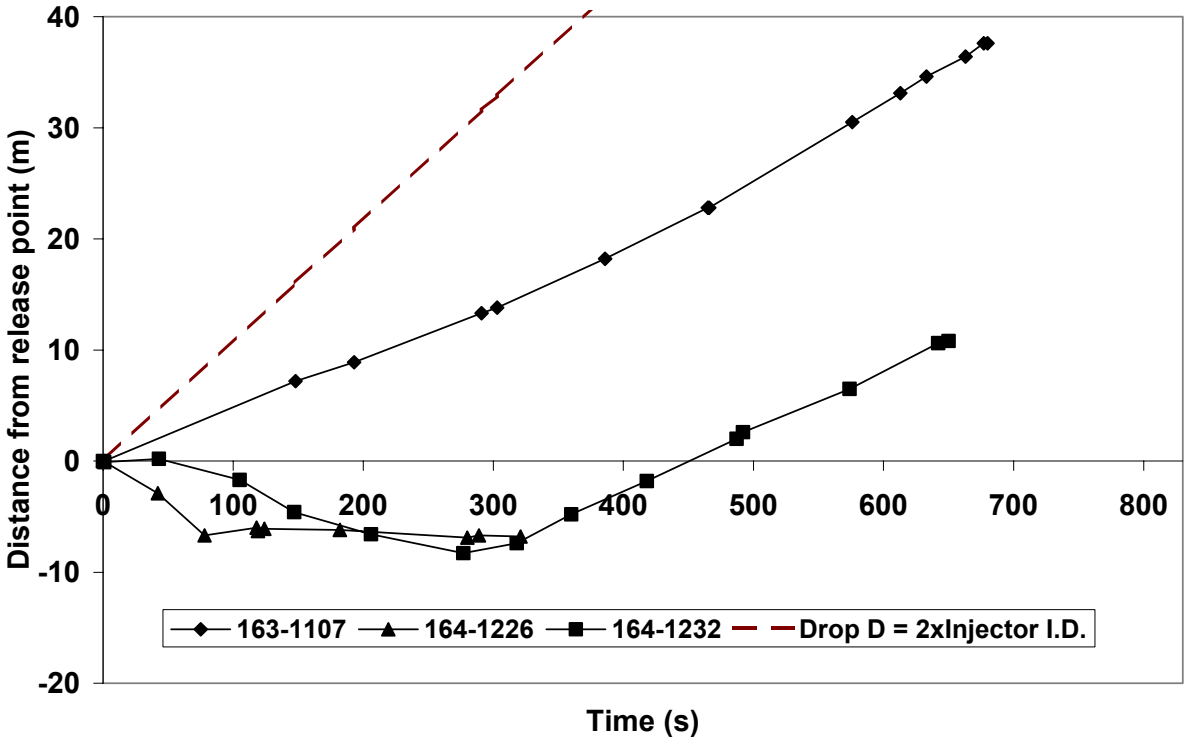
40
30
20
10
0
-10
-20
Distance from release point (m)
0
100
200
300
400
500
600
700
800
Time (s)
163-1107
164-1226
164-1232
Drop D = 2xInjector I.D.

FIGURE 4

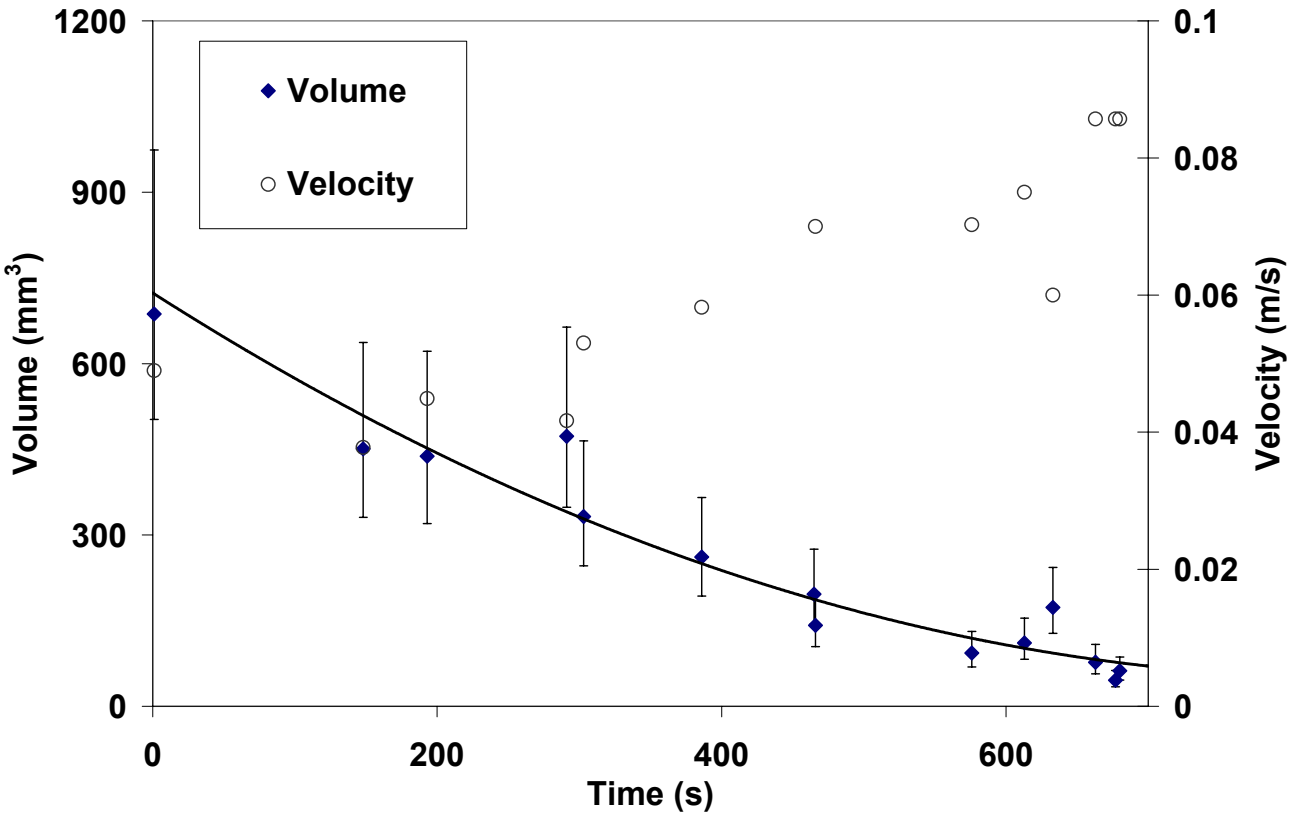
Volume
Velocity
1200
900
600
300
0
0.1
0.08
0.06
0.04
0.02
0
0
200
400
600
Time (s)
Volume (mm3)
Velocity (m/s)

FIGURE 5

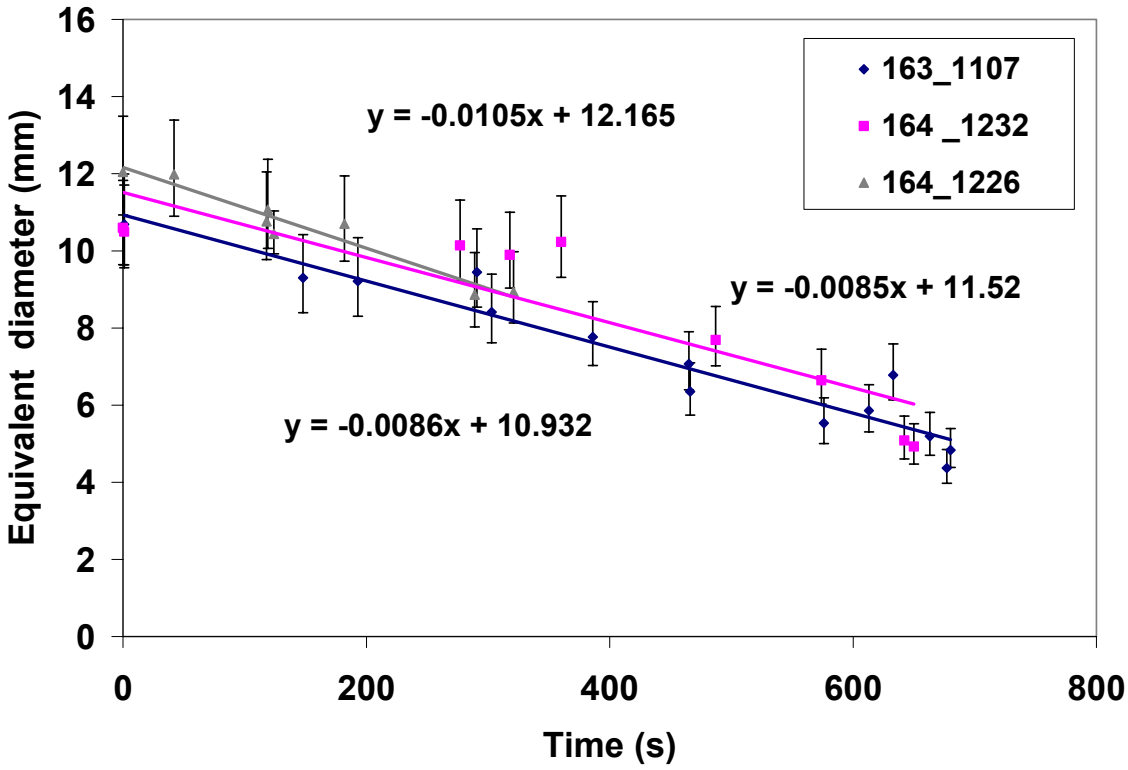
Equivalent diameter (mm)
Time (s)
163_1107
164 _1232
164_1226
y = -0.0105x + 12.165
y = -0.0085x + 11.52
y = -0.0086x + 10.932
0
2
4
6
8
10
12
14
16
0
200
400
600
800

FIGURE 6

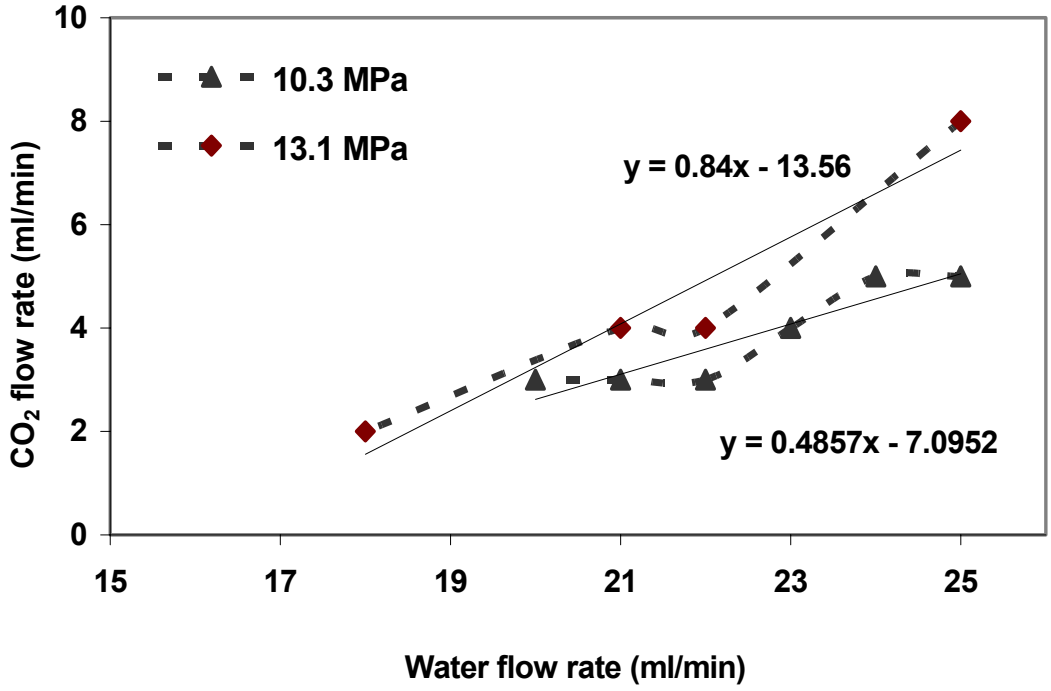
10
8
6
4
2
0
15
17
19
21
23
25
10.3 MPa
13.1 MPa
y = 0.84x - 13.56
y = 0.4857x - 7.0952
CO2 flow rate (ml/min)
Water flow rate (ml/min)

FIGURE 7

FIGURE 1. Schematics showing (A, top): laboratory design for injection of liquid CO_2 and water using a coflow jet reactor and (B, bottom): coflow jet reactor, syringe pumps, and flowmeters used for ocean injections of composite particles performed at 1000- to 1300-m ocean depth on the ROV *Ventana*. The Plexiglas box was open at the top and bottom, allowing the composite to freely rise or sink after injection.

FIGURE 2. The ROV Ventana carrying the experimental apparatus and about to enter the water. The front of the imaging box faces towards the vehicle. The lights arranged to illuminate the rear translucent screen are at the far left, the flow meters are on the box front corners, and the coflow reactor is mounted on the rear wall. The CO_2 cylinder and water pump are mounted under the vehicle, and connected by tubing to the valves mounted on the box.

FIGURE 3. Microphotographs of (A) laboratory and (B) ocean injections of CO_2 hydrate. (A) CO_2 hydrate injection in the Oak Ridge National Laboratory Seafloor Process Simulator using the coflow jet reactor at P = 10.5 MPa and T = 4.1 °C. Flow rates for water and CO_2 were 25 and 6 mL/min, respectively. (B) CO_2 hydrate injection in Monterey Bay, California, using the coflow jet reactor at 1290-m depth (P = 13.1 MPa and T = 3.2 °C). Flow rates for water and CO_2 were 50 and 10 mL/min, respectively. *Note:* The light on one of the particles in the field experiment comes from a Raman spectrometer that was unsuccessfully used to analyze composite particles.

FIGURE 4. Plot of particle depth versus time, indicating the vertical movement of particles after injection. Predicted path of liquid CO_2 droplet released at same depth as 163_1107 with a diameter twice that of the injector is also shown.

FIGURE 5. Volume and velocity histories of a particle after the 163_1107 injection at 1090-m depth.

FIGURE 6. Dissolution of composite particles.

FIGURE 7. Flow-rate limits of CO_2 and simulated seawater (3.5% NaCl aqueous solution) necessary for producing negatively buoyant composite particles in the Seafloor Process Simulator. Experiments were conducted with the vessel filled with a 3.5% NaCl solution. Composite produced using flow rates of CO_2 and NaCl solution above the line were positively buoyant, while those below the line sank.

Deep-sea field experiments on the biological impacts of direct deep-sea CO_2 injection

J.P. Barry, B.A. Seibel, J.C. Drazen, M.N. Tamburri, K.R. Buck, C. Lovera, L. Kuhnz, E.T. Peltzer, K. Osborn, P.J. Whaling, P. Walz, P.G. Brewer

Monterey Bay Aquarium Research Institute, 7700 Sandholdt Road, Moss Landing, CA 95039

ABSTRACT

Direct injection of CO_2 into the ocean, a radical idea suggested 25 years ago (Marchetti 1977), is among several carbon sequestration alternatives under consideration to offset the accelerating rise in anthropogenic greenhouse gases (Reichle et al 1999, Brewer et al. 1999). This issue raises important questions concerning the impacts of pH changes and elevated CO_2 levels for marine ecosystems and the role, if any, ocean sequestration should play in a national or global carbon management strategy. While there is uncertainty concerning physical responses to greenhouse gas forcing (Caldeira et al 2003), there is no doubt that oceanic CO_2 levels have risen significantly (Keeling and Whorf 2002, Barnola et al. 2003) and will continue to do so (Marland et al. 2001). Roughly $1/3^{rd}$ of current fossil fuel CO_2 emissions (~7 $GtCO_2y^{-1}$) enter the sea surface through air-sea exchange (Houghton et al. 1990, McNeil et al 2003), thereby acidifying the upper ocean (Sabine et al. 2002). Continued acidification by air/sea CO_2 exchange (Haugan and Drange 1992) or direct ocean CO_2 sequestration (Drange et al. 2001, Harvey 2003) will challenge the physiological tolerances of species inhabiting both shallow (Kleypas et al. 1999, Knowlton 2001) and deep (Tamburri et al. 2000, Seibel and Walsh 2003) marine ecosystems. Here we present the initial results of *in situ* deep-sea CO_2 release experiments off Central California, showing that various deep-sea taxa are sensitive to short-term (~ 1 mo.) exposure to CO_2-rich, low pH plumes emanating from deep-sea CO_2 pools.

INTRODUCTION

Warming of 0.75 ^oC over the Earth during the last century (Mann et al. 1999) has been accompanied by broad changes in marine and terrestrial ecosystems (Parmesan and Yohe 2003, Root et al. 2003). In this century, however, Earth's climate is expected to warm more rapidly; global CO_2 emissions are expected to increase from present rates near 7 GTCy-1 to 15 GtCy-1 by 2050 (Marland et al. 2001). Simultaneously, acidification of the surface ocean (-0.3 pH units by 2100; Haugan and Drange 1992) may place coral reefs and other shallow marine ecosystems in peril (Kleypas et al 1999, Knowlton 2001). Ocean sequestration would reduce atmospheric emissions, but would add to the accumulating burden of fossil fuel CO_2 in the ocean. And while "dangerous anthropogenic interference" with climate has been debated widely, no such debate has taken place over acceptable oceanic CO_2 levels. Thus, although direct deep-sea CO_2 injection is technically feasible (IPCC 2001), the environmental consequences of large-scale CO_2 sequestration remain unknown and may be substantial (Seibel and Walsh 2003).

Immersion in CO_2-laden, acidic seawater from CO_2 injection poses physiological challenges to marine animals that respond by tolerance, compensation, or death. Responses are based on physiological repertoires that have evolved over thousands of generations to tolerate the range of natural environmental variability encountered. Animals that have evolved in highly stable conditions typical of deep-ocean waters are, in general, more sensitive to a variety of environmental perturbations than shallow-water animals, including those associated with CO_2 injection (Seibel and Walsh 2003). The main CO_2-related stresses can include acidosis of intra- and extra-cellular fluids, requiring pH compensation and inducing respiratory stress, and metabolic suppression, associated with hypercapnia (Pörtner and Reipschläger 1996). Changes in ocean pH caused by direct sequestration or air/sea exchange that fall within the range of normal environmental variation are expected to be less stressful than more extreme perturbations. Over the world ocean, seawater pH varies today from ~7.3 to ~8.5, (www.nodc.noaa.gov), and differs

among ocean basins. pH varies most in the upper ocean; the mean (SD) pH in depths <1000 m for the Atlantic and North Pacific Oceans are 8.2 (0.15) and 7.9 (0.22), respectively, representing variation of 0.6 and 0.9 pH units). Deep-sea environments are less variable; pH between 3000-4000 m for these areas is 8.0 (0.02) and 7.8 (0.05), variation of 0.1 and 0.2 pH units. Individuals and populations are likely to experience even less natural pH variability.

We evaluated the biological impacts of direct CO_2 injection on deep-sea animals *in situ* during two experiments (E1, E2) exposing deep-sea animals to the dissolution plume from pools of liquid CO_2 released into PVC "corrals" on the seafloor at 3600 m depth off California (Fig. 1). Our experiments were designed to investigate the potential effects of direct ocean CO_2 sequestration and develop deep-sea experimental techniques for controlled ecosystem CO_2 enrichment (e.g. DeLucia et al. 1999). Liquid CO_2 is heavier than seawater at this depth, but dissolves slowly, producing a CO_2-rich, low-pH dissolution plume. We measured the survival of various groups of deep-sea organisms exposed to these plumes. Creation of a dissolving pool of CO_2 on the seafloor[0], selected here because it is experimentally tractable, is only one of many variants of proposed ocean CO_2 injection strategies (Haugan and Drange 1992, Drange et al 2001, Caldeira and Rau 2000).

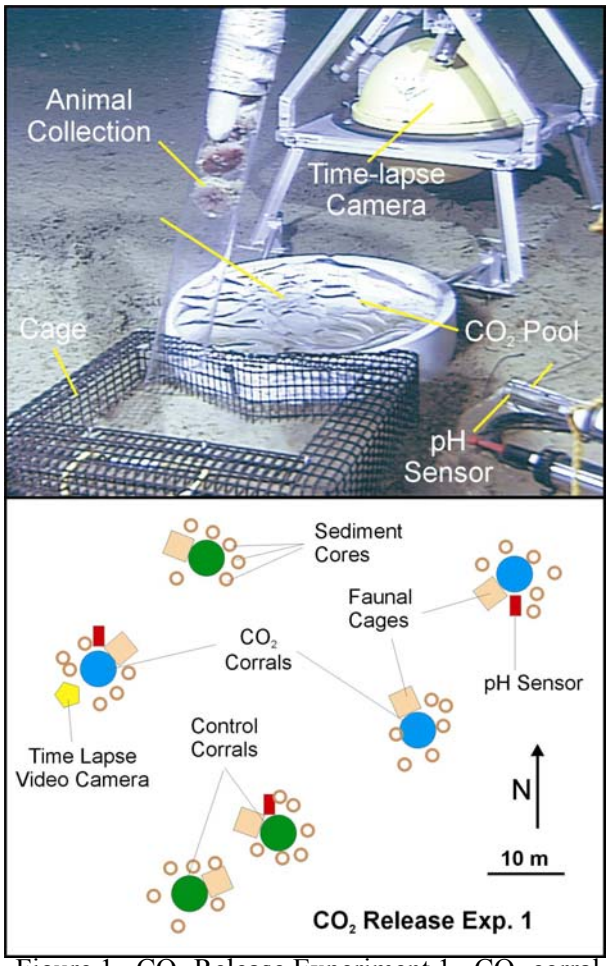

Figure 1. CO_2 Release Experiment 1. CO_2 corral filled with liquid CO_2, animal cage used to hold megafauna, pH sensor, and time-lapse video camera used in E1 (top). Sea urchins and holothurians are visible in acrylic tube, used as suction sampler to collect and deploy megafauna. Experimental layout of CO_2 release E1 at 3600 m depth shown in bottom image.

METHODS

An ROV-mounted CO_2-release system (Brewer et al. 1999) developed by the Monterey Bay Aquarium Research Institute was used to inject liquid CO_2 into PVC corrals placed on the seafloor on the continental rise in 3600 m depth, 85 nm off Moss Landing, CA (36° 42' 33.4" N, 123° 31' 22.0"W). The CO_2 persisted in liquid form, with a hydrate skin, throughout the study. We did not observe large volume changes from massive hydrate formation (Brewer et al. 1999).

In the first experiment (E1), 3 small (48 cm diameter x 15 cm high) PVC corrals were filled with ~twenty liters of liquid CO_2 (Fig. 1), and study animals were held in mesh cages (46 x 46 x 20 cm) placed nearby (<1m). The survival rates of megafauna held in cages and organisms inhabiting sediments adjacent to CO_2 corrals were compared with control groups near three empty corrals. Several individuals each of urchins (*Cystechinus* sp.) and holothurians (*Abyssocucumis* sp.) were collected from the seafloor nearby using a suction sampler and placed carefully in each mesh cage adjacent to CO_2 corrals (n=3) and control corrals (n=3). Sediment cores (7.5 cm diameter x 20 cm deep) were collected to obtain mud samples for microbial, meiofaunal, and macrofaunal counts and analyses (n=6 per corral). Sets of sediment cores were collected prior to dispensing the CO_2 and after 35d exposure. Macrofaunal samples were sieved (300 μm). Meiofaunal analyses were based on percol-gradient centrifugation technique. Microbial counts performed under epifluorescence microscopic inspection of DAPI-stained samples. Abundance, biovolume, or

indices of mortality (e.g. tissue degradation) were compared among treatments at the beginning and end of the experiment.

A second experiment (E2) was similar, but used a single, larger (93 cm diameter x 30 cm high) corral containing ~75 l of liquid CO_2. Study organisms included urchins and infaunal organisms used in E1, and common fishes (eelpout, *Pachycara sp.*; rattail, *Coryphaenoides armatus*). Fishes were collected in baited traps prior to CO_2 release. Fish traps and urchin cages were positioned 1, 5, 10, and 50 m from the central CO_2 pool. Infaunal organisms were sampled from sediment cores at these distances. CO_2 in experimental corrals was replenished after ~2 weeks in each experiment to ensure continued CO_2 dissolution. Both experiments were terminated after ~1 month.

The intensity of plume exposure was estimated from pH sensors positioned 3-5 cm above the seafloor and located 1 m (E1), 5 m, and 50 m (E2) from CO_2 corrals. Time-series records of pH were obtained from 1 m away from a CO_2 pool during E1, and from 5 m, and 50 m from the central CO_2 corral during E2.

The direction and speed of near-bottom currents at the site were measured using an acoustic doppler current meter deployed 2 m above the bottom during E1. Currents 15 m above the bottom were used for analyses. Current records were not obtained during E2.

CO_2 corrals used in E1 were 15 cm high, and filled completely with liquid CO_2, leading to fairly rapid dissolution, likely due to the direct exposure of the CO_2 surface to near bottom currents. During E2, a single larger PVC corral (33 cm high x 94 cm diameter) was filled only 2/3 full, partially insulating the CO_2 surface from bottom currents. This appears to have resulted in a slower dissolution rate and perhaps smaller pH excursions around the corral.

Because all animals collected from 3600 m depths died upon ascent to the surface, mortality caused by CO_2 exposure was distinguished from death during ascent by assessing amphipod tissue condition. A rating system from 1 (intact, "recent death") to 5 (nearly entirely degraded, tissues translucent to transparent, exoskeleton fragile) was used for tissue condition. Ratings of $\geq$4 had been dead for $\geq$2 weeks, based on comparisons with tissue degradation rates of amphipods measured at the site in separate assays. Mortality (% individuals dead) was calculated as the percentage of all individuals with tissue ratings of $\geq$4.

Natural variation in ocean pH was determined from inspection of pH measurements throughout the world ocean available from the National Ocean Data Center (http://www.nodc.noaa.gov/). Estimates of pH changes in the deep-sea caused by 100 y of CO_2 sequestration using injection rates of 0.25 and 4 gtCy-1 were calculated assuming no outgassing of injected CO_2 from the volume of the bottom 1 km of the ocean (~3.6 x 108 km^{-3}), alkalinity = 2400 $\mu m \cdot kg^{-1}$, depth = 3500 m, T = 1.5 ^{o}C, initial ΣCO_2 = 2350 $\mu m \cdot kg^{-1}$, and ending ΣCO_2 = 2356 and 2443 $\mu m \cdot kg^{-1}$, respectively.

RESULTS

In the first experiment (E1) changes in seawater pH around corrals were highly variable owing to changes in current direction with the tides, leading to large peak pH perturbations (ΔpH ~ –1.5 units were observed within 1 m of the CO_2 corrals) during periods when currents were flowing over pH sensors, and little or no pH change when currents carried the CO_2 dissolution plume away from pH sensors. Excursions in pH greater than 1 unit were rare (<5% of the time) even near CO_2 pools, and reductions of $\geq$ –0.2 units occurred only 25% of the time.

In the second experiment (E2) maximum pH shifts recorded 5 and 50 m from the CO_2 pool showed moderate (-0.2 pH units) to minor (-0.05 units) peak pH changes, and small average pH changes (-0.008, -0.003 units), respectively. Shifts of $\geq$ -0.2 units were recorded less than 2% of the time 5 m from the CO_2 pool. Unfortunately, the pH sensor adjacent (1 m) to the central CO_2 corral failed during E2.

Due to the rotary character of inertial and tidal currents at the site, pH perturbations were cyclical, exposing organisms to elevated CO_2 levels during short periods when they were in the path of the dissolution plume. Adoption of more complex experimental techniques analogous to terrestrial ecosystem studies (DeLucia et al. 1999) may be necessary to create steady pH fields. Near-bottom currents during E1 averaged 4.4 $cm \cdot s^{-1}$, with net transport to the SE at 1.7 $cm \cdot s^{-1}$. Fourier analysis of currents and variation in pH 1m (E1) and 5 m (E2) from CO_2 corrals all indicated strong periodicity near

TABLE 1. Summary of CO_2 Impacts

	1 m (E1)	1 m (E2)	5 m (E2)	10 m (E2)	50 m (E2)
Change in pH units: Max (mean)	-1.0 (-0.2)		-0.1 (-0.008)		-0.01 (-0.003)
Bacteria	-2 ns	0	0	0	0
Meiofauna					
Flagellates	64 **	65	33	23	0
Amoebae	67 *	68	34	24	0
Nematodes	63 **	0	0	0	0
Macrofauna					
Amphipod (*Haploops lodo*)	95 ***	15 *	2 ns	3 ns	3 ns
Epibenthic Megafauna					
Urchin – *Cystechinus* sp.	100 **	100	80	0	0
Holothurian – *Abyssocucumis* sp.	100 **				
Near-Bottom Deep-sea Fishes					
Zoarcid – *Pachychara* sp.		0	0		0
Macrourid - *Coryphaenoides armatus*		100	100		100

Table 1. Summary of faunal impacts during CO_2 release experiments. Changes in pH represent the maximum and (mean) perturbations to ambient pH levels during each experiment. Values for each taxon are percentage mortality estimates based on comparisons of CO_2 vs. Control treatments (E1) or initial vs. end samples (E2). CO_2 impacts were high for samples within areas of large pH shifts, and undetectable or non-significant for small pH shifts. Negative mortality listed for bacteria indicates an increase in cell counts. Failure of pH sensors prevented measurements of pH shifts near (1m) the CO_2 pool during E2. All faunal groups except bacteria exhibited high rates of mortality near CO_2 pools in E1. E1, E2 indicate Experiment 1, and 2, respectively. Blanks indicate no data. ns, *, **, *** indicate non-significant, $p<0.05$, $p<0.01$, $p<0.001$ for t-tests.

12.4 h, associated with the major semidiurnal lunar tidal constituent (M2). In effect, organisms 1m from CO_2 pools (E1) were bathed in CO_2-rich waters (ΔpH –1.0 or greater) for ~30 minutes, twice per day. The CO_2 plume was an order of magnitude weaker at 5 m during E2, where pH shifts of $\geq$0.1 unit persisted for ~15 minutes, twice per day.

Most organisms were sensitive to large pH changes in CO_2 dissolution plumes very near CO_2 pools. Urchins and holothurians mortality near (<1m) CO_2 corrals was high during exposure and dissolution of skeletal elements was observed in several urchins. Urchins in control cages appeared unharmed, and all holothurians in control cages were absent, and presumably escaped. Survival of the amphipod, *Haploops lodo*, was low after intense CO_2 exposure during E1. Its abundance and tissue condition were initially similar among treatments, but differed greatly after one month, indicating high mortality rates near CO_2 pools, and very low mortality near control corrals. Sediment-dwelling meiofauna showed similar declines in population density or condition after exposure to intense CO_2 stress. The abundance of flagellates and amoebae were similar near CO_2 and control corrals before CO_2 injection, but declined near CO_2 pools by the end of the experiment. Reduced densities of both groups probably reflect the death and decay of individuals impacted by CO_2. Nematodes, the most prevalent meiofaunal taxon declined only slightly in biovolume near CO_2 pools, apparently due the slow degradation of their chitinous cuticle. Detailed inspection of individuals stained with DAPI using epifluorescence microscopy (indicating the presence / absence of intact cell nuclei), however, indicated that most nematodes near CO_2 had died compared to low mortality near control stations. Unexpectedly, cell counts of sediment bacteria were similar between CO_2 and control corrals, despite the large pH shift and mortality of other groups, and even increased during the study near CO_2 pools.

Faunal responses to the apparently milder CO_2 plume produced during the second experiment were less severe than observed during E1, and decreased at distances of 5 m or greater where pH shifts were very small (Table 1). Urchins held in cages within 1m of the central CO_2 pool died during E2, but no obvious skeletal degradation was observed. Most urchins 5 m from CO_2 also died after exposure to pH reductions of only 0.1 to 0.3 units for less than 2% of the time during E2 and an average pH shift of only –0.008. No CO_2 effects were detectable for urchins held in distant cages (10, 50 m) where pH changes were small (ΔpH =< –0.05 units less than 1% of E2). The mortality rate for amphipods (*Haploops lodo*) near (1m) the CO_2 pool was much lower during E2 than measured in E1, but was greater than before CO_2 release (Table 1). Densities of the smallest meiofaunal groups (flagellates and amoebae) declined near the CO_2 pool, with detectable changes up to 10 m from the pool. Nematode mortality was low, however, suggesting that they were somewhat more tolerant to the milder pH changes during E2 than smaller taxa.

DISCUSSION

Our results support the expectation (Seibel and Walsh 2003) that deep-sea species may be sensitive to pH stress that will accompany a direct CO_2 injection sequestration program. CO_2-related physiological stress, if not lethal, will convey higher "costs of living" through the energetic costs of acid / base balance, restricted aerobic capacity, and inhibition of protein synthesis. These costs may be highest for deep-sea organisms, which typically have limited metabolic capacity. Physiological responses of individuals to increased CO_2 levels may translate into changes in the survival, growth, and reproduction rates of populations, and shifts in the ecosystem dynamics of deep-sea communities.

The scale of ecosystem impacts from a direct CO_2 sequestration program depends on the depths, locations, and certainly the volume of CO_2 injected. Since any CO_2 released will result in CO_2 dissolution plumes from pH ~4 in the boundary layer to background values, animals in close proximity to disposal sites are at risk. Plume effects over larger scale may be estimated coarsely from expected pH fields. For example, if 0.25 to 4 $GtCy^{-1}$ as CO_2 is injected for 100 y beneath 3000 m and disperses worldwide (see methods), the pH of the deep-waters of the entire world ocean will shift by –0.02 to –0.3 units. These levels are comparable to the pH changes observed ~5 m from our CO_2 pools, and overlap or exceed the present range of natural deep-ocean pH variability. Even larger pH perturbations will occur in mixing zones that may extend 10s to 100s of km around disposal sites (Haugan and Drange 1992, Caldeira and Wickett 2002).

Direct deep-sea CO_2 sequestration could partially mitigate the anthropogenic rise in atmospheric pCO_2 that will almost certainly accelerate through this century. Although fossil fuel conservation and alternative energy sources should be primary carbon management strategies, the decision to implement a direct ocean CO_2 sequestration program hinges on the balance between the lesser of two evils – the unabated effects of climate warming or acidification, or both, on terrestrial and shallow marine ecosystems, or damage to deep-sea ecosystems by CO_2 sequestration. Moreover, because most climate stabilization scenarios assume that CO_2 emissions will be balanced by removal, where the ocean is the largest CO_2 sink, it is likely that ocean pH will continue to decrease, with consequences that are currently not understood. Ongoing research should provide guidance concerning the risks of direct CO_2 injection, and may mandate other methods or more environmentally benign CO_2 sequestration approaches (e.g. accelerated carbonate dissolution; Caldeira and Rau 2000). Clearly, an ocean carbon sequestration program will be successful only if its intended benefits – a stabilization of atmospheric CO_2 and mitigation of climate warming consequences for terrestrial and shallow water ocean systems, outweigh its liabilities – energy expended on sequestration and damage to deep-sea ecosystems. Lacking presently is sufficient information on both sides of this balance.

REFERENCES

Barnola, J.-M., Raynaud, D., Lorius, C., & Barkov, N.I. Historical CO_2 record from the Vostok ice core. In *Trends: A Compendium of Data on Global Change*. Carbon Dioxide Information Analysis Center, Oak Ridge National Laboratory, U.S. Department of Energy, Oak Ridge, Tenn., U.S.A (2003).

Brewer, P.G., Friederich, G., Peltzer, E.T., & Orr, F.M. Jr. Direct experiments on the ocean disposal of fossil fuel CO_2. *Science* 284, 943-945 (1999).

Caldeira, K. & Wickett, M.E. Comparing pH impacts of oceanic CO_2 injection and atmospheric CO_2 release. *Eos Trans. AGU,* 83(1), Spring Meet. Suppl., Abstract OS51F-01 (2002).

Caldeira, K., & Rau, G.H. Accelerating carbonate dissolution to sequester carbon dioxide in the ocean: Geochemical implications. *Geophys. Res. Let*. 27, 225-228 (2000).

Caldeira, K., Jain, A.K., & Hoffert, M.I. Climate sensitivity uncertainty and the need for energy without CO_2 emission. *Science*, 299, 2052-2054 (2003).

DeLucia, E. H., J.G. Hamilton, S.L. Naidu, R.B. Thomas, J.A. Andrews, A. Finzi, M. Lavine, R. Matalama, J.E. Mohan, G.R. Hendrey, and W.H. Schlesinger. (1999) Net primary production of a forest ecosystem with experimental CO_2 enrichment. *Science*, 284, 1177- 1179.

Drange, H., Alendal, G., & Johannessen, O.M. Ocean release of fossil fuel CO_2: A case study. *Geophys. Res. Lett*. 28, 2637-2640 (2001).

Harvey, L.D.D. Impact of deep-ocean carbon sequestration on atmosphereic CO_2 and on surface-water chemistry. *Geophys. Res. Lett.* 30, 1237-1240 (2003).

Haugan, P.M., & Drange, H. Sequestration of CO_2 in the deep ocean by shallow injection. *Nature* 357, 318-320 (1992).

Houghton, J.T. et al., *Climate Change: The IPCC Scientific assessment. Intergovernmental Panel on Climate Change*, Cambridge University Press (1990).

IPCC. In *Climate Change 2001: The Scientific Basis* (eds Houghton, J.T., et al., Cambridge University Press, Cambridge, 896 p, 2001).

Keeling, C.D. & Whorf, T.P. Atmospheric CO_2 records from sites in the SIO air sampling network. In *Trends: A Compendium of Data on Global Change*. Carbon Dioxide Information Analysis Center, Oak Ridge National Laboratory, U.S. Department of Energy, Oak Ridge, Tenn., U.S.A. (2002)

Kleypas, J.A. *et al*., Geochemical consequences of increased atmospheric carbon dioxide on coral reefs. *Science* 284, 118-120 (1999).

Knowlton, N. The future of coral reefs. *Proc. Nat. Acad. Sci.* 98, 5419-5425 (2001).

Mann, M.E., Bradley, R.S. & Hughes, M.K. Northern hemisphere temperatures during the past millennium: interferences, uncertainties, and limitations. *Geophys. Res. Lett*. 26, 759-762 (1999).

Marchetti, C. On geoengineering and the CO_2 problem. *Climate Change* 1, 59-69 (1977).

Marland, G., Boden, T.A., & Andres, R.J. Global, Regional, and National CO_2 Emissions. In *Trends: A Compendium of Data on Global Change*. Carbon Dioxide Information Analysis Center, Oak Ridge National Laboratory, U.S. Department of Energy (2001; http://cdiac.esd.ornl.gov/trends/trends.htm).

McNeil, B., Matear, R.J., Key, R.M., Bullister, J.L., & Sarmiento, J.L. Anthropogenic CO_2 uptake by the ocean based on the global chlorofluorocarbon data set. *Science* 299, 235-239.

Parmesan, C. & Yohe, G. A globally coherent fingerprint of climate change impacts across natural systems. *Nature* 421, 37-42 (2003).

Pörtner, H.-O., Reipschläger, A. In, *Ocean Storage of CO_2. Environmental, Workshop 2: Environmental Impact* (eds Ormerod, B., Angel, M.) 57-81 (IEA Green house and Gas R & D Programme, Southampton Oceanography Centre, UK, 1996).

Reichle, D. et al. *Carbon Sequestration: Research and Development* (Office of Science, Office of Fossil Energy, U.S. Dept. of Energy, 1999).

Root, T.L., et al. Fingerprints of global warming on wild animals and plants. *Nature* 421, 57-60 (2003).

Sabine, C.L., et al. Distribution of anthropogenic CO_2 in the Pacific Ocean. *Global Biogeochemical Cycles* 16, 1083-1099 (2002).

Seibel, B.A. & Walsh, P.J. Biological impacts of deep-sea carbon dioxide injection inferred from indices of physiological performance. *J. Exp. Biol.* 206, 641-650 (2003).

Tamburri, M.N., Peltzer, E.T., Friederich, G.E., Aya, I., Yamane, K., & Brewer, P.G. A field study of the effects of CO_2 ocean disposal on mobile deep-sea animals. *Mar. Chem.* 72, 95-101 (2000).

ACKNOWLEDGEMENTS

This research was supported by MBARI (projects 200001, 200002), the U.S. Dept. of Energy, Fossil Energy Group (Grant DE-FC26-00NT40929), and the U.S. Department of Energy, Ocean Carbon

Sequestration Program, Biological and Environmental Research (BER), (grant #DE-FG03-01ER63065). Deep-sea experiments would not have been possible without the excellent support of the crews of the R/V Western Flyer and ROV Tiburon.

27
Direct Injection of CO_2 in the Ocean

Peter G. Brewer

It is now 25 years since Marchetti (1977) first suggested bypassing atmospheric disposal of some fraction of industrial CO_2 emissions and using direct deep-ocean disposal as one means of ameliorating climate change. After all, the alkalinity of the ocean already provides the dominant long-term sink for atmospheric CO_2, and deep-ocean injection may logically be seen as simply accelerating a "natural" process. Behind this apparently simple suggestion lies great complexity, fascinating science, and strongly held opinions. The scale of modern CO_2 fluxes, and the interest in finding safe and economically viable ways to avoid "dangerous anthropogenic interference with climate," has led to new efforts to investigate this possible solution. Until very recently, only cartoon sketches were available to describe the possibilities of this field (Hanisch 1998). Now, important and challenging small-scale field experiments (Brewer et al. 1999) and new ocean modeling studies (Drange et al. 2001; Caldeira et al. 2002) have been conducted, and they illuminate both the possibilities and the challenges facing this strategy. A significant international scientific literature now exists (Handa and Ohsumi 1995), and the field has become established as a growing part of ocean science.

There are many variants of proposed ocean CO_2 disposal strategies. For example, Caldeira and Rau (2000) proposed using limestone to neutralize saturated solutions of captured CO_2, followed by shallow ocean disposal of the resulting solution. All of these concepts will have to be subjected to experimental test, and much of this work remains to be done. Early experiments on small-scale CO_2 injections form the basis of this background chapter.

The scale of surface ocean CO_2 uptake from the atmosphere is now so large that any distinction between a "natural" process and an industrial policy of only slightly indirect surface ocean disposal is hard to maintain. The average rate of surface ocean CO_2 uptake for the 1980s and 1990s was approximately 2.0 petagrams of carbon per year (PgC y^{-1}). This is 21 million tons of CO_2 per day, and fluxes of such scale will have biogeochemical impacts. Surface ocean waters are already>0.1 pH units lower than in

preindustrial times (Brewer 1997), and if the IS92A "business-as-usual" scenario of the Intergovernmental Panel on Climate Change (IPCC) is followed, by the end of this century surface ocean carbonate ion concentrations will drop by 55 percent, with anticipated major effects on coral reef systems (Langdon et al. 2000) and calcareous plankton (Riebesell et al. 2000).

With this as background, it is clear that the enormous engineering demands would limit any industrial effort to dispose of CO_2 by direct injection in the deep sea to a very small fraction of the massive current and future surface fluxes. Nonetheless, such techniques could be very useful as part of a portfolio of atmospheric stabilization strategies, if they are shown to be safe and cost-effective. The criticisms leveled at this approach are essentially that it would be harmful to marine life (Seibel and Walsh 2001) and that it would inevitably increase the already large oceanic burden of fossilfuel CO_2.

Such comments at once expose scientific unknowns, for there are simply no standards to refer to here, and standards are urgently needed. How sensitive are marine animals to pH changes? If we permit atmospheric CO_2 levels to rise to ~600 parts per million (ppm) and remain there, then surface ocean waters, and eventually all ocean waters, will experience an ~0.3 pH change from preindustrial levels. Is that an acceptable limit, and why? What burden of fossil fuel CO_2 is "acceptable" for climate or geochemical or biological reasons? How might we view the trade-off between the direct effects of CO_2 and the induced effects of climate and temperature? The focus of the ocean science community has been on observing the evolving fossil-fuel CO_2 tracer signal,

and these questions have simply (and astonishingly) not yet been posed. It is clear that the atmosphere, and therefore also the ocean, has experienced very large changes in CO_2 over Phanerozoic time (Berner 1990). And in today's ocean there are large pH gradients between the Atlantic and Indo-Pacific oceans and within ocean basins. Many marine animals migrate vertically through large pH gradients each day. How these observations relate to the modern fossil-fuel signal remains to be tested.

Given these questions, the current series of deep-ocean CO_2 injection experiments can be viewed not simply as disposal strategy tests, but also as controlled enrichment experiments that may allow us to mimic the elevated CO_2 levels of a future ocean in much the same way that ecosystems are manipulated on land (DeLucia et al. 1999; Shaw et al. 2002).

The cost of CO_2 capture dominates the economics of both geologic and oceanic disposal schemes. An excellent introduction to this problem is provided by the International Energy Agency's Greenhouse Gas Program (http://www.ieagreen.org.uk/). The most widely used technology is scrubbing the gas stream with an amine solvent and regenerating the pure CO_2 by heating the amine. This technique is routinely used in the food and beverage industries and for capturing CO_2 for geologic disposal in the Sleipner Field off Norway. The costs of the capture process presently exert an ~25 percent energy penalty, and there are now strenuous efforts to improve this.

The Near-Field Fate of CO_2 in Seawater

Ocean scientists are well versed in the thermodynamics and ocean distributions of the extraordinarily dilute (~2.2 millimolar [mM]) oceanic CO_2 system (Wallace 2001). But such concepts must be radically extended to investigate the science of deep-ocean CO_2 injection. Figure 27.1 shows the phase diagram for pure CO_2 superimposed on an oceanic pressure-temperature (P-T) scale (Brewer et al. 1999), with a temperature profile from a station off northern California overlaid.

The shaded area in Figure 27.1 indicates the zone in which CO_2 will react with seawater to from a solid hydrate ($CO_2.6H_2O$), with profound changes in physical behavior.

For the P-T profile indicated, CO_2 gas will first form a hydrate at a depth of about 350 meters (m). The transition from gas to liquid occurs at about 400 m deep. For warm water regions (such as the Sargasso and Mediterranean Seas), these profiles will be shifted, but Figure 27.1 is generally applicable over much of the world's oceans. Liquid CO_2 is highly compressible, and at depths <2,750 m, it is less dense than seawater; thus CO_2 released will form a buoyant plume that will dissolve in the surrounding ocean (Alendal and Drange 2001). The dissolution rate of CO_2 droplets is close to 3 micro-

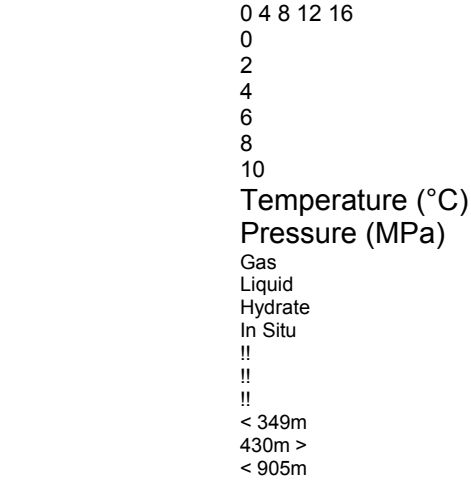

Figure 27.1. The phase behavior of CO_2 in seawater, showing the gas-liquid and hydrate phase boundaries with a typical in situ P-T profile (from Brewer et al. 1999).

moles per square centimeter per second ((mol cm^{-2} sec^{-1}) (Brewer et al. 2002a), with the result that, for a release of small droplets, 90 percent of the plume is dissolved within 30 minutes and within about 200 m above the release point.

Below a depth of about 3,000 m, the high compressibility of liquid CO_2 results in formation of a fluid of greater density than seawater, and a gravitationally stable release is possible. This finding has led to suggestions of storing liquid CO_2 as a "lake" on the deep ocean floor. Here considerable complexity exists. The solubility of CO_2 in seawater is so high ((0.8 molar at 1(C and 30 megapascals [MPa]) and the partial molal volume so low ((31 milliliters per mole [ml mol_{-1}]) that a dense boundary layer can form (Aya et al. 1997), inhibiting mixing with the ocean above. Such a system would have much in common with naturally occurring pools of dense brines on the seafloor. The formation of hydrate in such a system, however, can occur spontaneously, with complex self-generated, fluid dynamic instabilities and resulting large volume changes from the incorporation of six molecules of water for every molecule of CO_2 (Brewer et al. 1999). A spectacular example of this is shown in Figure 27.2, where an experimental pool of CO_2 placed on the seafloor at 3,600 m depth has penetrated the upper sediments and formed a massive hydrate "frost heave."

It was earlier thought that the formation of a hydrate would possibly result in "per-

Figure 27.2. A "frost heave" of CO_2 hydrate on the sea floor at 3,600 m depth resulting from massive hydrate formation).

manent" storage of CO_2 on the seafloor as a hydrate because the P-T conditions are so strongly favorable. The essential condition for hydrate stability, however, is equality of the chemical potential in all phases. Because seawater is so strongly undersaturated with respect to CO_2, the hydrate will dissolve. The oceanic dissolution rates of both hydratecoated CO_2 droplets (Brewer et al. 2002b) and of the solid hydrates (Rehder et al. 2002) have been directly measured.

Possible technologies for future applications may include either pipeline or tanker injection techniques (Aya et al. 2003). With either approach, injection depth, physical state, or local pH perturbation can be optimized.

The Far-Field Fate of CO_2 in Seawater

Once fossil-fuel CO_2 injected into deep-ocean water becomes dissolved in the background ocean, it yields a tracer signal that can be modeled. Aumont et al. (2001) compared seven ocean models to explore the long-term fate of purposefully injected CO_2. Essentially all show a strong correlation between depth of injection and efficiency of retention. For injection at 3,000 m ocean depth, overall retention efficiencies are ~ 85 percent over a 1,000-year timescale. Some surface ocean reexposure and reabsorption from the atmosphere is included in this estimate. For a 3,000 m injection, this fraction is about 25 percent of the total.

Experimental Activities

For many years, only model concepts and sketches were available to describe this field. Plans for a medium-scale experiment (several tons CO_2) off the coast of Hawaii, and later off the coast of Norway, were frustrated by environmental permitting issues. This situation changed in 1996, with the successful adaptation of remotely operated vehicle (ROV) technology to contain and release small, controlled quantities of CO_2 in the deep ocean for scientific study (Brewer et al. 1998). Rapid advances in technique then led to the ability to conduct experiments at great depth (Brewer et al. 1999). These experiments have now been extended to elegant biological response studies (Barry et al. 2002) and sophisticated chemical measurements (Brewer et al. 2002b).

The most recent experimental system used is a 56-liter (l), carbon-fiber, composite piston-accumulator (Hydratech, Fresno, CA), with a 23-centimeter (cm) outside diameter and 194-cm length, rated at 3,000 pounds per square inch gauge (psig), for ROV operation (Figure 27.3). Two tandem cylinder pumps, with capacities of 128 milliliters (ml) and 970 ml, provide power for accurate delivery of the contained CO_2. The CO_2 cools and compresses during descent to ocean depth, so that under typical conditions

(900 psig on deck at 16(C; 1.6(C at 3,600 m), 45 l are available per dive for experimental purposes.

The availability of these experimental quantities permits tests of ecosystem responses

to elevated deep-ocean CO_2 levels. One recent experimental arrangement is shown in Figure 27.4. Here, a set of small CO_2 "corrals" has been placed on the seafloor at a depth of 3,600 m, where the liquid CO_2 is sufficiently dense to be gravitationally stable. Around these CO_2 sources are arranged animal cages, and cores are taken to investigate the benthic infauna. Current meters, a time-lapse camera, and recording pH sensors complete the observing system.

Such experiments are at a very early stage, and rapid progress is expected. The challenges of carrying out field experiments in the deep sea should, however, not be underestimated. For example, the well-known tidal flows force the low pH plume from the CO_2 corrals, so that the experimental cages are exposed to varying pH signals (Figure 27.5). It should be possible to advance experimental design to improve this.

Conclusions

Deep-ocean CO_2 sequestration is clearly technically possible, although there are many variants in the details, and few of these have yet been explored thoroughly. The primary costs of any CO_2 capture and disposal technology lie in the capture step, and this situation is the same for either geologic or oceanic disposal. Early ideas of "permanent" dis-

Figure 27.3. A 56 l carbon-fiber-wound CO_2 delivery system installed on ROV Tiburon, showing end cap with gauges, delivery pumps on top, and valves to the left. The dispensing valve is attached to the robotic arm in front of the vehicle and is not shown (from Brewer et al. 2003).

Figure 27.5. The pH signals recorded at distances of 1 m, 5 m, and 50 m from a CO_2 source placed on the seafloor. The effects of electrode drift have been removed, and the data sets are offset for visual clarity. The background oceanic pH is about 7.6. The effect of the tidal velocity ellipse is to advect the CO_2 plume past each sensor with about a 12.4-hour period (from Barry et al. 2002).

Figure 27.4. A sketch of a deep-sea CO_2 enrichment experimental site designed to investigate the response of marine organisms to locally elevated CO_2 levels. Note that deep ocean CO_2 levels will rise even in the absence of any active carbon sequestration program (from Barry et al. 2002).

posal as a hydrate on the seafloor are not realistic because the hydrate will readily dissolve in the unsaturated ocean water. Concepts of a "lake" of CO_2 on the seafloor, with a stable, dense boundary layer above, remain to be tested, but these would be locally specific solutions where seafloor topography permits. In most locations, CO_2 would quickly become dissolved in seawater and transported as a tracer plume by the abyssal circulation. The mean ventilation time of the Atlantic Ocean is ~250 years, and that of the Pacific Ocean ~550 years (Stuiver et al. 1983). Models show the expected Antarctic atmospheric reexposure of CO_2 on approximately these timescales. Much of the CO_2 is reabsorbed, with the result that, over a timescale of about 1,000 years, the injection is some 85 percent efficient.

The primary concerns over oceanic injection are the possible effects on marine life,

and the fact that it will add to the already substantial ocean fossil-fuel CO_2 burden. There are as yet no standards to refer to here, and these are urgently needed. The current invasion rate of fossil-fuel CO_2 from the atmosphere to the surface ocean now approximates 20 million tons per day. This flux has already changed surface ocean pH, and a 0.3 pH reduction in ocean waters can be expected if atmospheric CO_2 is held at about 600 ppm. Thus, deep-sea ecosystems will inevitably experience change, and it is likely that any disposal strategy will be of significantly smaller scale than the surface invasion signal.

Release of CO_2 directly into the ocean may be less harmful than release of CO_2 into the atmosphere. In this case, if injected CO_2 results in diminished atmospheric peak concentrations, then direct injection of CO_2 in the ocean could reduce the overall adverse consequences of fossil-fuel burning. If oceanic injection simply adds to atmospheric releases, however, overall adverse consequences could increase. Thus, the ability of oceanic injection to contribute to diminished adverse consequences of fossil-fuel use depends both on the science and technology of oceanic CO_2 injection and on the roles that that science and technology might play in our energy economy.

Acknowledgments

I acknowledge the David and Lucile Packard Foundation, the U.S. Department of Energy Ocean Carbon Sequestration Program, and an international research grant from the New Energy and Industrial Technology Organization for support of this research.

Literature Cited

Alendal, G., and H. Drange. 2001. Two-phase, near field modeling of purposefully released CO_2 in the ocean. *Journal of Geophysical Research* 106:1085–1096.

Aumont, O., J. C. Orr, A. Yool, K. Plattner, F. Joos, E. Maier-Reimer, M.-F. Weirig, R. Schlitzer, K. Caldeira, M. Wickett, and R. Matear. 2001. Efficiency of purposeful CO_2

injection in the deep ocean: Comparison of seven ocean models. *IGBP Open Science Conference 2001, Amsterdam, The Netherlands*. http://www.ipsl.jussieu.fr/OCMIP /phase2/poster/aumont.pdf.

Aya, I., K. Yamane, and H. Nariai. 1997. Solubility of CO_2 and density of CO_2 hydrate at 30 MPa. *Energy* 22:263–271.

Aya, I., R. Kojima, K. Yamane, P. G. Brewer, and E. T. Peltzer. 2003. In situ experiments of cold CO_2 release in mid-depth. Pp. 739–744 in *Greenhouse gas control technologies,* edited by J. Gale and Y. Kaya. Amsterdam: Pergamon.

Barry, J., B. A. Seibel, J. Drazen, M. Tamburri, C. Lovera, and P. G. Brewer. 2002. Field experiments on direct ocean CO_2 sequestration: The response of deep-sea faunal assemblages to CO_2 injection at 3200m off Central California. *Eos, Transactions, American Geophysical Union* 83:OS51F-02.

Berner, R. A. 1990. Atmospheric carbon dioxide levels over Phanerozoic time. *Science* 249:1382–1386.

Brewer, P.G. 1997. Ocean chemistry of the fossil fuel CO_2 signal: The haline signature of "business as usual." *Geophysical Research Letters* 24:1367–1369.

Brewer, P. G., F. M. Orr Jr., G. Friederich, K. A. Kvenvolden, and D. L. Orange. 1998. Gas hydrate formation in the deep sea: In situ experiments with controlled release of methane, natural gas, and carbon dioxide. *Energy and Fuels* 12:183–188.

Brewer, P. G., G. Friederich, E. T. Peltzer, and F. M. Orr Jr. 1999. Direct experiments on the ocean disposal of fossil fuel CO_2. *Science* 284:943–945.

Brewer, P. G., E. T. Peltzer, G. Friederich, and G. Rehder. 2002a. Experimental determination of the fate of rising CO_2 droplets in seawater. *Environmental Science and Technology* 36:5441–5446.

Brewer, P. G., J. Pasteris, G. Malby, E. T. Peltzer, S. White, J. Freeman, B. Wopenka, M. Brown, and D. Cline. 2002b. Laser Raman spectroscopy used to study the ocean at 3600-m depth. *Eos, Transactions, American Geophysical Union* 42:469–470.

Brewer, P. G., E. T. Peltzer, G. Rehder, R. Dunk. 2003. Advances in deep-ocean CO_2 sequestration experiments. Pp.1667–1670 in *Greenhouse gas control technologies,* edited

by J. Gale and Y. Kaya. Amsterdam: Pergamon.
Caldeira, K., and G. H. Rau. 2000. Acclerating carbonate dissolution to sequester carbon dioxide in the ocean: Geochemical implications. *Geophysical Research Letters* 27:225–228.
Caldeira, K., M. E. Wickett, and P. B. Duffy. 2002. Depth, radiocarbon and the effectiveness of direct ocean injection as an ocean carbon sequestration strategy. *Geophysical Research Letters,* doi:10.1029/2001GL014234.
DeLucia, E. H., J. G. Hamilton, S. L. Naidu, R. B. Thomas, J. A. Andrews, A. Finzi, M. Lavine, R. Matalama, J. E. Mohan, G. R. Hendrey, and W. H. Schlesinger. 1999. Net primary production of a forest ecosystem with experimental CO_2 enrichment. *Science* 284:1177– 1179.
Drange, H., G. Alendal, and O. M. Johannessen. 2001. Ocean release of fossil fuel CO_2: A case study. *Geophysical Research Letters* 13: 2637–2640.
Handa, N., and T. Ohsumi. 1995. *Direct ocean disposal of carbon dioxide.* Tokyo: Terra.
Hanisch, C. 1998. The pros and cons of carbon dioxide dumping. *Environmental Science and Technology* 32:20–24A.
Langdon, C., T. Takahashi, C. Sweeney, D. Chipman, J. Goddard, F. Marubini, H.

Aceves, H. Barnett, and M. J. Atkinson. 2000. Effect of calcium carbonate saturation state on the calcification rate of an experimental coral reef. *Global Biogeochemical Cycles* 14:639–654.
Marchetti, C. 1977. On geoengineering and the CO_2 problem. *Climatic Change* 1:59–68.
McNeil, B., R. J. Matear, R. M. Key, J. L. Bullister, and J. L. Sarmiento. 2003. Anthropogenic CO_2 uptake by the ocean based on the global chlorofluorocarbon data set. *Science* 299:235–239.
Rehder, G., S. H. Kirby, W. B. Durham, L. Stern, E. T. Peltzer, J. Pinkston, and P. G. Brewer. 2002. Dissolution rates of pure methane hydrate and carbon dioxide hydrate in undersaturated sea water at 1000m depth. *Geochimica et Cosmochimica Acta* (submitted).
Riebesell, U., I. Zondervan, B. Rost, P. D. Tortell, R. E. Zeebe, and F. Morel. 2000. Reduced calcification of marine plankton in response to increased atmospheric CO_2. *Nature* 407:364–367.
Seibel, B., and P. J. Walsh. 2001. Potential impacts of CO_2 injection on deep-sea biota. *Science* 294:319–320.
Shaw, H. R., E. S. Zavaleta, N. R. Chiariello, E. L. Cleland, H. A. Mooney, and C. B. Field. 2002. Grassland responses to global environmental changes suppressed by elevated CO_2. *Science* 298:1987–1990.
Stuiver, M., P. D. Quay, and H. G. Ostlund. 1983. Abyssal water carbon-14 distribution and the age of the world oceans. *Science* 219:849–851.
Wallace, D. W. R. 2001. Storage and transport of excess CO_2 in the oceans: The JGOFS/WOCE Global CO_2 survey. In *Ocean circulation and climate*, edited by G. Siedler, J. Church, and J. Gould. San Diego: Academic Press.

First Expeditionary Deployments of the Deep Ocean Raman In Situ Spectrometer

S. N. White (sheri@mbari.org), P. G. Brewer (brpe@mbari.org), E. T. Peltzer, W. Kirkwood Monterey Bay Aquarium Research Institute, Moss Landing, CA 95039
J. D. Pasteris Washington University, Dept. of Earth & Planetary Science, St. Louis, MO 63130
N. Nakayama Hokkaido University, Div. of Earth and Planetary Science, Sapporo, Hokkaido 0600810, Japan

OS32A
0235

ABSTRACT

MBARI's *in situ* laser Raman spectrometer (DORISS – Deep Ocean Raman In Situ Spectrometer) was deployed at gas vents in Guaymas Basin, Gulf of California in 2003. The first *in situ* Raman spectra of natural gas venting from the sea floor were obtained. These spectra were compared to GC analyses of samples collected at the same vent and Raman analyses of pure methane deployed as a standard for at-sea testing.

Laser Raman spectroscopy is a powerful technique for analyzing the chemical composition and molecular structure of solids, liquids, and gases. The prototype deep-ocean Raman instrument is based on an off-the-shelf laboratory model from Kaiser Optical Systems, Inc. Engineering test deployments conducted over the past 1.5 years have shown that Raman spectra of high quality can be obtained in the deep ocean. We have acquired spectra from solid, liquid and gaseous specimens deployed as deep as 3600 m in the ocean. We are currently in the next phase of development which consists of using DORISS for exploratory measurements of natural targets in the deep ocean.

During an expedition to the Gulf of California on the R/V Western Flyer in 2003, DORISS was deployed successfully by the ROV Tiburon at natural gas vents on the sea floor (~1582 m depth). Spectra were collected of gas samples at the vent site and at depths above the hydrate stability zone. Bands for methane dominate the spectra. Attempts to collect spectra of natural gas hydrates at the vent were difficult in part due to the stringent positioning requirements of the probe head when analyzing solid, opaque targets. This problem has been addressed by the development of a precision underwater positioner (PUP) that provides a stable platform for analyses and precision movement of the probe head (see following poster OS32A-0236).

DORISS Instrument

DORISS is based on a laboratory model spectrometer from Kaiser Optical Systems, Inc. It consists of a 532 nm Nd:YAG laser, a holographic transmissive grating, a 2048 x 512 CCD camera from Andor Technology, and a holographically filtered optical head with interchangeable sampling optics. The duplex grating covers the 100-4400 cm^{-1} spectral region and splits the spectrum into two stripes on the face of the CCD, providing a mapping of ~1 cm^{-1} per pixel.

The DORISS instrument is divided into three pressure housings :

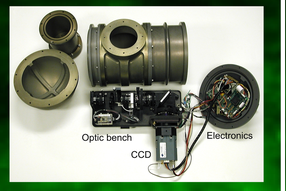

Spectrometer Housing — spectrometer, CCD and associated electronics

Probe Head Housing — optical head; deployed to the target via ROV manipulator,

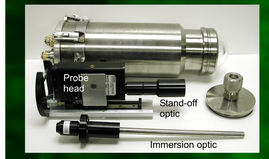

Electronics Housing — laser, power supply, and single-board computer

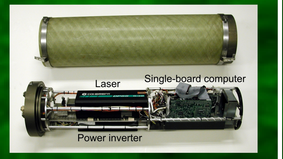

The two sampling optics were used during this expedition (both shown above left):

Stand-off optic – a 10X objective used behind a dome window
- ~3 mm depth of focus in water, 0-10 cm working distance in water
- larger depth of focus provides greater flexibility but lower power density

Immersion optic – 2 mm focal distance lens at the end of 10 in. long, 0.5 in. diameter metal tube with a plane sapphire end window protruding through a flat endcap with a gland seal (pictured at right)
- ~1 mm depth of focus, 1-7 mm working distance in water
- higher power density preferred when analyzing gases, but small depth of focus requires precision positioning when used on opaque targets

Calibration

DORISS was calibrated routinely during the cruise. The Kaiser calibration kit includes a neon source for wavelength calibration, a tungsten source for intensity calibration, and a cyclohexane standard for laser wavelength calibration. A diamond plate was installed in the laser path within the probe head but off focus. The strong, stable 1332 cm^{-1} line is superimposed on all spectra providing a calibration reference during deployment.

Instrument details can be found in Brewer et al., in press.

Gulf of California Expedition

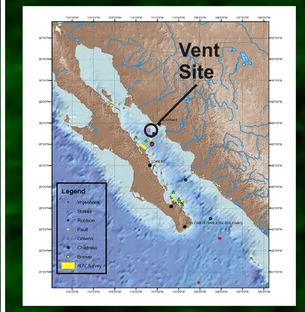

During the Spring of 2003 the R/V Western Flyer and ROV Tiburon traveled to the Gulf of California. (Expedition map at left.) During Leg 5 of this expedition (April 21st – May 11th), we had the opportunity to use DORISS to analyze natural gas seeping from the sea floor along a transform ridge just north of Guaymas Basin. Seeps were located acoustically at this site in 1980 [Merewether et al., 1985], and visited with the submersible Alvin in 1985 [Simoneit et al., 1990].

We were able to locate a single gas vent at 27°35.5'N, 111°28.5'W, 1582 m (right). During four ROV dives to this site we attempted to collect *in situ* Raman spectra of natural gas bubbling from the sea floor, and solid gas hydrates found in the sediment. We were also able to collect gas samples for GC shore-side analysis to verify the *in situ* data.

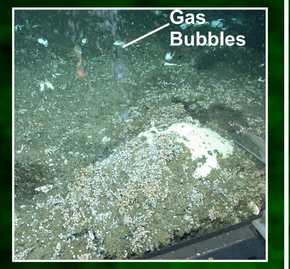

Gas collection

Raman Samples

Two experimental set-ups were used to collect gas and hydrate samples for *in situ* Raman analysis. One configuration consisted of the Raman probe head with the stand-off optic mounted on an off-loadable frame in a downward looking orientation (right). Two specially designed funnels could be positioned below the probe head in the laser beam path – one with a sealed glass top for capturing gas, the other with a mesh top to capture chunks of hydrate while allowing gas to escape. Unfortunately, the hydrate fragments excavated in this area were too small to be captured and thus no spectra of solid hydrate were obtained. Spectra of gas samples were analyzed in this configuration both at the sea floor and during ascent.

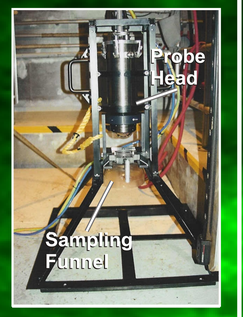

The preferred method of obtaining gas spectra was through use of the immersion optic protruding into an open-bottomed cube (picture A below). Gas was trapped in the cube forming a gas space around the immersion optic (i.e., no seawater was present in the beam path). Both configurations were successful for analyzing gas samples. The one problem was the formation of a partially-opaque hydrate skin on the window of the immersion probe and the glass top of the sampling funnel. This partially blocked both the exiting beam and the backscattered signal, thus greatly reducing the sensitivity. Once the sample was brought above the hydrate stability zone (~585 m depth, ~7.0°C) clean, high quality spectra could be obtained.

Gas Samples

Gas samples for shore based analysis were collected in 150 ml stainless steel cylinders. Three evacuated cylinders were integrated into a sampling funnel with a heating element (picture B below). During sample collection gas hydrate formed in the sampling funnel which could clog the lines to the cylinders. The heating element was used to heat the sample and melt the hydrate. The gas could then be pulled into an evacuated cylinder by actuating a valve. Sixteen samples were collected in this manner. These samples include gas bubbling from the vent, gas bubbles captured above the vent, gas within the sediment, and melted hydrate from within the sediment.

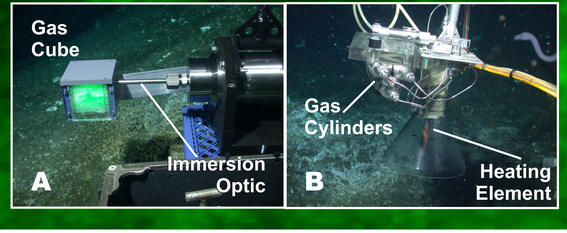

Raman Analysis

Raman spectroscopy, which is capable of identifying covalently bonded gas species, can be used to determine the composition of natural gas [e.g., Diller and Chang, 1980]. The primary constituent of the vent gas was assumed to be methane which has a strong Raman peak at ~2917 cm^{-1} (, vibrational mode), and smaller peaks at 1535 ($_2$), 3020( ), and 3070 cm^{-1} (2 $_2$). Non-methane hydrocarbons (NMHC) were also assumed to be present in measurable quantities. Raman spectra of the vent gas were obtained at the sea floor (1582 m, ~3.0°C) and at various depths in the water column using both sampling optics.

Data processing was performed with the GRAMS/AI spectral processing package from ThermoGalactic. The GRAMS peak fitting algorithm deconvolves the peaks, calculates and subtracts the baseline function, and determines peak positions (Raman shift), heights, widths and areas.

Changes in the position and intensities of the gas bands can indicate changes in gas density. The , methane peak (~2917 cm^{-1}) is known to experience a downshift in wavenumber with increasing density [Seitz et al.,1993]. The graph to the left shows the position of the , methane peak with respect to depth (pressure, density) as measured by DORISS. Our data show the peak shifting by 0.003 cm^{-1} per meter depth.

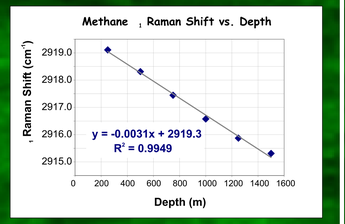

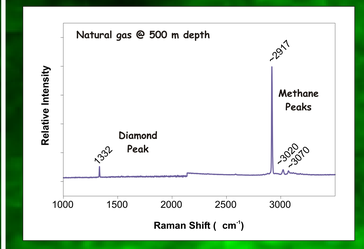

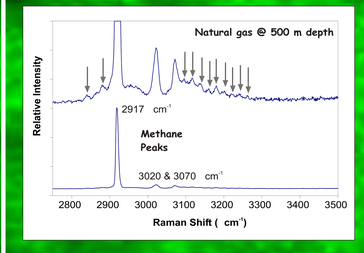

The highest quality spectra were collected with the immersion optic after the sample was raised above the hydrate stability zone (such that the hydrate skin formed on the optical window was dissipated). The spectrum at left was collected at a depth of 500 m. The 1332 cm^{-1} diamond standard peak is clearly visible in the spectrum. The step at ~2200 cm^{-1} is where the two spectral windows are joined.

There are three main observations from this data:

1) Methane is the only component that has been identified in the spectra to date. While other higher hydrocarbons may be present, they are not in high enough concentrations to be detected by Raman analyses. GC analysis on shore verified that methane is present at ~97%.

2) Brunsgaard Hansen et al. [2002] observed that the pressure (density) of a methane mixture can be inferred from the ratio of the 3020 ($_3$) and 3070 cm^{-1} (2 $_2$) bands. The intensity ratios we observed are similar to those observed by Brunsgaard Hansen et al. [2002]:

0.67 @ 1582 m (~16.1 MPa); 1.75 @ 250 m (~2.6 MPa).

3) The intensity and resolution of the spectra reveal not only vibrational bands of methane (e.g., 2917, 3020, and 3070 cm^{-1}), but also coupled rotational-vibrational bands (indicated by arrows at left) from intramolecular Coriolis forces.

GC Analysis

Methods

Vent gases, some containing decomposed hydrate samples, were collected in stainless steel evacuated cylinders (right) for later analysis. In the laboratory we determined C_1–C_5 hydrocarbons and CO_2 concentrations using a Hewlett Packard, 5890 gas chromatograph with a flame ionization detector (FID) for hydrocarbons and a thermal conductivity detector (TCD) for CO_2. He was the carrier gas at a 36 ml/min constant flow rate. Samples were transferred to a calibrated volume loop (0.1 ml and 1.0 ml) at atmospheric pressure through a glass tube packed with Drierite for water removal before injection into the GC column (2 m Porapak-Q 60/80 mesh). Run conditions were 40°C for 2 min, increasing at a rate of 16°C/min to 200°C and held at this temperature. Calibration was performed using hydrocarbon gas standards of known concentration (Scotty IV calibration gas (HC-MIX #9)). Precision for replicate analyses was ± 0.33 mole% for C_1–C_5 and ± 1.5 mole% for CO_2.

Results

The hydrocarbon gas and CO_2 concentrations measured, and the $C_1/(C_2+C_3)$ ratios are listed in Table 1. The hydrocarbons detected consist of methane to iso-pentane. Methane is the major component (96.7 - 98.8%). NMHC are trace components (<0.28%). CO_2 is 2.7 - 3.2% except for sample T0578 (1.4%). The ratios of $C_1/(C_2+C_3)$ (<10^3) suggest the contribution of small amounts of thermogenic gases. In sample T0578, the material recovered contained both primary gas and hydrate fragments released by sediment disturbance. The hydrocarbon results are similar to the other samples. The presence of trace quantities of iso-C_5, and undetectable n-C_5 suggests some fractionation mechanism. We note that structure-H hydrate could provide this as iso-C_5 can be included in this structure but n-C_5 cannot. However, we have no direct evidence for the presence of this hydrate form. For T0563 and T0573, we see small changes in the concentration of C_1 and CO_2 gases near 5 m and 8–10 m above the vent. This may be controlled by bubble dissolution and rise rate, with the highly soluble CO_2 component (solubility ~10.5 greater than methane) being rapidly lost.

Table 1. Molecular compositions of vent gases and hydrates from the sea floor in Guaymas Basin, Gulf of California.

Dive #	Cylinder	C_1	C_2	C_3	i-C_4	n-C_4	i-C_5	CO_2	$C_1/(C_2+C_3)$	Description
		mole %								
T0563	Red	96.7	0.25	0.042	0.013	0.001	0.003	2.95	332	Main gas vent @ 1 m
	Blue	96.7	0.24	0.042	0.013	0.001	0.003	2.73	344	Main gas vent @ 5 m
	Black	97.3	0.25	0.042	0.013	0.002	0.003	2.88	333	Main gas vent @ 0 m
T0566	Red	98.0	0.25	0.041	0.013	0.002	0.003	2.91	337	Main gas vent @ 0 m
	Blue	97.6	0.25	0.269	0.062	0.052	0.009	2.94	188	Main gas vent @ 0 m
	Black	97.5	0.25	0.283	0.065	0.053	0.009	2.95	182	Duplicate of Blue
T0573	Red	97.4	0.27	0.078	0.017	0.002	0.004	3.15	283	Main gas vent @ 0 m
	Blue	97.0	0.26	0.077	0.017	0.002	0.004	3.06	290	Main gas vent @ 2-3 m
	Black	96.9	0.27	0.080	0.018	0.003	0.004	3.08	281	Main gas vent @ 8-10 m
T0576	Red	98.1	0.25	0.083	0.019	0.003	0.004	2.81	297	Sediment gas bubbles
	Blue	98.1	0.26	0.078	0.017	0.003	0.004	3.11	290	DORISS excavation vent
	Black	98.8	0.26	0.082	0.018	0.003	0.004	2.91	293	3rd sample from disturbed site
T0578	Red	98.4	0.26	0.077	0.016	0.002	0.004	3.04	295	Small vent as DORISS
	Blue	97.8	0.26	0.077	0.017	0.002	0.004	3.09	293	Main gas vent
	Black	98.4	0.26	0.077	0.017	0.003	0.004	3.03	294	Duplicate of Blue
T0582	Red	98.2	0.17	0.118	0.027	0.006	0.008	1.43	337	Sediment gas + clathrate

Conclusions & Future Work

DORISS successfully obtained *in situ* Raman spectra of natural gas emanating from a vent on the sea floor. As verified by shore-based GC analysis, the gas was composed primarily of methane (~97%). Trace constituents were not present in high enough concentrations to be detected by Raman analysis. Two significant lessons were learned from this expedition. 1) When analyzing gases within the hydrate stability zone, a heater can and should be used to remove hydrate skin formed during collection. This was successfully done for the gas sample collection and would have greatly improved the Raman data collected on the sea floor. 2) Precision position is necessary when collecting Raman spectra of opaque targets (such as solid hydrate, hydrate skin, or rocks). This requirement is dictated by the focal depth of the sampling optics. A new Precision Underwater Positioner (PUP) has been built for this purpose and is described in the following poster (OS32A-0236).

Raman spectroscopy is a powerful analytical tool that can now be used to analyze targets *in situ* in the deep ocean. We plan to continue expeditionary deployments of the DORISS instrument in 2004 during an expedition to Hydrate Ridge and the Cleft Segment of the Juan de Fuca Ridge. At these locations we will attempt to use Raman spectroscopy to analyze gas hydrates *in situ* (using the PUP positioner), and to analyze various targets in hydrothermal vent environments – vent fluids, bacterial mats, sulfides, etc.

Acknowledgements

We would like to acknowledge the work of the engineering team: George Malby, Mark Brown, and Danelle Cline; our collaborators at Washington University John Freeman, and Brigitte Wopenka; the captain and crew of the R/V Western Flyer; the pilots of the ROV Tiburon. Funding was provided by a grant to MBARI from the David and Lucile Packard Foundation; by the U.S. Dept. of Energy Ocean Carbon Sequestration Program (Grants No. DE-FC26-00NT40929 and DE-FC03-01ER6305); and by a grant from the Japan Society for the Promotion of Science.

References

Brewer, P.G., G.E. Malby, J.D. Pasteris, S.N. White, E.T. Peltzer, B. Wopenka, J. Freeman, and M.O. Brown, Development of a laser Raman spectrometer for deep-ocean science, Deep-Sea Research, in press.

Brunsgaard Hansen, S., R.W. Berg, and E.H. Stenby, How to determine the pressure of a methane-containing gas mixture by means of two weak Raman bands, $_3$ and 2 $_2$, Journal of Raman Spectroscopy, 33, 160-164, 2002.

Diller, D.E., and R.F. Chang, Composition of mixtures of natural gas components determined by Raman spectroscopy, Applied Spectroscopy, 34 (4), 411-414, 1980.

Merewether, R., M.S. Olsson, and P. Lonsdale, Acoustically detected hydrocarbon plumes rising from 2-km depths in Guaymas Basin, Gulf of California, Journal of Geophysical Research, 90 (4), 3075-3085, 1985.

Seitz, J.C., J.D. Pasteris, and I.-M. Chou, Raman spectroscopic characterization of gas mixtures. I. Quantitative composition and pressure determinations of CH_4, N_2, and their mixtures, American Journal of Science, 293, 297-321, 1993.

Simoneit, B.R., P.F. Lonsdale, J.M. Edmond, and W.C. Shanks, Deep-water hydrocarbon seeps in Guaymas Basin, Gulf of California, Applied Geochemistry, 5, 41-49, 1990.

Background Image: The 532 nm green laser of DORISS illuminates a cube filled with natural gas hydrate from a deep-sea gas vent at Guaymas Basin during the 2003 MBARI Gulf of California Expedition.